UNIVERSIDADE ESTADUAL PAULISTA
JÚLIO DE MESQUITA FILHO
PROGRAMA DE PÓS-GRADUAÇÃO EM ENGENHARIA ELÉTRICA

TOOL CONDITION MONITORING IN THE DRESSING PROCESS THROUGH ELECTROMECHANICAL IMPEDANCE AND MACHINE LEARNING

PEDRO DE OLIVEIRA CONCEIÇÃO JUNIOR

Ph.D. Thesis
Bauru, SP
03-2020

UNIVERSIDADE ESTADUAL PAULISTA
JÚLIO DE MESQUITA FILHO
PROGRAMA DE PÓS-GRADUAÇÃO EM ENGENHARIA ELÉTRICA

TOOL CONDITION MONITORING IN THE DRESSING PROCESS THROUGH ELECTROMECHANICAL IMPEDANCE AND MACHINE LEARNING

PEDRO DE OLIVEIRA CONCEIÇÃO JUNIOR

A thesis submitted to São Paulo State University (UNESP), School of Engineering (FEB), Bauru, São Paulo, as part of the requirements for the doctoral degree (Ph.D.) in Electrical Engineering.

Advisor: Full Prof. Paulo Roberto de Aguiar (Department of Electrical Engineering, UNESP)

Co-Advisor: Assis. Prof. Fabricio Guimarães Baptista (Department of Electrical Engineering, UNESP)

Co-Advisor Abroad: Assoc. Prof. Doriana Marilena D'addona (Department of Chemical, Materials and Production Engineering, *Università Degli Studi di Napoli Federico II*, Italy)

Ph.D. Thesis
Bauru, SP
03-2020

Conceição Junior, Pedro de Oliveira.

Tool Condition Monitoring in the Dressing Process through Electromechanical Impedance and Machine Leaarning / Pedro de Oliveira Conceição Junior, 2020

122 f. : il.

Orientador: Paulo Roberto de Aguiar

Tese (Doutorado)–Universidade Estadual Paulista. Faculdade de Engenharia, Bauru, 2020

1. Monitoramento da condição da ferramenta. 2. Retificação. 3. Processo de dressagem. 4. Impedância eletromecânica. 5. PZT. 6. Aprendizagem de máquina. I. Universidade Estadual Paulista. Faculdade de Engenharia. II. Título.

UNIVERSIDADE ESTADUAL PAULISTA

Câmpus de Bauru

ATA DA DEFESA PÚBLICA DA TESE DE DOUTORADO DE PEDRO DE OLIVEIRA CONCEIÇÃO JÚNIOR, DISCENTE DO PROGRAMA DE PÓS-GRADUAÇÃO EM ENGENHARIA ELÉTRICA, DA FACULDADE DE ENGENHARIA - CÂMPUS DE BAURU.

Aos 06 dias do mês de março do ano de 2020, às 14:00 horas, no(a) Anfiteatro da Pós-graduação / FEB, reuniu-se a Comissão Examinadora da Defesa Pública, composta pelos seguintes membros: Prof. Dr. PAULO ROBERTO DE AGUIAR - Orientador(a) do(a) Departamento de Engenharia Elétrica / Faculdade de Engenharia de Bauru - UNESP, Prof. Dr. BRUNO ALBUQUERQUE DE CASTRO do(a) Departamento de Mecatrônica / FATEC - Faculdade de Tecnologia de Garça, Prof. Dr. FABIO ROMANO LOFRANO DOTTO do(a) - / Farol Pesquisa, Desenvolvimento e Consultoria, Prof. Dr. ALESSANDRO ROGER RODRIGUES do(a) Departamento de Engenharia Mecânica / USP - São Carlos, Prof. Dr. BRENO ORTEGA FERNANDEZ do(a) Departamento de Engenharia Elétrica / Centro Universitário de Lins - UNILINS, sob a presidência do primeiro, a fim de proceder a arguição pública da TESE DE DOUTORADO de PEDRO DE OLIVEIRA CONCEIÇÃO JÚNIOR, intitulada **TOOL CONDITION MONITORING IN THE DRESSING PROCESS THROUGH ELECTROMECHANICAL IMPEDANCE AND MACHINE LEARNING** . Após a exposição, o discente foi arguido oralmente pelos membros da Comissão Examinadora, tendo recebido o conceito final: Aprovado . Nada mais havendo, foi lavrada a presente ata, que após lida e aprovada, foi assinada pelos membros da Comissão Examinadora.

Prof. Dr. PAULO ROBERTO DE AGUIAR

Prof. Dr. BRUNO ALBUQUERQUE DE CASTRO

Prof. Dr. FABIO ROMANO LOFRANO DOTTO

Prof. Dr. ALESSANDRO ROGER RODRIGUES

Prof. Dr. BRENO ORTEGA FERNANDEZ

À Minha Familia

ACKNOWLEDGMENTS

My deep gratitude goes first to God.

Secondly, I would like to express the deepest appreciation to my advisor and head of the “Data Acquisition and Signal Processing Laboratory (LADAPS)” Dr. Paulo Roberto de Aguiar, Full Professor at Department of Electrical Engineering (DEE), São Paulo State University (UNESP), who has provided me with the guidance, patience, and careful supervision to make this achievement possible. Without his valuable insights and encouragement, this project would never have taken shape.

I sincerely acknowledge my co-advisor abroad Assoc. Professor Doriana Marilena D’Addona, who provided me the possibility to do a research internship during my Ph.D. program at the Department of Chemical Engineering, Materials and Industrial Production (DICMAPI), University of Naples Federico II. Her fully technical review and her supportive discussions had been a great help to support this Ph.D. thesis. I am also grateful to Professor Roberto Teti, director of “Fraunhofer Joint Laboratory of Excellence on Advanced Production Technology (Fh_JLEAPT)”, who provided me the possibility to carry out part of this research at that center.

I am deeply indebted to my colleague Ph.D. candidate Salvatore Conte for his unconditional support and friendship during the time I worked in Naples, Italy.

I sincerely acknowledge the Fraunhofer Jh_LEAPT laboratory team and I am grateful to my colleagues Dr. Alberto Botillo, Ing. Roberta Angellone, Dr. Francesco Napolitano, Dr. Alessandra Caggiano and Dr. Tiziana Segreto for their unconditional support during the period of this research work. I appreciate also the support of Ing. Roberta Angellone for her technical help with microscopic measurements.

I would like to thank all my colleagues at DICMAPI, University of Naples Federico II, and all those who have provided much support directly or indirectly during the time, I worked in Naples, Italy.

I am grateful to my co-advisor Assoc. Professor Fabricio Baptista who provided technical support and guidelines to carry out this research work.

I appreciate also the support of the Full Professor Eduardo Bianchi for his sincere support during my study providing essential guidance and the necessary equipment to support this research work.

In LADAPS, where I met many great people during all these years, I am grateful to my colleagues Dr. Marcelo Marchi, M.Sc. Luiz Gilli Fabiano, M.Sc. Fabio Isaac, Dr. Rogerio Thomazella, M.Sc. Carine Tavora, Ing. Bárbara Lopes, Ing. Leonardo Simões, Ph.D. student Reinaldo Gotz, Dr. Breno Fernandez, and all other members of the lab in general. I will not mention them all, so it was a pleasure to work with you, and good luck to all. A particular reward has to be given to the colleagues I worked with: M.Sc. Felipe Alexandre, Ph.D. Student Martin Viera, M.Sc. Wenderson Lopes, and M.Sc. Danilo Ribeiro, for their unconditional support, confidence, open mind, and time spent to make this project go ahead at every moment this work going on. In the same manner, I would like to express my sincere gratitude to Dr. Fabio Dotto for their contribution to this work, numerous advice, friendship, and time spent sharing his experience with me.

I also place on record, my sense of gratitude to all my colleagues and professors at DEE UNESP-Bauru SP and numerous other people that have been involved for different tasks: helping to perform experiments, discussing scientific results, and dealing with administrative issues. A particular thought goes to Dr. Bruno Castro with who I also spent great times at work, and sometimes later. Thank you for all the laughs.

I would like to thank the São Paulo Research Foundation - FAPESP, under grants #2016/02831-5 and #2017/16921-9 for supporting this research work.

I am grateful to the jury members that accepted to read the manuscript and made valuable recommendations that was of great help to improve this thesis.

Last but not least, I would like to express my sincere gratitude to Aline Lima and my deep sense of tranks towards my family for their unconditional support and encouragement extended to me. In particular, I am grateful to My mother Maria Carvalho for giving birth to me in the first place and supporting me throughout my life.

“It is dark in front of the grinding grain”

Tönshoff & Grabner

ABSTRACT

The electromechanical impedance (EMI) has attracted increasing attention as an effective sensor monitoring technique for applications in many engineering sectors. Due to the considerable potential of lead zirconate titanate (PZT) diaphragm transducers in terms of excellent electromechanical coupling properties, low implementation cost and wide-band frequency response, this technique provides a new alternative approach for tool condition monitoring (TCM) in grinding processes competing with the conventional and expensive indirect sensor monitoring methods. This research work aimed to develop a new approach for TCM in dressing operation using the PZT-EMI-based technique in cooperation with machine learning algorithms. The research activities proposed in this work involved in diagnosing different wear and failure ranges on dressing tools through experimental tests of dressing operation into different dressing conditions. Further, the proposed system was tested for sensory position independence and for different types of dressing tools to ensure its capability for real-time application. The proposed approach was validated on the basis of the dressing tool condition information obtained from representative damage indices computed at different frequency bands. The proposed intelligent diagnosis system was able to select the most damage-sensitive features, such as damage classification and location, based on the optimal selection of the suitable frequency band. The best results showed less than 2% of general average errors to determine the actual tool condition. This thesis contributes to an effective monitoring system of the dressing operation capable of avoiding replacement of the dressing tool before the end of its service life as well as the operation being performed with damaged tools, since the proposed approach can identify different sates of the tool life span.

Keywords: tool condition monitoring, grinding, dressing process, electromechanical impedance, PZT, machine learning.

RESUMO

A impedância eletromecânica (EMI – *electromechanical impedance*) tem atraído cada vez mais atenção como uma técnica eficiente de monitoramento a base de sensores em diversos setores de engenharia. Devido ao considerável potencial dos transdutores piezelétricos de titanato e zirconato de chumbo (PZT) do tipo diafragmas em termos de excelentes propriedades de acoplamento eletromecânico, baixo custo de implementação e resposta a uma banda ampla de frequência, esta técnica fornece uma nova alternativa para monitoramento da condição de ferramentas (TCM – *tool condition monitoring*) no processo de retificação competindo com os métodos convencionais e caros de monitoramento indireto por sensores. Assim, a presente pesquisa visou desenvolver uma nova abordagem para o TCM na operação de dressagem por meio do método EMI-PZT em conjunto a algoritmos de aprendizado de máquina (*machine learning*). As atividades de pesquisa propostas neste trabalho envolveram o diagnóstico de diferentes níveis de desgaste e de falhas nas ferramentas de dressagem por meio de ensaios experimentais em diferentes condições de dressagem. O sistema proposto também foi testado para diferentes posições de transdutores quanto à aquisição de dados, bem como para diferentes tipos de dressadores visando expandir sua capacidade de aplicação em tempo real. O sistema proposto foi validado com base na informação da condição da ferramenta de dressagem extraída por meio de índices de danos calculados para diferentes bandas de frequência. O sistema inteligente foi capaz de selecionar as características mais sensíveis ao dano, tais como classificação e localização de danos, com base na seleção da faixa de frequência ideal. Os resultados mais satisfatórios apresentaram erros gerais abaixo de 2% quando da determinação da condição real da ferramenta de dressagem. Esta tese contribui com a proposta de um sistema de monitoramento da operação de dressagem eficaz e capaz de evitar a substituição da ferramenta antes do tempo, bem como que a operação de dressagem seja realizada com dressadores danificados, uma vez que o sistema proposto pode identificar diferentes estágios da vida útil da ferramenta de dressagem.

Keywords: monitoramento da condição da ferramenta, retificação, processo de dressagem, impedância eletromecânica, PZT, aprendizagem de máquina.

CONTENTS

LIST OF FIGURES

LIST OF TABLES

SYMBOLS & ABBREVIATIONS

Symbols:

$\parallel$	*Parallel connection*
$\emptyset_p$	*Active element diameter [mm]*
σ_D	*Standard deviation of the damaged signature*
σ_H	*Standard deviation of the healthy signature*
α_d	*drag angle [degrees]*
a	*Depth of cut [μm]*
a_d	*Dressing depth [μm]*
b_d	*Dressing tool active width [mm]*
C	*Static capacitance of the transducer [μF]*
Cov	*Covariance*
d_{iklj}	*Piezoelectric constants*
D_i	*Electrical displacement*
D_s	*Wheel diameter [mm]*
D_w	*Workpiece diameter [mm]*
ε_{ik}^T	*Permittivity component at constant stress*
E_k	*Electric field*
j	*Unit imaginary number*
l_c	*Length of contact [mm]*
Re	*Real part of the impedance*
r_d	*Diamond curvature radius*
s_{ijkl}^E	*Elastic compliance at a constant electric field*

S_{ij}	*Strain component*
T_{kl}	Traction vector component
U_d	*Overlap ratio*
v_d	*Crossfeed velocity [m/s]*
ω	*Angular frequency [rad/s]*
ω_1	*Initial frequency [rad/s]*
ω_F	*Final frequency [rad/s]*
$x(t)$	*Analogic excitation signal [V]*
$x[n]$	*Digital excitation signal [V]*
$y(t)$	*Analogic response signal [V]*
$y[n]$	*Digital response signal [V]*
Z_B	*Electrical impedance of the PZT diaphragm brass plate [Ω]*
Z_E	*Electrical impedance of the transducer [Ω]*
Z_D	*Electrical impedance of the PZT diaphragm [Ω]*
Z_{IN}	*Electrical impedance of the analog input* [Ω]
Z_{k_D}	*Electrical impedance under damaged conditions* [Ω]
Z_{k_H}	*Electrical impedance under damaged conditions* [Ω]
Z_p	*Mechanical impedance of the transducer [N.s/m]*
Z_s	*Mechanical impedance of the structure [N.s/m]*

Abbreviations:

ABDI - *Agência Brasileira de Desenvolvimento Industrial*

ADC- *Analogic-digital conversion*

AE – *Acoustic emission*

AI – *Artificial intelligence*

ANN – *Artificial neural networks*

BP – *Backpropagation*

BP – *Backpropagation*

CAD – *Computer-aided design*

CBN - *Cubic boron nitride*

CC – *Correlation coefficient*

CCDM- *Correlation coefficient deviation metric*

CIRP- *International Academy for Production Engineering*

CNC – *Computer numeric control*

CNN – *Convolutional neural networks*

CPS - *Cyber-physical systems*

CTF – *Catastrophic tool failure*

CVD - *Chemical vapor deposition*

CTF – *Catastrophic tool failure*

DAC- *Digital-analogic conversion*

DAQ – *Data acquisition*

DNN – *Deep neural networks*

DPO – *Deviation of power*

ECCD - *Electrochemical in-process control dressing*

ECDD - *Electro contact discharge dressing*

ECMD - *Electrochemical discharge dressing*

EDD - *Electrical discharge dressing*

ELID - *Electrolytic in-process dressing*

EMI – *Electromechanical impedance*

FFT – *Fast Fourier transform*

k-NN- *k-nearest neighbor*

LVM - *Levenberg–Marquardt*

MF- *Membership function*

MFC – *Microfiber composite*

MLP – *Multilayer perceptron*

MD – *Mechanical dressing*

NDE – *Non-destructive evaluation*

NFS- *Neuro-fuzzy systems*

NN – *Neural networks*

PC – *Personal microcomputer*

PCA- *Principal component analysis*

PLB- *Pencil lead break*

PNN – *Probabilistic neural networks*

PSD – *Power spectral density*

PZT – lead zirconate titanate

RNN – *Recurrent neural networks*

RMS – *Root mean square*

RMSD- *Root mean square deviation*

ROP – *Ratio of power*

SOM- *Self-organizing maps*

STFT- *Short-time Fourier transform*

SHM – *Structural health monitoring*

TDNN – *Time-delay neural network*

USB- *Universal serial bus*

WT – *Wavelet transform*

PUBLICATIONS

OLIVEIRA, P.C.; MARCHI, M.; MARTINS, C.H.; D'ADDONA, D.M.; AGUIAR, P.R.; BIANCHI, E.C. Spectral Estimation of Vibration Signal for Monitoring the Wear of Single-Point Dresser. ***Matéria****, v. 21, 04, 2016. DOI: 10.1590/S1517-707620160004.0079.*

OLIVEIRA JUNIOR, P.C.; SOUZA, R.V.C.G.; FERREIRA, F.I.; MARTINS, C. H.; AGUIAR, P.R.; BIANCHI, E.C. Wear Monitoring of Single-Point Dresser in Dry Dressing Operation Based on Neural Models. **Modelling, Identification and Control***, 2017, Innsbruck. Calgary: ACTAPRESS. DOI: 0.2316/P.2017.848-054.*

OLIVEIRA JUNIOR, P.C.; FERREIRA, F.I.; AGUIAR, P.R.; BATISTA, F.G.; BIANCHI, E.C.; DADDONA, D. M. Time-domain Analysis Based on the Electromechanical Impedance Method for Monitoring of the Dressing Operation. ***PROCEDIA CIRP****, v. 67, p. 319-324, 2018. DOI: 10.1016/j.procir.2017.12.220.*

OLIVEIRA JUNIOR, P.C.; RUZZI, R.S.; LOPES, W.N.; ALEXANDRE, F.A.; BAPTISTA, F.G.; AGUIAR, P.R.; BIANCHI, E.C. A New Approach For Dressing Operation Monitoring Using Voltage Signals Via Impedance-Based Structural Health Monitoring. ***KnE Engineering****, v. 3, p. 942, 2018. DOI: 10.18502/keg.v3i1.1514.*

OLIVEIRA JUNIOR, P.C.; D'ADDONA, D.M.; AGUIAR, P.R.; TETI, R. Dressing Tool Condition Monitoring through Impedance-Based Sensors: Part 1—PZT Diaphragm Transducer Response and EMI Sensing Technique. **Sensors***, 2018,* 18*, 4455. DOI: 10.3390/s18124453.*

OLIVEIRA JUNIOR, P.C.; D'ADDONA, D.M.; AGUIAR, P.; TETI, R. Dressing Tool Condition Monitoring through Impedance-Based Sensors: Part 2—Neural Networks and k-Nearest Neighbor Classifier Approach. ***Sensors****, 2018, 18, 4453. DOI: 10.3390/s18124455.*

OLIVEIRA JUNIOR, P.C.; D'ADDONA, D.M.; CONTE, S.; AGUIAR, P.R., BAPTISTA, F.G.; BIANCHI, E.C. Failure Diagnosis in Multi-Point Diamond Dressers Using Electromechanical

Impedance Technique. ***International Conference on Industrial Internet of Things and Smart Manufacturing****, London, UK, September 5-6, 2018. ISBN: 978-1-912532-06-3.*

OLIVEIRA JUNIOR, P.C.; CONTE, S.; D'ADDONA, D.M.; AGUIAR, P.R.; BAPTISTA, F.G.; BIANCHI, E.C.; TETI, R. Damage patterns recognition in dressing tools using PZT-based SHM and MLP networks. Procedia CIRP, v.79, p.303-307, 2019. DOI: 10.1016/j.procir.2019.02.071.

OLIVEIRA JUNIOR, P.C.; D'ADDONA, D. M.; ALEXANDRE, F.A.; RUZZI, R.S.; AGUIAR, P.R.; BAPTISTA, F.G.; BIANCHI, E.C. **.** *Impedance-based PZT Transducer and Fuzzy Logic to Detect Damage in Multi-point Dressers* ***. Springer Nature Switzerland AG: Advances in Manufacturing II*** *- Volume 4, LNME, pp. 213–222, 2019. DOI: 10.1007/978-3-030-16943-5_19.*

OLIVEIRA JUNIOR, P.C.; D'ADDONA, D. M.; ALEXANDRE, F.A.; RUZZI, R.S.; AGUIAR, P.R.; BAPTISTA, F.G.; BIANCHI, E.C **.** *Enhancement of Impedance-Based Damage Classification Using Self-Organizing Maps* ***. CIRP ICME '19 - 13th CIRP International Conference on Intelligence Computation in Manufacturing Engineering****, 19-21 July, 2019, Guilt of Naples, Italy.*

PATENT

Title: BR1020190256648 “Sistema e Método de Monitoramento de Desgaste de Ferramentas para Dressagem de Rebolos”. **Inventors:** OLIVEIRA JUNIOR, P.C.; AGUIAR, P.R.; BAPTISTA, F.G.; D’ADDONA, D.M.; BIANCHI, E.C. **Holders:** OLIVEIRA JUNIOR, P.C.; AGUIAR, P.R.; BAPTISTA, F.G.; D’ADDONA, D.M.; BIANCHI, E.C.; UNESP; UNINA; FAPESP. **Intellectual property organization:** Instituto Nacional da Propriedade Industrial (INPI). **Deposition year**: 2019.

GRANT INFORMATION

Grantor: São Paulo Research Foundation (FAPESP)

Grant numbers: #2016/0281-5 (research scholarship in Brazil – Ph.D, "*Sistemas de Monitoramento da Integridade Estrutural de Dressadores baseado no Método da Impedância Eletromecânica*"); #2017/16921-9 (Research Internship Abroad – BEPE, "*A New Approach for Dressing Operation Monitoring based on Electromechanical Impedance and Computational Intelligence*").

Home Institution: Faculdade de Engenharia (FE), Universidade Estadual Paulista (UNESP), Bauru. Bauru, SP, Brazil.

Host Institution: UNINA - Università Degli Studi di Napoli Federico II, Dipartimento di Chimica, Materiali e Ingegneria della Produzione Industriale; Piazzale Vincenzo Tecchio, 80, 80125 Napoli NA, Italy

Supervisor abroad: Assoc. Prof. Doriana Marilena D'Addona

Reference Group at the host institution: Fraunhofer Joint Laboratory of Excellence on Advanced Production Technology (Fh_JLEAPT – Director: Prof. Roberto Teti).

DI C Ma PI

Dipartimento di Ingegneria Chimica, dei Materiali e della Produzione Industriale

Università degli Studi di Napoli Federico II

Fraunhofer J_LEAPT

Chapter 1

INTRODUCTION

Nowadays, the Industry 4.0 paradigm, a German strategic initiative, is focused on high technology and can result in unemployment for those who do not face the transition to the new manufacturing concept. As a result, industries must shift to more cost-effective manufacturing solutions and innovative monitoring systems in order to meet a new demand: novel systems need to be robust, reconfigurable, reliable, intelligent and inexpensive. In 2018, Li presented a paper titled: “China's manufacturing locus in 2025: With a comparison of ‘Made-in-China 2025’ and ‘Industry 4.0’” (LI, 2018). That survey compared Germany's “Industry 4.0” and China's “Made-in-China 2025” and estimated China's locus in “Made-in-China 2025”. China became a global leader in manufacturing systems and the second-largest economic power in the world. On the other hand, Germany is the world-leading industrialized nation and its Industry 4.0 is a strategic plan to compete in the global market (Volkswagen, BMW, and SAP, just to name a few of its prestigious companies). This way, both nations have recognized guiding principles to enhance industrial capability through innovation-driven manufacturing and achieve green development. The main remarks include: industrial information integration, manufacturing digitization, Internet of Things (IoT), and artificial intelligence (AI).

With respect to economic motivations, the Fraunhofer society (Fraunhofer-Gesellschaft), which is one of the most important research institutions in Europe, presented the state-of-the-art technologies for the factory of the future through the brochure titled: “Trend in *Industrie* 4.0” (FRAUNHOFER-GESELLSCHAFT, 2016). A survey conducted by Fraunhofer and reported by its president Dr. R. Neugebauer indicates that Industry 4.0 could participate in a boost in productivity worth some 78 billion euros by the year 2025. Again, those hot topics previously mentioned are targeted with particular reference to: secure production in Industry 4.0, adjusting production processes in real-time, production without rigid plans, among others.

In a similar way to the Brazilian scenario, according to a survey conducted by Agência Brasileira de Desenvolvimento Industrial (ABDI), it is expecting to reduce costs by approximately 73 billion R$ (reais) per annum from industry 4.0 digitization (ABDI, 2019). Likewise, Brazilian industrial companies are becoming familiar with the use of digital technologies, including the adoption of digital automation with sensors for process control. According to a 2018 survey conducted by Confederação Nacional das Indústrias (CNI), almost half (48%) of large industrial companies plan to invest in these technologies. The percentage of responses (%) is shown in Figure 1, as addressed by CNI (2018).

Figure 1- Digital technology investment forecast in 2018

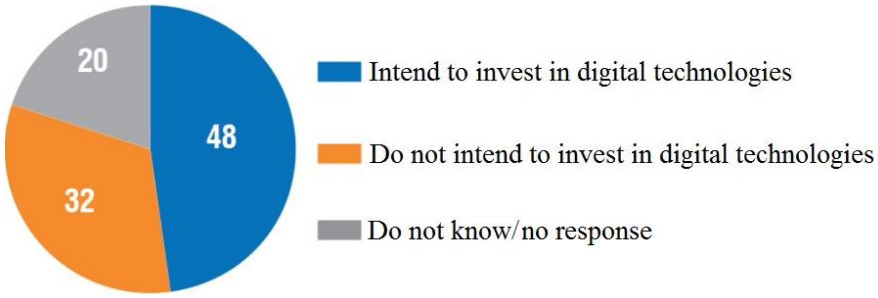

Source: (CNI, 2018)

In the context of Industry 4.0, production systems are updated to a smart level taking advantage of advanced information and manufacturing technologies to achieve flexible, smart, and reconfigurable manufacturing operations in order to address a dynamic and global market. Some technologies also have machine learning techniques and sensor monitoring systems, which allows manufacturing operations to learn from experiences and sensing devices in order to optimize industrial practice. Accordingly, machining processes are widely used in manufacturing systems, and then the use of innovative sensor systems for monitoring machining operations became more commonplace to enhance productivity in the new round of industrial revolution.

The advanced monitoring of machining processes can represent economy and facility due to the fact that it is supporting of tool wear diagnosis, surface roughness, burn and anomalies during material cutting that can cause loss, damage, and other impairing factors in the process. For example, in terms of cutting tools, U.S. manufacturers consumed $ 206.3 million worth of them during April 2018, as addressed by the U.S. Cutting Tool Institute (USCTI). Tool wear and related failures could result in significant increases in energy and power consumption, poor surface quality, and loss of dimensional accuracy. Owing to that, tool condition monitoring (TCM) is a crucial element in modern manufacturing systems because it allows an optimal tool life exploitation through condition-based replacement strategies. In addition, TCM systems provide the possibility for identifying the dangers of severe damage or catastrophic failures to machine tool components in precision plant manufacturing. In this context, many approaches have been proposed to accomplish sensor monitoring of machining operations and a number of these were successfully employed in TCM. The International Academy for Production Engineering (CIRP) has a long and comprehensive record of research and publication on this subject. A comprehensive survey was the publication of the CIRP keynote paper titled “Advanced monitoring of machining operations” by Teti *et al*. (2010) where a large number of contributions on the development and implementation of sensor-based TCM was compiled. Further examples are summarized next.

The use of sensor systems for TCM in machining was already considered since before the 1980s to enhance productivity. For example, in 1995 Teti compiled a review of the TCM literature database containing over 500 publications in the time frame 1960-1995 (TETI, 1995). In the same manner, the CIRP scientific-technical committees (STC) members structured a roadmap for consultation on the status of research and industrial application in TCM, as reported by the CIRP keynote paper published by (BYRNE *et al*., 1995). Some other examples of past contributions on sensor-based TCM were: wear-related loading of the grinding wheel using AE signal processing (Dornfeld (1984)); grinding wheel tool life and quality monitoring through EA signal processing (Inasaki; Okamura (1985)); neural network sensor fusion for TCM (Dornfeld; Devries (1990)); on-line prediction of the tool life (Novak; Wiklund (1996)); catastrophic tool failure (CTF) detection through EA signal processing (Jemielniak; Otman (1998)); tool wear state identification by fuzzy logic data processing (Teti (1998)); integrated condition monitoring and fault diagnosis for modern manufacturing systems (Zhou *et al.* (2000)); and AE tool contact sensing in reliable grinding monitoring (Oliveira; Dornfeld (2001)). Moreover, numerous other techniques and methods of signal processing for feature extraction on the basis of tool condition information published in the time frame 2002-2009 were documented by (Teti, *et al.* (2010)).

Nevertheless, the involvement of sensor monitoring for tool conditions until nowadays was reported in many recent investigations. For example, an approach towards data-driven smart manufacturing was presented by Li; Liu; Wu (2019) to improve the accuracy of tool wear prediction using audio-based signal processing. Likewise, an in-process machine vision monitoring of tool wear for cyber-physical production systems was proposed in the research activities published by Lins; Araujo; Corazzim (2020). In the same way, Cheng *et al.* (2019) proposed an in-process TCM system through deep convolutional neural networks. Accordinly, Teti *et al*. (2020) proposed a robust ANN-based machine learning paradigm to make smart actions o the timerly execution of tool change. Some other recent contributions are therefore available in publications by Martins *et al*. (2014), Arun *et al*. (2018), D'addona *et al*. (2018), Jemielniak (2019), Rehorn; Jiang; Swain *et al*. (2019), and Lins; Araujo; Corazzim (2020).

Based on this concept, this thesis contributes to a grinding case with the aim of performing TCM during the dressing process. The focus is to use the electromechanical impedance (EMI), which is an innovative sensor monitoring technique in machining operations, in order to meet the demands of industrial practice optimization. Some publications resulting from the scope of this thesis include the following: Oliveira Junior *et al.* (2018a,b,c) Oliveira Junior *et al.* (2019). Therefore, this chapter provides an overview of the present research work, including the grinding importance and the challenges in dressing operation monitoring. Subsequently, the thesis motivation is defined, and the thesis objectives are specified. At the end, the organization of the document is provided.

1.1 Overview and scope of the thesis

Grinding is a finishing process widely used in the manufacturing activities of many industrial components (well known for many of its strategic sectors, biomedical, aerospace, and automotive, to name a few). Due to its stochastic nature of undefined geometrical cutting edges and grain distribution, grinding is a complex process that depends on several parameters. The main topics include, but are not limited to: grinding wheel, coolant, workpiece, grinding machine, environment, temperatures, power, dressing performance, and dressing tool. A systematic view of the most important parameters of the grinding process, addressed by Rabiey (2010), is summarized in Figure 2.

The success of any grinding process is critically dependent on the performance of the grinding wheel. However, during grinding, the wheel progressively loses its cutting capacity due to wheel wear and fracture (attrition wear, grain fracture, bond fracture). Excessive grinding wheel wear leads to an unexpected increase in power consumption, loss of workpiece surface quality and integrity, and occurrence of thermal damages. The dressing operation is then carried out to guarantee an optimal abrasive wheel topography and, consequently, a satisfactory surface quality for the final component (OLIVEIRA JUNIOR *et al.* 2018a; POMBO *et al.*, 2017).

The slogan: "grinding is dressing", kept in the grinding community, points out the importance of dressing processes on the manufacturing results, besides all the other relevant parameters for grinding performance (WEGENER *et al.*, 2011). A typical dressing setup is composed of stationary or rotary dressing tools. This way, stationary dressing tools, which include single-point or multi-point diamond dressers, are more often applied in industrial dressing operations because the dressing parameters are simpler to control (MALKIN; GUO, 2008; POMBO *et al.*, 2017; WEGENER *et al.*, 2011). On the other hand, the dressing performance is critically dependent upon dressing tool conditions, i.e. wear and related problems (e.g.: dressing temperature, tool breakage, etc.) can diverse affect the dressing tool shape, as reported by Pombo *et al.*(2017). Further, dressers containing worn diamonds provide less sharpness on the grinding wheel and are consequently responsible for unsatisfactory grinding operations. Owing to that, an efficient system is a desirable element that can monitor the in-process dressing tool conditions and predict its remaining useful life for improving grinding quality and saving cost. On this subject, TCM in the dressing process has long been a consensus in the literature (BADGER; MURPHY; DONNELL, 2018; INASAKI; OKAMURA, 1985; OLIVEIRA JUNIOR *et al.* 2018a; MAKSOUD; ATIA, 2007; MARTINS *et al.*, 2014; OLIVEIRA; DORNFELD, 2001; POMBO; PORTILLO, 2016).

Figure 2- A systematic view of the most important parameters of the grinding process

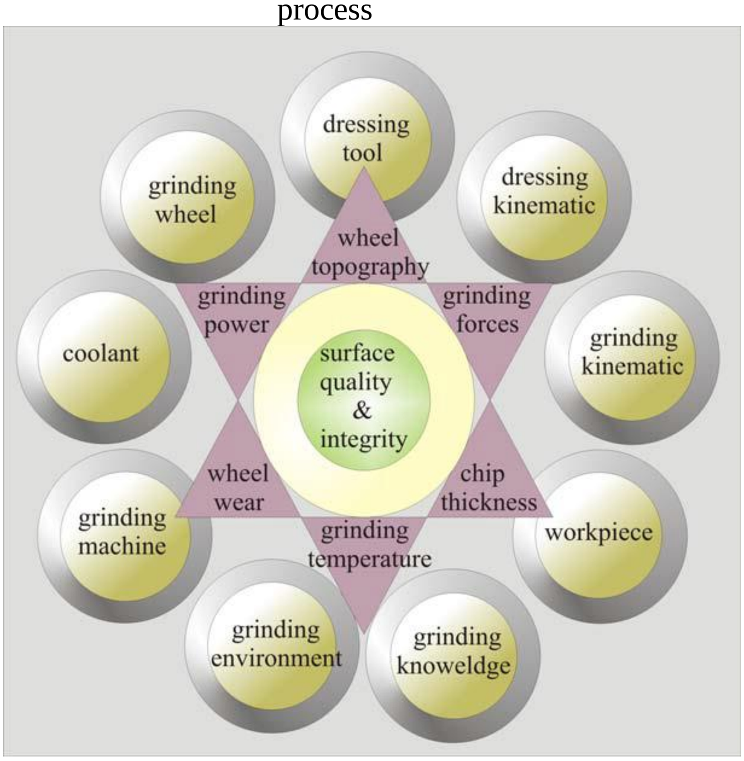

Source: (RABIEY, 2010)

Researchers have made efforts to establish precision monitoring and diagnostic of dressing tool wear using direct and indirect TCM systems. Previous studies published on the subject of direct monitoring were made on dressing tool wear measurement by fixing optical, laser and touch probe techniques (CEARSOLO *et al.*, 2016; HABRAT; BATSCH; PORZYCKI, 2005;

POMBO *et al.*, 2017). These procedures, however, require that the machine be stopped for tool extraction and visual inspection, resulting in machine downtime and human user intervention cost. In contrast, indirect monitoring systems operate according to the variables that are prospectively effective for machining process monitoring, which can be measured by the application of appropriate physical sensors, such as: acoustic emission (AE), vibration, force, motor current, and power. Furthermore, the signals measured by these sensors are subjected to digital signal processing and provide information for process optimization, i.e. the signal features are correlated with tool state and/or process conditions (TETI, R. *et al.*, 2010). For example, Kwak; Ha (2004) proposed to detect the grinding wheel dressing time using force signals and wavelet transform signal processing. Aguiar *et al.* (2009) used sensor fusion technology based on AE combined with power signals to accomplish the same goal. D'addona *et al.* (2016); Oliveira Junior. *et al.* (2017); Martins *et al.* (2014); and Miranda *et al.* (2015) accomplished the single-point dressing tool condition monitoring by data processing of AE, vibration and power signal through artificial neural networks (ANN) and fuzzy systems.

On the other hand, the piezoelectric impedance-based method for damage detection has become popular due to the fact that it has a suitable potential for practical applications in the areas of structural health monitoring (SHM) (CHEN; XUE, 2018; KIM; WANG, 2014a). The detection is achieved using the electromechanical impedance (EMI), which is a nondestructive evaluation (NDE) technique characterized by its simple methodology of using cheaper cost, smart, quick response, and compact piezoelectric devices (FAN *et al.*, 2018). Overall, the most common EMI framework involves a lead zirconate titanate (PZT) transducer (piezoceramic patch or thin-disk piezoelectric diaphragm) that is attached to the host structure, excited in a suitable frequency range, and acts in its both sensing and actuation capacities. Subsequently, a relationship between the mechanical impedance of the host component and the electrical impedance of the PZT transducer is established (BAPTISTA; VIEIRA FILHO; INMAN, 2010). (GIURGIUTIU; ZAGRAI, 2000; INMAN *et al.*, 2005; LIM; SOH, 2014; LIN; XU, 2017; MARUO *et al.*, 2015; NA, WONGI; BAEK, 2018; PARK, GYUHAE *et al.*, 2003; VENU GOPAL MADHAV ANNAMDAS; CHEE KIONG SOH, 2010; YANG; LIM; SOH, 2008). This way, a significant number of researches, taking into account the EMI-based approach, have been conducted on the field of SHM focusing mostly on impedance spectrum analysis through representative damage evaluation metrics (FAN *et al.*, 2018; HU; ZHU; WANG, 2014; LIN; XU, 2017; SILVEIRA; CAMPEIRO; BAPTISTA, 2017; ZHOU, PIN; WANG; ZHU, 2018). In addition, several EMI-based damage classification enhancement methodologies have been developed (e.g.: using numerical analysis, wavelet transform, and machine learning) (CHOI *et* *al.*, 2018; DE OLIVEIRA, MARIO A.; MONTEIRO; VIEIRA FILHO, 2018; HUYNH; DANG; KIM, 2018; INMAN; VIEIRA; GUIMAR, 2011; NA, S.; LEE, 2013; OLIVEIRA, M. ANDERSON DE *et al.*, 2013).

In the past few years, thin-disk piezoelectric diaphragms (also named as PZT diaphragms in this thesis work) have become a promising device used to accomplish SHM on the basis of EMI method (BUDOYA; CAMPEIRO; BAPTISTA, 2019; FREITAS *et al.*, 2017; FREITAS; BAPTISTA, 2016). They are low-cost, compact and lightweight components widely used in a diversity of electronic devices (telephone ringers, audible alarms, piezoelectric transducers) (FREITAS *et al.*, 2017). In several SHM cases of studies, these devices presented damage indices with values similar to those of conventional PZT ceramic transducers, which are most commonly used from a commercial point of view (BUDOYA *et al.*, 2017; FREITAS *et al.*, 2017; FREITAS; BAPTISTA, 2016; SILVEIRA; CAMPEIRO; BAPTISTA, 2017). On the other hand, they were also used as passive transducers in partial discharge monitoring in power transformers (CASTRO *et al.*, 2016), surface roughness discrimination (LIANG *et al.*, 2017), burn detection and in the grinding process (RIBEIRO *et al.*, 2017), grinding wheel acoustic mapping (DOTTO *et al*., 2019) and ceramic grinding monitoring (VIERA *et al.*, 2019a,b).

The scope of this thesis is to develop a new approach for TCM in dressing operation using the PZT-EMI-based technique in cooperation with machine learning algorithms. The main contribution of the present research work is that the PZT diaphragms along with the EMI technique provide a new alternative for dressing operation monitoring versus the conventional sensor-based TCM systems (such as those based on commercial sensors of force, vibration, and AE). Explicitly, the research activities proposed in this thesis involves in diagnosing different wear and failure ranges on dressing tools through experimental tests of dressing operation into different dressing conditions. Further, the proposed system is tested for sensory position independence and for different types of dressing tools to ensure its capability for real-time application. The context and thesis motivation are summarized in the next section.

1.2 Context and motivation

In 2015 Marchi *et al.* published a pioneer study on the subject of sensor monitoring of grinding operation through the EMI technique by the paper titled “Grinding process monitoring based on electromechanical impedance measurements” (MARCHI *et al.*, 2015). That investigation showed a new approach for monitoring the surface grinding process with particular reference to the surface integrity of the ground SAE 1020 steel workpieces. An important finding was the quantification of the wear pattern during the grinding process through representative damage indices commonly used in the SHM applications. This way, the approach initially conceived by Marchi *et al*. represented a breakthrough in the research on real-time monitoring of the grinding process in view of the innovative sensor monitoring technique.

Three years later, in 2018, Batista Silva *et al*. presented another paper showing an investigation on the surface integrity of hardened ABNT N2711 steel after the grinding operation by using a conventional abrasive wheel and various cutting conditions based on the EMI technique (BATISTA SILVA *et al.*, 2018). It was an expansion of the research activities published by Marchi. The main topics included: measurements of microhardness and surface roughness of the machined surfaces, as well as measurements of grinding power, in order to detect any damage in the machined surface and validate the EMI technique.

In the following year of 2019, Ferreira *et al*. discussed correlations between EMI, input (equivalent chip thickness) and output (roughness, microhardness, and power) grinding parameters, including real and imaginary part of the electrical impedance for several frequency bands (FERREIRA *et al.*, 2019). Such a study was of utmost importance to understand the behavior of the EMI for a broader situation when applied to the grinding process.

It is interesting to note that the EMI technique has come to the forefront in grinding operations due to its considerable potential for condition monitoring. The shift has been towards the future enhancement of machining systems and their operational performance. In the context of industry 4.0, this approach forms a paradigm shift from traditional sensor monitoring systems to a new perspective using an alternative and nondestructive evaluation technique, such as the EMI integrating low-cost PZT transducers. In addition, the effective implementation of the proposed approach for industrial grinding operations can be taken into account in computer numeric control (CNC) machines with low cost and without significant changes in the usual cycle times. However, although promising results of the EMI technique for the grinding process, none of the previous approaches focused on TCM in dressing operation. In summary, the main motivations of the present study are:

- The dressing operation is critically dependent upon the dressing tool condition. Therefore, a damaged dressing tool leads to unexpected malfunctions to the manufacturing process, such as: unsatisfactory grinding wheel preparation, loss of workpiece surface quality, and power consumption (POMBO *et al.*, 2017).
- Though findings on dressing operation monitoring showed satisfactory classification rates and accuracy as it was reported in the above-cited papers in Section 1.1,

considerable data processing time and high costs in terms of computing hardware were required.

- The notable potential of a PZT diaphragm transducer as it was demonstrated in section 1.1: their low-cost compared to commercial sensors for AE detection, i.e., PZT diaphragm transducers have an average cost ranging from few cents of dollars (MURATA, 2018) versus the high average cost of the AE commercial sensors, ranging from hundreds to thousands of dollars (PHYSICAL-ACOUSTIC, 2018).
- The EMI setup uses a simple methodology in terms of hardware instrumentation following the approach presented by Baptista; Vieira Filho (2009).

1.3 Thesis objectives

The goal of this thesis is to develop an innovative TCM sensory system for dressing tool wear and failure monitoring in the grinding operation. Unlike existing methods, this goal is achieved by employing the EMI technique along with PZT diaphragms from which the collected sensor signals are used as input data to a proposed intelligent diagnosis system. To accomplish this, the research work has been divided into two tasks: (i) TCM for dressing tool wear and failure in grinding process through EMI along with PZT diaphragms sensorial data processing; (ii) enhancement of damage identification in (i) through machine learning. By utilizing the approach proposed in this thesis, a reduction in manufacturing costs can be expected because the tool replacement will be based on the actual tool condition. This practice avoids that the dressing tool being substituted before their end of life or that the dressing operation being performed with damaged tools. Further, the proposed approach may contribute to the improvement of TCM in the grinding process.

1.4 Thesis organization

The rest of this document is structured as followed:

- Chapter 2 provides a state of the art on TCM in grinding, including trends, sensor technology, and previous works related to this thesis.
- Chapter 3 provides a background related to the EMI technique from an SHM perspective, including theoretical aspects, methods for transducer characterization, and procedures for damage evaluation.

- Chapter 4 details the equipment and experimental procedures applied for the implementation of the proposed approach.
- Chapter 5 discusses the most relevant results obtained with the proposed approach.
- Chapter 6 concludes the thesis, summarizing its contributions to the existent knowledge, as well as future developments and challenges.

Chapter 2

A STATE OF THE ART ON TCM IN GRINDING

In this chapter, a state of the art on tool condition monitoring (TCM) in grinding is reported. The past contributions on the subject of TCM over the last 30 years are reviewed, and an up-to-date inspection of sensor monitoring trends is provided. From this, the role of grinding and dressing as well as the dressing tool wear and related problems are explained. At the end of this chapter, a summary of related works is presented.

2.1 The role of the grinding process and dressing operation in manufacturing

In the field of industrial production, the main function of the grinding process is to produce a required surface by removing a designated amount of material from the component. To accomplish this goal, there are several types of grinding operations (surface grinding, cylindrical grinding, internal grinding, and centerless grinding) that depends on the workpiece shape and related features. Grinding is a key technology for the production of high-quality and high accuracy products. Further, it accounts for about 20 % ~ 25 % of the total industrial cost on material removing processes in industrialized countries (MAGGIONI; MARZORATI, 2013; MALKIN; GUO, 2008; MARINESCU *et al.*, 2016; ROWE, 2014). Examples of precision machined components (aeronautical and automotive) along with industrial grinding processes is shown in Figure 3.

A typical grinding framework can be decomposed into input versus output parameters, as addressed by Tian (2009). As shown in Figure 4, the decomposition includes the relative motion of input parameters (process parameters, consumable tools, machine tool, and workpiece), technical output (heat, force, power, vibration, etc.), and output (geometric accuracy, surface quality, and economic). However, as reported by Tian (2009), it is worth mentioning that the correlation between input and output parameters may not be drawn in a simple way due to the complex nature of the grinding process.

Figure 3 – Examples of precision machined components and industrial grinding process

Source: (BOST, 2019; DUVAL, 2019; JFS, 2019)

Figure 4 – Grinding process decomposition

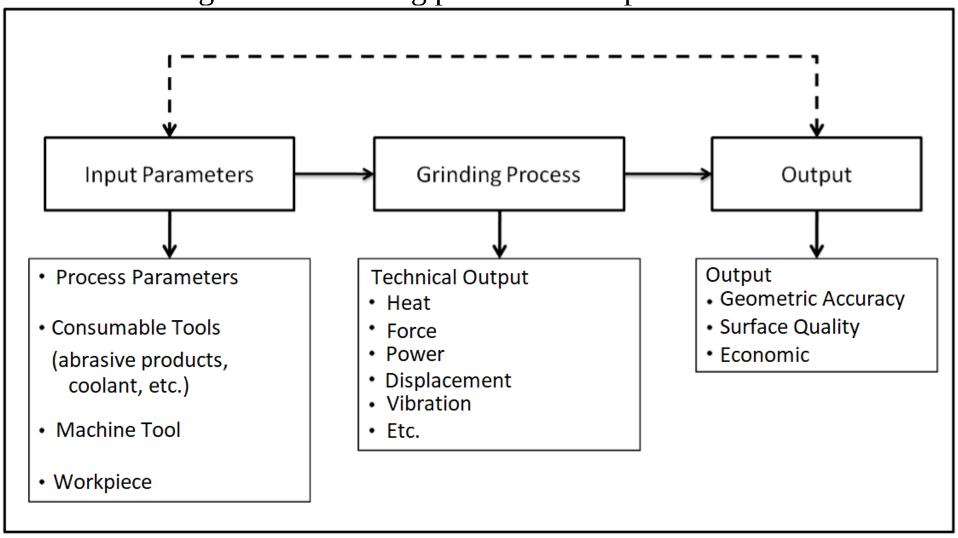

Source: (TIAN, 2009)

Surface grinding, which often involving the grinding of flat surfaces (Figure 5), is one of the most common. However, since it uses a grinding wheel which is made up of a great number of randomly distributed abrasive grains, surface grinding is a complex removal process influenced by many factors. The random nature of the grain position on the grinding wheel surface makes it more difficult to accomplish (MAGGIONI; MARZORATI, 2013; TIAN, 2009). As shown in Figure 6, the process is influenced by (in parenthesis: the employed symbols, derived from CIRP and German general cutting terminology commonly used in grinding, where they are dealt with): kinematic (cutting speed v_s, and workpiece speed v_w); and geometrical parameters (wheel diameter D_s, workpiece diameter D_w, depth of cut a, the length of contact l_c, and average chip thickness h_m), (GOSTIMIROVIĆ *et al.*, 2015; MARINESCU *et al.*, 2016a).

Furthermore, according to Malkin; Guo (2008), the grinding wheels are segmented into the general class of bonded abrasive tools and, according to Wegener et al. (2011), they are classified with respect to their abrasive material (Figure 6a), such as: (i) conventional (e.g.: aluminum oxide and silicon carbide (SiC)), and (ii) superabrasive/single-layer (e.g.: cubic boron nitride (CBN) and diamond). In addition, they are further distinguished regarding their bonding method, i.e., ceramic, resinoid, and metal bond grinding wheels.

Figure 5 – Surface grinding process examples

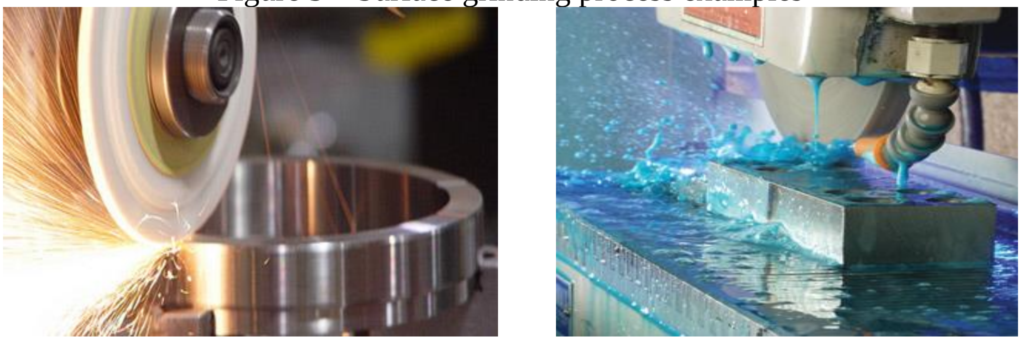

(a) **(b)**

Source: (CARNIEL, 2017; DYNAMIC PRECISION, 2013)

Figure 6 - Related mechanisms of the surface grinding process

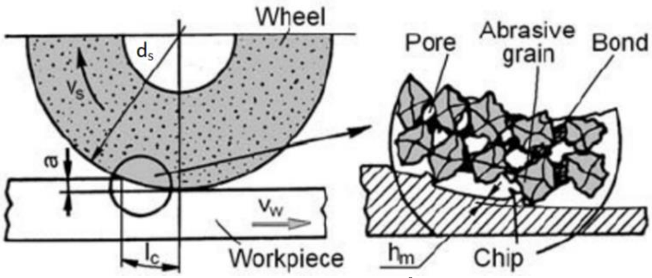

Source: (GOSTIMIROVIĆ *et al.*, 2015)

Moreover, during grinding, the wheel is subject to several types of loads (mechanical, chemical, thermal, etc.) due to the contact between cutting edges and workpiece surface material. This leads to macro wear (loss of macro geometry), microwear (wear on the grain level as illustrated in Figure 6b), bond wear (bond bridge, bond breakage), and pullout (complete grain removed), (WEGENER *et al.*, 2011). In addition, once the grain is worn flat or cutting edges are inactive, the wheel progressively loses its sharpness and needs more power consumption and energy to interact with the workpiece surface. As a result, it leads to a lot of process malfunctions and negative results to the final component (e.g.: decreases in the surface quality and accuracy, loading, and grinding burns), especially when performing grinding of complex parts, such as cutting tools, aerospace components, turbine blades and gears (DENG; XU, 2019; MAGGIONI; MARZORATI, 2013; TIAN, 2009).

In order to maintain the correct geometry and sufficient sharpness during the grinding operation, the grinding wheel must be periodically dressed. The dressing is also performed on a grinding wheel before performing a grinding operation. The term "grinding is dressing" has long been a consensus in the grinding community. Nevertheless, understanding the most influential parameters of the dressing process is critical to achieving optimum performance in grinding. The most important aspects of the dressing process are described in the following subsections.

Figure 7 – Grinding wheel: (a) configuration; and (b) microwear mechanisms

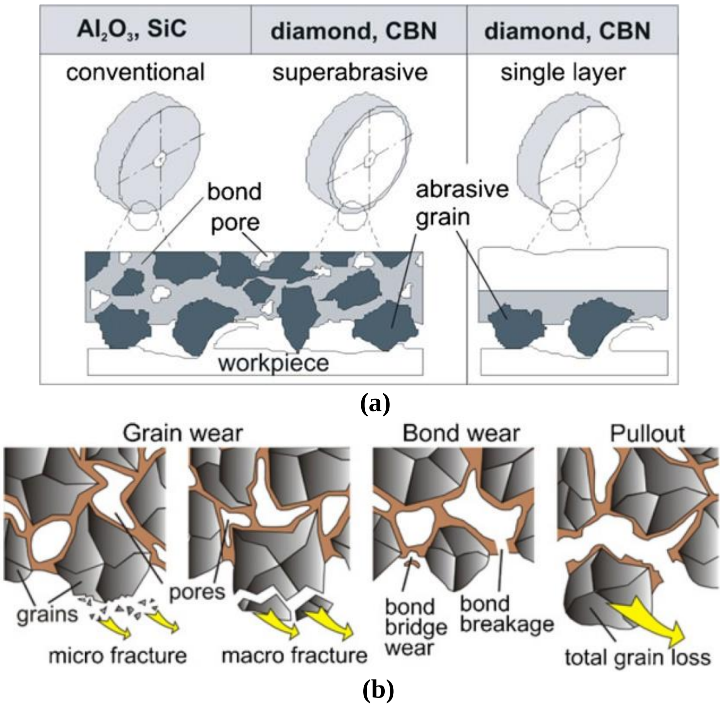

Source: (WEGENER *et al.*, 2011)

2.1.1 The dressing process

Following the definition given by Wegener *et al.* (2011) and Deng; Zhou (2019), dressing operations can be categorized into distinct classes:

- *Mechanical dressing*: dressing with stationary diamond tools (e.g.: multi-point dressing, single-point dressing, block sharpening, and free grinding); and dressing with rotating diamond tools (e.g.: form roller, profile roller, touch dressing, diamond gears dressing, cup wheel dressing, and sharpening using SiC rollers). Applications include: bonded abrasive wheels focusing mostly on conventional grinding operations.

- *Electrochemical and electro physical dressing*: electrical discharge dressing (EDD), electrolytic in-process dressing (ELID), electrochemical in-process control dressing (ECCD), electrochemical discharge dressing (ECDM), and electro contact discharge dressing (ECDD). Applications include: metal bonds grinding wheels (usually most difficult to accomplish through mechanical dressing).
- *Laser dressing methods*: tangential profiling, and radial sharpening. It is adopted along with bonded abrasive wheels, especially in cases where accuracy and precision along with a very high surface finish is required.
- *Combination dressing (hybrid technologies)*: ultrasonic-assisted conditioning, mechanical-laser combination dressing, mechanical-ELID dressing, and mechanical-EDD dressing. Are made to develop or adopt a process that gives the best result towards required wheel sharpness.

In the surface grinding process, mechanical dressing of bonded abrasive grinding wheels is the most common especially when it is performed with stationary dressing tools (i.e., single-point and multipoint), (WEGENER *et al.*, 2011). Examples of mechanical dressing are shown in Figure 8. According to Marinescu *et al.* (2016); Rowe (2014), the framework of mechanical dressing process includes: (i) truing to remove deviations from designated form; (ii) dressing to obtain a suitable sharpness and uniform cutting edges distribution; (iii) conditioning to remove bonds from around the abrasive grits (mostly used for superabrasive grinding wheels); and (iv) cleaning up to eliminate an abrasive layer that is usually loaded with workpiece surface material.

According to Malkin; Guo (2008), in mechanical dressing, grinding wheels are usually conditioned by feeding a dressing tool, in a crossfeed (traverse) velocity v_d, versus the rotating grinding wheel surface (Figure 9a). Subsequently, a layer of depth (a_d) is removed from the radius while creating a dressing lead s_d from the axial feed of the dressing tool per revolution of the grinding wheel (typical drag angle α_d lies between 10° and 15° in single-point dressing operation). Further, according to Wegener *et al.* (2011), the depth of the dressing a_d determines the active width of the dressing tool b_d with a diamond curvature radius r_d. A further influencing parameter is the overlap rate in dressing (U_d), which indicates the relationship of the b_d and the dressing lead s_d (Figure 9b). As the following example illustrates (Figure 9b), the U_d is directly connected with the sharpness that the dressing operation produces on the grinding wheel.

Figure 8- Mechanical dressing operation with stationary tools: (a) single-point; (b) multipoint

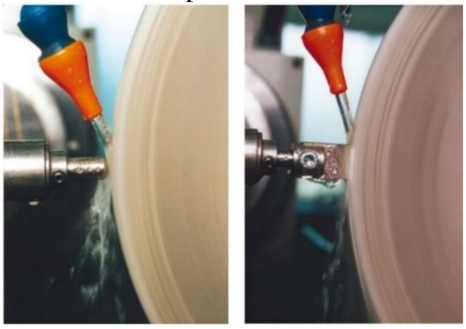

(a) **(b)**

Source: (LACH DIAMOND, 2019)

Figure 9 – Single-point dressing: (a) dressing of conventional wheels; (b) generation of wheel topography

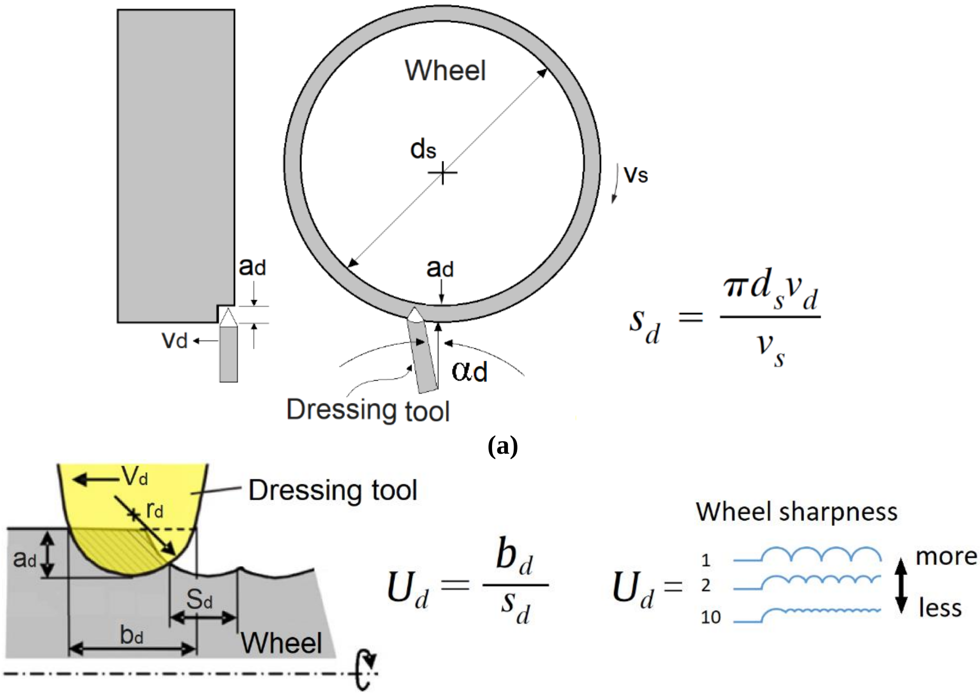

(b)

Source: Adapted from (MALKIN; GUO, 2008; WEGENER *et al.*, 2011)

In mechanical dressing of conventional grinding wheels, single-point or multi-point tools made of natural or synthetic diamonds are commonly applied. Since natural diamond is the hardest material with the highest thermal conductivity known in nature, diamond tools have many advantages as compared with common ceramic and SiC tools especially when performing the dressing operation. However, natural diamond dressers' lifetime can vary relatively greatly due to the fact that they are influenced by their crystallographic irregularities, shape differences, crystal purity, and sizes. On the other hand, the introduction of synthetic diamonds provides a solution for high-quality usage. The advantages of synthetic diamonds lie in their homogenous crystalline structure and constant wear resistance. The production of synthetic diamond is chategorized into: (i) monocrystalline diamond (MCD); and (ii) polycrystalline diamond (PCD), which can be made with or without binder phase. The PCB without binder phase is the most common process due to the fact that it uses a production method called chemical vapor deposition (CVD). In this case, the dressing tool are referred just as CVD diamond (JACKSON; DAVIM, 2011; MARINESCU *et al.*, 2016). The main characteristics of single-point and multi-point diamond dressing tools are summarized in the following subsections.

2.1.2 Single-point diamond dressing tools

Single-point diamond-dressing tools (Figure 10) are more often applied in the mechanical dressing of conventional abrasive wheels and can give excellent dressing achievement when adjusted correctly (ROWE, 2014).

Figure 10- Examples of single-point dressers: (a)typical designs; (b) CVD diamond; (c) natural diamond

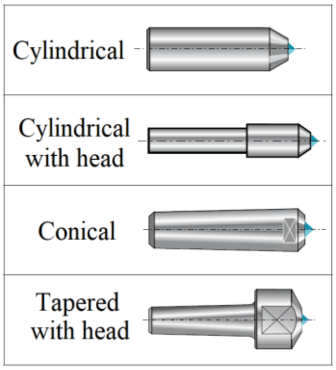

(a)

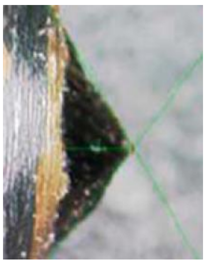

(b)

(c)

Source: adapted from (a, b): (WIRZ-DIAMANT, 2014)DENG; XU, 2019); author (c)

A single-point dresser, the simplest dressing tool, consists of a single diamond mounted in a metal binder, which is well-enough defined for replicable dress action and must to form a clean drag angle (see, for instance, Figure 9a) in relation to the grinding wheel surface. In general, typical designs of the single-point diamond dresser are categorized as shown in Figure 10a. Examples of single-point of natural diamond and CVD diamond are shown in Figure 10b and Figure 10c (MALKIN; GUO, 2008; MARINESCU *et al.*, 2016).

2.1.3 Multipoint diamond dressing tools

Multipoint diamond dressing tools are mostly used in the dressing of vitrified CBN grinding wheels. They also have many advantages as compared with single-point tools. For example: they are lower cost because smaller and less expensive diamonds are used; their lifetime tends to remain more consistent; and their wear volume lies at less than one percent of the volumetric wheel removal in dressing of resin-bonded CBN wheels (MALKIN; GUO, 2008; MARINESCU *et al.*, 2016; ROWE, 2014). In relation to the multipoint dressing parameters, the dressing lead s_d and dressing depth a_d have similar nuances as with the single-point dressing process (MALKIN; GUO, 2008). In general, as shown in Figure 12, multipoint dressers consists of multiple well-defined (surface plate) or random geometry (multiple grain dresser) diamonds mounted on metallic tool-holders (POMBO *et al.*, 2017; WEGENER *et al.*, 2011). Examples of multipoint dressers with CVD and natural diamond, respectively, are illustrated in Figure 12.

Figure 11 – Multipoint dressing tools

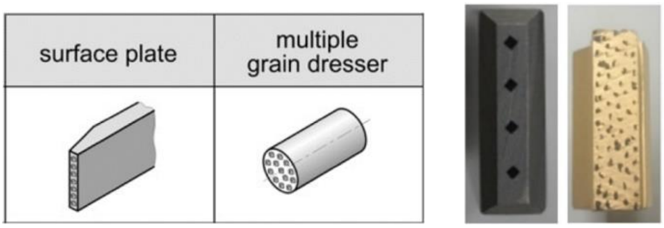

Source: Adapted from (MARINESCU *et al.*, 2016b; POMBO *et al.*, 2017)

2.1.4 Dressing tool wear and related problems

The dressing performance is critically dependent upon dressing tool conditions, i.e. wear and dressing temperatures can diversely affect the dressing tool shape, as reported by Pombo *et al.* (2017). A dressing tool is subject to wear flats at the tip as a result of tool modifications in the course of the dressing operation. Figure 12 confirms that the diamond wears progressively increasing along the dressing passes, as addressed by Martins *et al*. (2014). Worn dressing tools can affect the grinding performance in several ways (MARINESCU *et al.*, 2016; ROWE, 2014). For example, Pombo *et al*. (2017) pointed out that the increase of the dresser wear makes that the active width of dressing tool b_d also increases (Figure 13). In addition, according to Marinescu *et al.* (2016) and Rowe (2014), it leads to loss of grinding wheel sharpness and rapid reduction in grinding power due to grain fracture and abrasive dislodgement, which may entail increases of workpiece roughness and temperature.

Figure 12 – Diamond wear evolution as function of the number of dressing passes

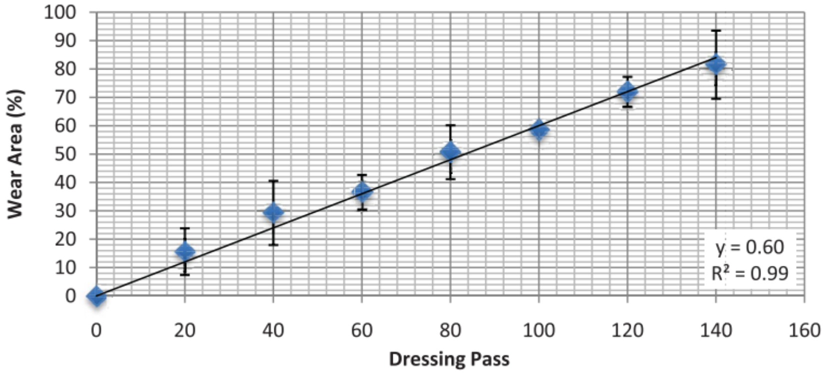

Source: (MARTINS, CESAR H. R. *et al.*, 2014)

Figure 13- Diamond wear analysis

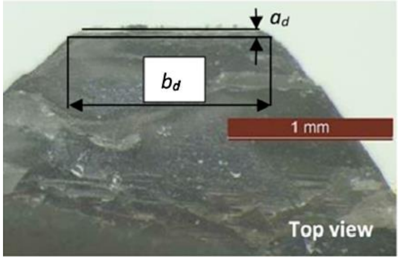

Source: (POMBO *et al.*, 2017)

The phenomena involved in dressing tool wear has been the key focus of literature in an attempt to achieve the most influential parameter for the process control. This way, much attention has been paid to: the dressing parameters, the consumed dressing power, the nature of the diamond and tool holder, and the temperature in the contact zone (COELHO; OLIVEIRA; CAMPOS, 2000; DENG; XU, 2019; INASAKI; OKAMURA, 1985; POMBO *et al.*, 2017; WEGENER *et al.*, 2011). The study conducted by Pombo *et al.* (2017) provided a more in-depth analysis of the relationship between dressing temperatures and dressing tool wear (Figure 14).

Figure 14- Wear level of diamonds using different materials in the tool holder

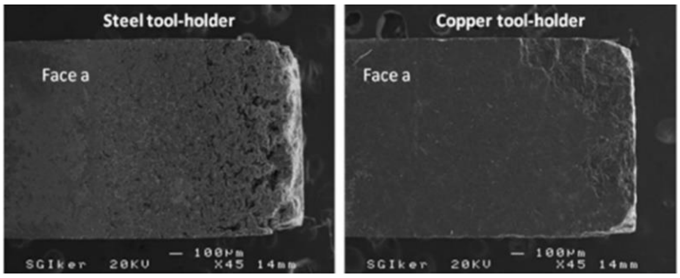

Source: (POMBO *et al.*, 2017)

They pointed out the following main conclusions: (i) a higher contact area, as defined on the basis of the dressing parameters, is related to higher temperatures on the diamond tip; (ii) a relationship can be drawn between contact area and dressing power consumption; (iii) as it can be seen in the scanning electron microscopy (SEM) picture (Figure 14), the wear that has suffered the diamond mounted on a copper tool-holder dresser was much lower than that mounted on a steel tool-holder dresser; and (iv) temperatures on the dressing tool surface can be reduced by as much as 35% when using a copper tool-holder.

2.2 Trends in tool condition monitoring

TCM is a kind of preventive and predictive maintenance in which the tool condition is diagnosed on the basis of process information sensing and analysis. According to Teti (2015), almost 50 % of monitoring applications have been, therefore, related to TCM (Figure15).

Figure 15- Machining process monitoring scopes

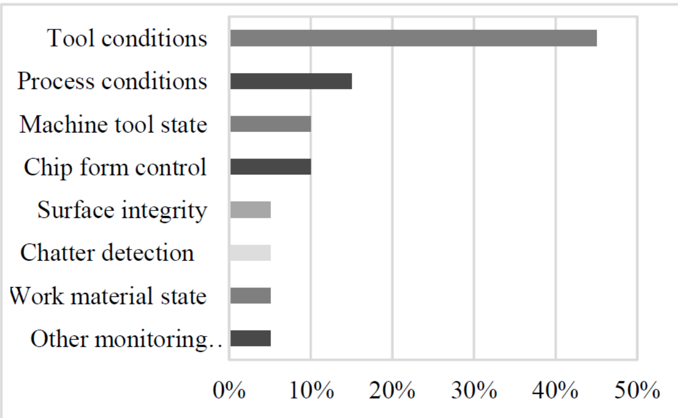

Source: (Teti, 2015)

For more than 30 years, a vast amount of work has been done in the field of TCM concerning tool wear, tool breakage, tool chipping, catastrophic tool failure (CTF), etc. Previous contributions were reported by Inasaki; Okamura (1985); Byrne et al. (1995); Teti (1995); Rehorn; Jiang; Orban (2005); Teti et al. (2010); Bhuiyan; Choudhury (2014); Swain et al. (2019); and Jemielniak, Krzysztof (2019).

Furthermore, following the definition given by Teti (2015), the sequence of activities in sensor-based TCM can be summarized as follows: the most relevant features related to the tool condition can be sequentially detected, processed and selected through a sensorial perception in cooperation with advanced signal processing and machine learning algorithms. A typical sensor-based TCM architecture, addressed by kothuru (2017), is shown in Figure 16. Table 1 summarizes the entire signal processing and machine learning roadmaps for TCM. Further light on this definition includes the following subsections.

Figure 16 – Architecture of a typical TCM system

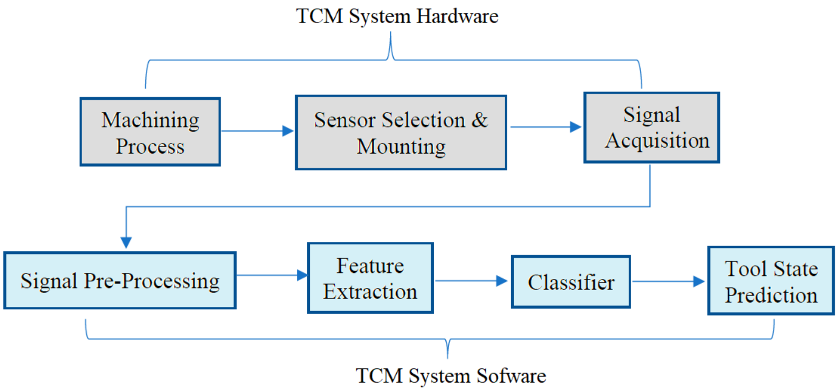

Source: (KOTHURU, 2017)

Table 1- Framework of signal processing and machine learning for TCM

Signal processing		**Machine learning**		**Tool state**
Signal pre-processing	**Feature extraction**	**Techniques**	**Features**	
Filtering; Amplification; Bias/offset suppression; A/D conversion; Segmentation.	*Time-domain*: average value, standard deviation, RMS, event counts, kurtosis, deviation of power (DPO), digital filter realization, etc. *Frequency-domain*: fast Fourier transform (FFT), power spectral density (PSD), and ratio of power (ROP); *Time-frequency domain*: STFT, and WT (spectrograms, level decompositions, etc.);	ANN (*feedforward backpropagation (BP), self-organizing maps (SOM)*,); Fuzzy logic and fuzzy systems; *k*-nearest neighbor; *k*-means; Support vector machine; Principal component analysis.	Classification; Prediction; Estimation; Regression; Clustering; Pattern recognition; Etc.	Wear; Breakage; Fracture; Chipping; CTF; Etc.

2.2.1 Sensor technology

Sensors and sensor systems are the basis for indirect and automated TCM. They are devices that sequentially detect physical stimulus changes and turn them into signals (usually electrical). The most common sensors utilized for TCM are categorized as: (i) feed and spindle quantities (current, power, speed, and position); and (ii) close to process (acoustic emission (AE), vibration, force, torque, strain, and temperature). Sensor-based TCM is accomplished through measurements of appropriate auxiliary quantities (cutting force, vibrations, power, temperature, AE on the contact zone, etc.) where the actual tool condition is deduced via correlations through signal processing and machine learning (TETI *et al*., 2010; TETI 2015). Besides choosing the most appropriate types of sensors and their best appropriate location, the use of multiple sensors at a time (usually termed as sensor fusion) is also considered to investigate the entire events in which the single sensor application is marginal or incapable of providing a reliable and unambiguous TCM (BHUIYAN; CHOUDHURY, 2014; ZHOU, YUQING; XUE, 2018).

Piezoelectric sensing materials have been the subject of sensor technology including thin membrane, seismic mass, and quartz (most commonly applied in dynamometers, accelerometers and AE sensors). Also, the ongoing development of alternative crystal materials has facilitated the realization of piezoceramic sensor technology such as PZT transducers (see Chapter 3). More recently, new classes of sensors and sensor systems have nevertheless emerged in the field of machining monitoring focusing mostly on smart and wireless devices, and cyber-physical systems (LUO; CHONG; LIU, 2018; LINS; CORAZZIM, 2020; LUO *et al.*, 2018; ZHONG *et al.*, 2017).

2.2.2 Signal processing for feature extraction

The analog sensor signals are first pre-processed (Table 1) through amplification, filtering, bias/offset suppression, analog to digital (A/D) conversion, etc., so that digital time-domain signals are obtained. Subsequently, the useful information related to the tool condition is extracted and selected through popular signal processing techniques. There are several techniques and methods of signal processing for feature extraction and selection. A more comprehensive review of the whole subject is given by Lauro *et al.* (2014); Lee; Mendis; Sutherland (2019); and Teti *et al.* (2010). To summarize (see Table 1), the most common are: (i) extraction of signal features in the time domain (e.g.: standard deviation, effective value (root mean square - RMS), deviation of power - DPO, digital filter realization, kurtosis, etc.); (ii) frequency domain signal representations (e.g.: fast Fourier transform - FFT, power spectral density - PSD, and ratio of power - ROP); and (iii) time-frequency domain signal representations (e.g.: short-time Fourier transform - STFT, wavelet transform - WT).

2.2.3 Machine learning for decision making

The features selected and extracted from sensor signals can feed feature vectors representative for the decision-making implementation through knowledge-based machine learning algorithms. They are based on the estimation of parameters in order to perform an intelligent and automated TCM. The machine learning techniques most employed for the purpose of TCM were briefly summarized in Table 1. Concerning the supervised and unsupervised learning paradigms, artificial neural networks (ANNs) are most frequently used. A typical neural network (NN) has a single layer of input neurons connected to at least one layer of hidden neurons, and then to a layer of output neurons. In supervised learning, the backpropagation (BP) with Levenberg–Marquardt (LM) optimization, which implements multi-layer (ML) feedforward NN, is the most common algorithm (Figure 17). From this, the training process is performed by changing connection weights from the initial weight values. At the end, the output error is therefore compared to the expected result (typical tasks are: classification, estimation, regression, prediction, and pattern recognition). Further examples of supervised NN are: probabilistic NN (PNN); recurrent NN (RNN); neuro-fuzzy systems (NFS); and, more recently, deep NN (DNN). Some examples of publications on the subject of TCM are: Azmi (2015); Caggiano *et al.* (2018); Cheng *et al.* (2019); and Lopes Silva; Hassui (2016).

On the other hand, in unsupervised learning, only input stimuli are given to the NN, which organizes itself during the training process. For example, the self-organizing maps (SOM) is a kind of unsupervised NN whose learning rules are based on a competitive approach. This means that the neurons compete for the privilege to remain active, in such a way that the neuron with greater activity, i.e. the winning neuron or the best-matching unit (BMU), is the main participant in the learning stage (winner-takes-all) (HAYKIN, 2008; KATUNIN; AMAROWICZ; CHRZANOWSKI, 2015). Other examples of supervised and unsupervised learning paradigms are: (i) k-nearest neighbor (k-NN) classifier, which is based on the allocation of new unclassified examples to the class to which the majority of its k-nearest neighbors belongs (supervised learning); (ii) k-means, which identifies *k* number of centroids and then allocates every data point to the nearest cluster (unsupervised learning); (iii) support vector machine (LVM), which is a non-probabilistic binary linear classifier that outputs a model that categorizes new examples from a given labeled training dataset (supervised learning); and (iv) principal component analysis (PCA), which is an unsupervised linear projection that converts a set of (possibly) correlated variables into a (smaller) set of uncorrelated variables denominated principal components. These promising techniques have been the subject of research in TCM as addressed by Caggiano *et al.* (2018); Kong *et al.* (2019); Martins *et al.* (2014); Shi *et al.* (2016); and Rui Silva (2010).

Figure 17- Training process using the BP algorithm

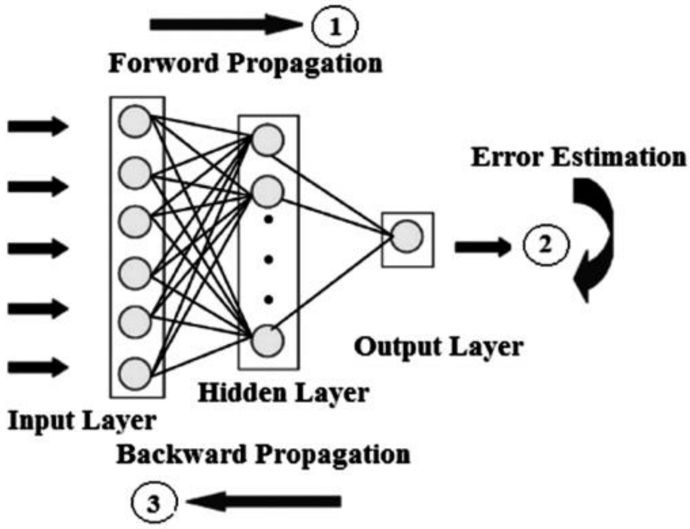

Source: (ABEDINI *et al.*, 2012)

Another promising machine learning technique is nevertheless Fuzzy logic (FL), which accommodates the uncertainty of the real world and model actions from specialist knowledge. Thus, in a fuzzy inference system, the input variables are taken through a mechanism that is composed of parallel “If-Then” rules as well as fuzzy logic operations in order to reach the output space. Moreover, it can contain elements with a membership degree between completely belonging to the set and completely not belonging to the set. In this context, a membership function (MF) is a curve that defines the character of the fuzzy set by assigning to each element the corresponding degree value, usually in a closed unit interval [0, 1]. As it is well-known, there are five common forms of membership function, such as triangle, trapezoidal, Gaussian, generalized bell, and sigmoidal. In addition, the three-level fuzzy system with fuzzy sets "Low", "Medium" and "High" is often applied to represent a practical situation. In this case, the most fundamental logical operations are AND, OR and NOT. In contrast with the standard logical operation, operands A and B are association values within the range [0, 1]. In the fuzzy inference process, the parallel “If-Then” rules form the inferencing mechanism that indicates how to design input variables onto output space (WANG, 2015).

Overall, three types of fuzzy inference methods are covered in the literature, such as Mamdani, Sugeno, and Tsukamoto. The fuzzy inference of Mamdani is one of the most common fuzzy-based approaches applied for scientific problems and it was one of the first proposed control systems by means of fuzzy set theory. It was proposed in 1975 by Ebrahim Mamdani (Mamdani; Assilian (1975)) as an attempt to synthesis a controller for a model industrial plant. In the Mamdani system, the consequent of the "If-Then" rule is defined by the fuzzy set. The fuzzy output set of each rule will be reshaped by a corresponding number and the defuzzification is required after the aggregation of all these reconfigured fuzzy sets. Therefore, the Mamdani type fuzzy inference process consists of five steps: fuzzification of input variables, fuzzy apply operator, apply the implication method, apply the aggregation method, and defuzzification. The following publications are some examples of fuzzy-based TCM: Bobyr; Yakushev; Dorodnykh (2020); Cuka; Kim (2017); and Ren *et al.* (2014).

2.2.4 Outlook on current trends

Nowadays, new guiding principles to enhance the industrial capability of machining operations are emerging. An example is illustrated in Figure 18.

Figure 18 - Cloud manufacturing framework for smart TCM

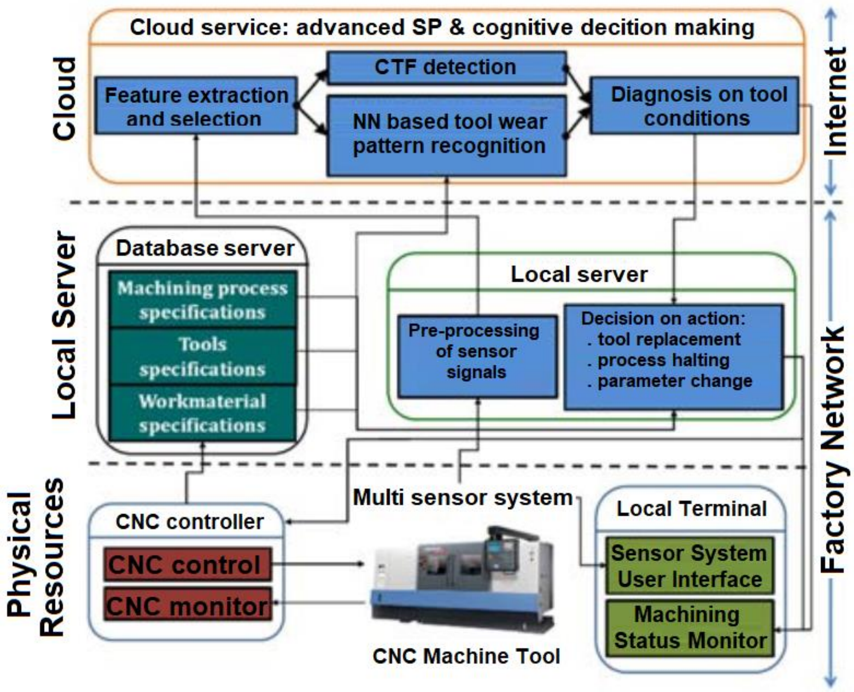

Source: Adapted from (CAGGIANO, 2018)

Driven by the Industry 4.0 framework, the scope is to enable the industrial information integration and manufacturing digitization. This way, some aspects of monitoring of machining in the context of Industry 4.0 were analyzed by Zębala; Struzikiewicz (2020). Unsurprisingly, innovative and reconfigurable sensor systems, signal processing approaches, and machine learning algorithms took place. They are also supplemented or expanded by the following industry 4.0 key enabling technologies: (i) industrial internet of things (IIoT); (ii) cloud computing; (iii) cyber-physical systems (CPS). A cloud manufacturing framework was conceived by Caggiano (2018) with the aim of performing a smart TCM in manufacturing operations (Figure 18). The authors drew on future developments of monitoring systems where manufacturing services are extended to several machines and machining processes, allowing to communicate and cooperate with each other. Some other recent developments on this subject were carried out by Lee; Mendis; Sutherland (2019); Li; Liu; Wu, (2019); Lins; Araujo; Corazzim (2020); Liu *et al.* (2020); and Luo *et al.* (2018).

2.2.5 TCM developments in the grinding process

The enhancement of monitoring technologies is essential to make the grinding process more reliable and economical. Tönshoff; Friemuth; Becker (2002) summarized the various elements and approaches of a monitoring system during grinding. The general need is expressed in Figure 19. This way, there are a great number of input variables and the mechanisms of grinding process change with time: the main aspects were reported in Section 2.1.

Figure 19- Grinding process monitoring framework

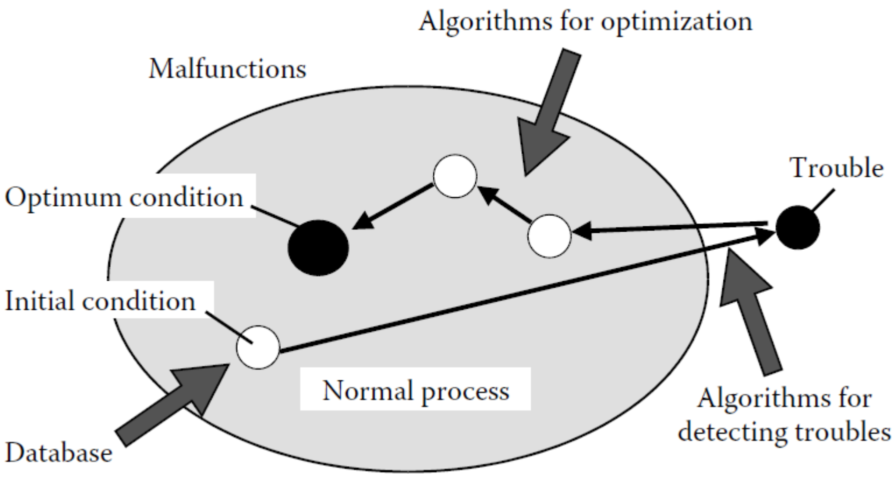

Source: (TÖNSHOFF; FRIEMUTH; BECKER, 2002)

TCM is a key factor to improve the grinding process because it supports the tool wear diagnosis, tool breakage, grinding machine tool state, temperature effects, and among other faults that occur during the material removal stage (JEMIELNIAK, KRZYSZTOF, 2019; LAURO *et al*., 2014; ZHANG, CUNJI et al., 2016). TCM in dressing operations conducted so far follows the same frameworks reported in the previous subsections. These methods are typically based on sensor signal detection and processing (AE, vibration, force, power) for the monitoring of dressing tool wear and related damages (e.g.: dressing tool lifespan, ideal point to replace it, thermal damages, and CTF), as well as the optimal dressing moment through grinding wheel wear and sharpness (AGUIAR *et al*., 2009; MARTINS *et al*., 2014; MIRANDA *et al*., 2015; MOIA *et al*., 2015; LOPES *et al.*, 2017; ALEXANDRE *et al*., 2018; OLIVEIRA JUNIOR *et al*., 2019).

A trend toward automated dressing is available in publications by Oliveira, Dornfeld, Winter (1994); Oliveira, Dornfeld (2001); and Oliveira, Bottene, França (2010). These papers focused on the use of the AE mapping technique through an image construction procedure for fast RMS analysis (Figure 20) and the inscription of pre-configurable patterns (textures) on the grinding wheel (Figure 21). The latter is transferred to the workpiece surface during the grinding operations. In summary, the method provides information about the grinding wheel topography, the dressing performance and the interaction between the grinding wheel and workpiece.

Figure 20- AE mapping technique based on image construction procedure for fast RMS analysis

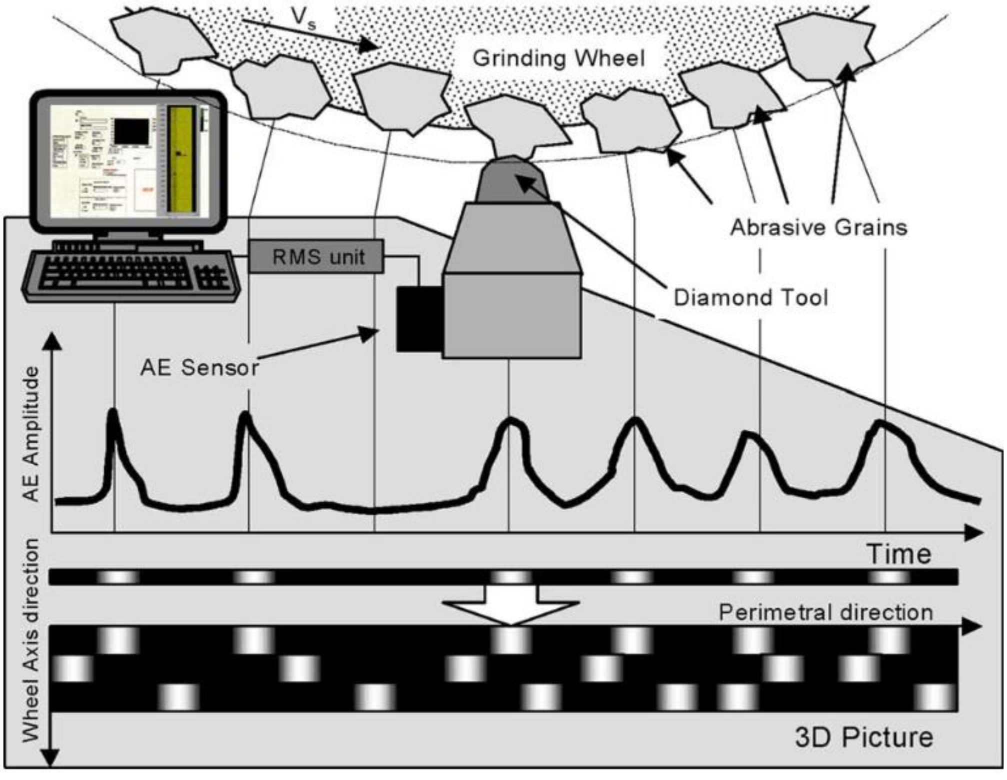

Source: (LEE, D E *et al.*, 2006)

Figure 21 - A novel dressing technique for texturing of ground surfaces

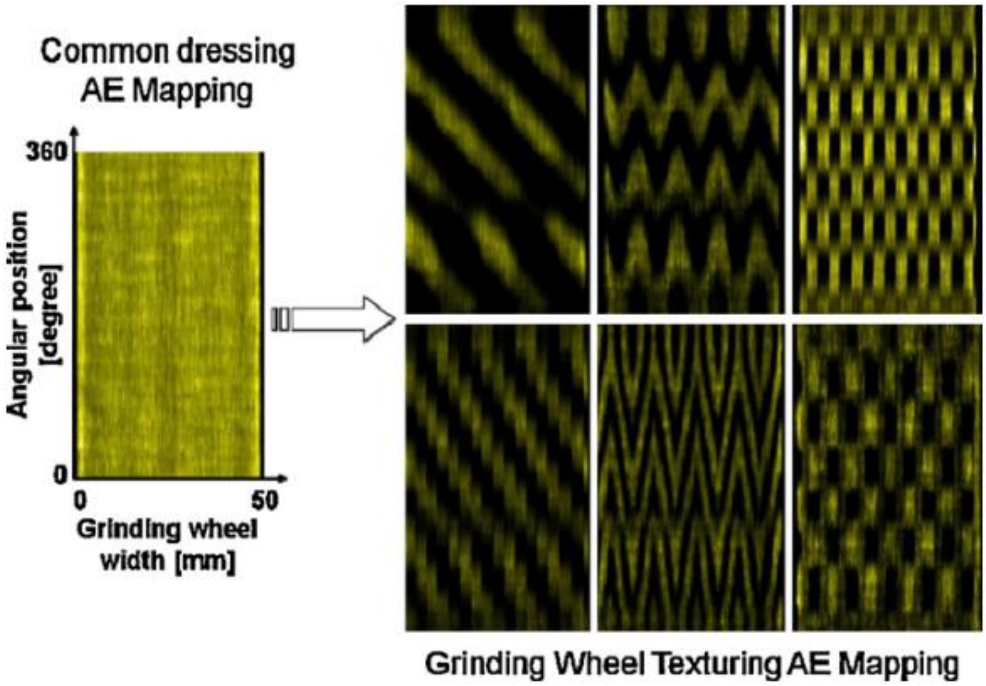

Source: (OLIVEIRA, J F G; BOTTENE; FRANÇA, 2010)

More recently, a novel sensor monitoring technique was developed in the research activities published by Dotto *et al.* (2019) dealing with AE mapping. These authors focused mostly on the application of low-cost piezoelectric transducers as a substitute for conventional and consolidated AE sensors as well as the selection of the optimal frequency bands from the sensor signals. The maps obtained by means of the piezoelectric diaphragm, which represents the wheel topography with two simulated faults (plus (+) and tee (T) symbols deliberately machined on the grinding wheel surface), are shown in Figure 22.

Figure 22 – In dressing acoustic map by low-cost piezoelectric transducer

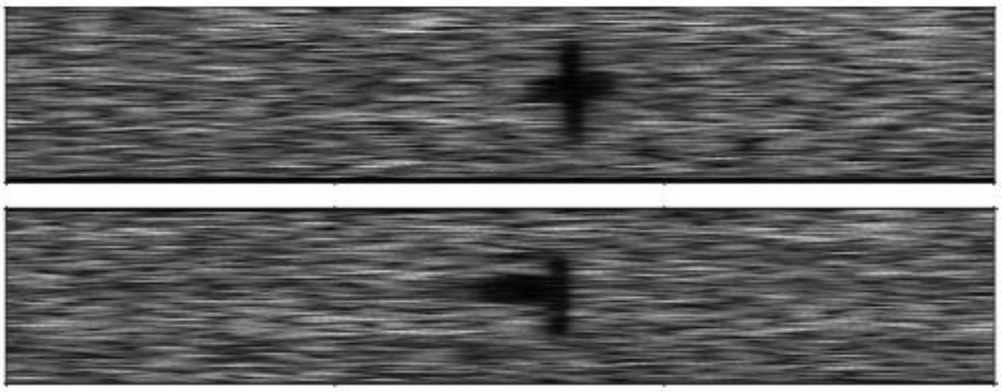

Source: (DOTTO *et al.*, 2019)

2.2.6 TCM for dressing tool wear and related problems

Many approaches have been proposed to accomplish sensor-based TCM for dressing tool wear and related problems and a number of these were employed in stationary dressing operation. A comprehensive study conducted by Martins *et al.*, (2014) described a method to characterize the wear condition of stationary single-point dressers from AE signal and ANN-based machine learning (Figure 23). From this, the features of the AE signal were obtained from the RMS and ROP metrics at nine representative frequency bands selected from AE spectra. Combinations of two frequency bands were evaluated as inputs to several NN models, which have been compared with their tool wear classification ability.

Figure 23 – Dressing tool wear monitoring using: (a) AE RMS; and (b) machine learning based on k-NN algorithm

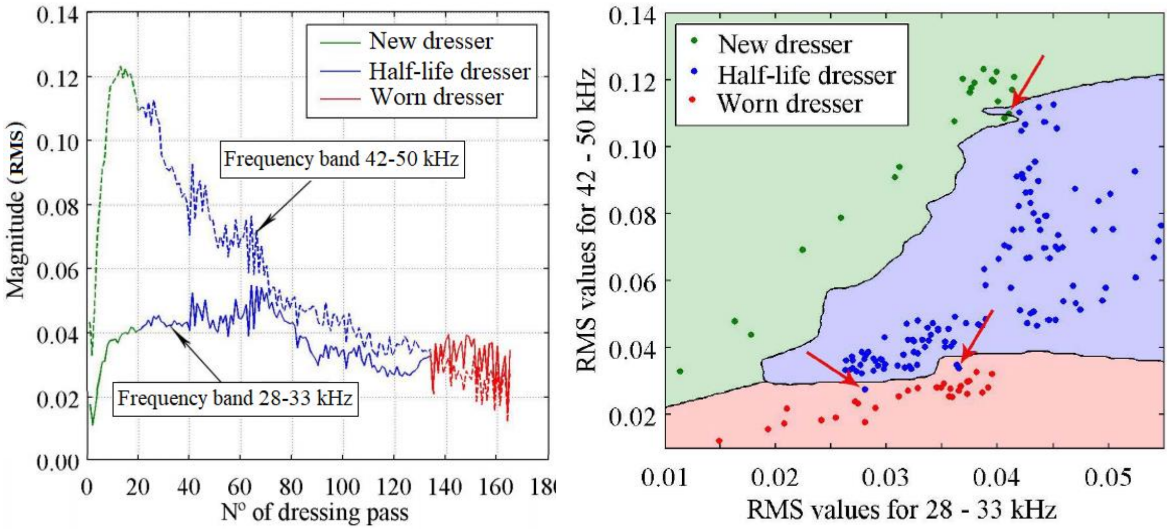

Source: (MARTINS *et al.*, 2014)

In particular, those authors found that the combination of the frequency bands of 28–33 and 42–50 kHz best characterized the dresser wear condition. The RMS for the best frequency bands is shown in Figure 23a. Also, Figure 23b shows the boundary regions, obtained through the application of the *k*-NN algorithm in which the data of each level of tool wear are located.

Further works related to stationary dressing operation are summarized next. For example: D'addona *et al.* (2017, 2018), Denkena; Jacobsen; Kramer (2005), Kwak; Ha (2004), and Lopes *et al.* (2017) focusing on optimal dressing moment detection; Inasaki; Okamura (1985), Oliveira; Dornfeld (2001), Wehmeier; Inasaki (2002), Naghdy; Cook; Engineering (2002), Mochida *et al.* (2009), Oliveira; Bottene; França (2010), and Ferreira *et al.* (2019) focusing on dressing performance; and Egana *et al.* (2006), Martins *et al.* (2013, 2014), Miranda *et al.* (2015), D'addona *et al.* (2016), and Oliveira Junior *et al.* (2016, 2017) covering dressing tool wear control/estimation. Of these, AE detection (Inasaki; Okamura (1985), Oliveira; Dornfeld (2001), Denkena; Jacobsen; Kramer (2005), D'addona *et al.* (2016, 2017), Lopes *et al.*(2017); Ferreira *et al.* (2019)), force and power (Inasaki; Okamura (1985), Kubo; Tamaki (2010), Kwak; Ha (2004)) and vibration (D'addona *et al.* (2016), Junior *et al.* (2017), Kubo; Tamaki (2010), Miranda *et al.* (2015)) have been employed. Moreover, sensor signal processing for feature extraction and selection were applied focusing mostly on: (i) time-domain analysis (i.e.: RMS (Oliveira; Dornfeld (2001), Martins *et al*. (2014); Wehmeier; Inasaki (2002), D'addona *et al.* (2017)), ROP (D'addona *et al.* (2016, 2018); Lopes *et al.* (2017)), and event counts (D'addona *et al.* (2018), Lopes *et al.* (2017))); (ii) frequency domain analysis (including FFT (Inasaki; Okamura (1985); Wehmeier; Inasaki (2002), Kubo; Denkena; Jacobsen; Kramer (2005), Tamaki (2010); Martins *et al*. (2014)) and PSD (Oliveira Junior *et al*. (2016); Lopes *et al*., (2017))); and (ii) time-frequency domain analysis (e.g.: STFT (Oliveira Junior *et al*. (2016, 2017)) and WT (Egana *et al.* (2006), Kwak; Ha (2004))). In addition, reliable machine learning paradigms, which take into account ANN (D'addona *et al*. (2017), Oliveira Junior *et al*. (2017); Martins *et al*. (2013, 2014), Ferreira *et al*. (2019)) and fuzzy inference systems (Miranda *et al*. (2015)), have been applied as well. A brief summary of these viable solutions as a function of the monitoring scopes is reported in Table 2.

In conclusion, while numerous sensor-based TCM techniques discussed above have been effective and viable solutions, the dressing tool wear and related problems remain a challenge up to now. The main reason seems to be that it has been conducted mainly under theoretical conditions and few of these achievements are found on the factory floor because it is not realistic to implement some of the important sensor monitoring procedures such as complex signal processing and decision making roadmaps. Accordingly, the cost reduction is still a challenge for these monitoring systems, i.e., conventional techniques present high computational cost because of the several phases of data processing and the systems require expensive instrumentation and devices. On the other hand, there is an increasing trend toward Industry 4.0 concepts focusing mostly on innovative, inexpensive, more autonomous, and simpler sensor monitoring techniques (the main achievements were reported in subsection 2.2.4) which have attracted researchers in TCM areas (see, for instance, Lins et al. (2019) and Li, Liu, Wu (2019)). Alternatively, the electromechanical impedance (EMI) method, which has emerged as a promising and cost-effective solution for real-time damage diagnosis, can provide an actual breakthrough in the research on sensor-based grinding process monitoring. Thereby, a background related to the EMI is reported in the next Chapter.

Table 2 – Summary of related works

Sensor system	**Feature extraction**	**Decision-making paradigm**	**Monitoring scope**	**Published by**
AE and power	FFT		Detection of the optimal dressing time	INASAKI; OKAMURA, 1985
AE	RMS		Detection of the optimal dressing time/dressing performance	OLIVEIRA; DORNFELD, 2001
AE	RMS and FFT		Dressing performance	WEHMEIER; INASAKI, 2002
Force	FFT and WT		Detection of the optimal dressing time	KWAK; HA, 2004
AE and power	DPO, DPKS		Detection of the optimal dressing time	AGUIAR *et al.*, 2009
AE	RSM, ROP, and FFT	MLP NN	Dressing tool wear	MARTINS *et al.*, 2014
AE and vibration	RMS and ROP	Fuzzy logic	Dressing tool wear	MIRANDA *et al.*, 2015
AE	RMS and FFT	MLP NN	Detection of the optimal dressing time	MOIA *et al.*, 2015
Vibration	RMS and FFT	MLP NN	Dressing tool wear/tool failure and breakage	D'ADDONA *et al.*, 2016
AE	Event counts, ROP and PSD		Detection of the optimal dressing time	NASCIMENTO LOPES *et al.*, 2017
Vibration	RMS, ROP, and STFT	MLP NN	Dressing tool wear/tool failure and breakage	JUNIOR *et al.*, 2017
AE	RSM, FFT, and CFAR	TDNN	Dressing performance	FERREIRA *et al.*, 2019

Chapter 3

THE ELECTROMECHANICAL IMPEDANCE METHOD

In this chapter, a background related to the EMI method from an SHM perspective, including theoretical aspects, methods for transducer characterization, and procedures for damage evaluation, is presented.

3.1 SHM technology

Structural health monitoring (SHM) systems often find varied applications in civil, mechanical, and aerospace engineering projects (Figure 24) because these systems can promote human safety and reduce the economic impacts of unforeseen failures. To ensure reliability and safety, an SHM system provides important information on the structural condition in terms of damage occurrence (FARRAR, 2013; CASTRO; BAPTISTA; CIAMPA, 2019). A typical SHM framework consists of detecting incipient damages and can be decomposed through the integration of four-steps following a general statistical pattern recognition paradigm defined by Farrar (2013): (i) operation evaluation; (ii) data acquisition and normalization; (iii) feature selection and information condensation; and (iv) statistical modeling for feature discrimination.

Numerous approaches and strategies exist to achieve the SHM purpose. Among them, non-destructive evaluation (NDE) methods, focusing mostly on vibration analysis and wave propagation (e.g.: AE detection, lamb waves, ultrasonic guided waves, optical-based methods, etc.), are emphasized because they are flexible in the application of various types of structures and minimally invasive to the component under study (BUDOYA; BAPTISTA, 2018; FARRAR, 2013; CASTRO; BAPTISTA; CIAMPA, 2019a; KIM; WANG, 2014b; SELVA *et al.*, 2013). Recently, the electromechanical impedance (EMI) has become a promising tool within NDE methods due to the fact that it uses smart piezoelectric devices and a low-cost methodology capable of identifying small-sized damages (KIM; WANG, 2014; NA; BAEK, 2018). In summary, the EMI-based damage identification activities include: (i) the excitation of the transducer in a suitable frequency range; (ii) the electrical impedance measurements of the transducer (response); (iii) the establishment of a relationship between the mechanical impedance of the structure and the electrical impedance of the transducer; (iv) the detection of possible damages through representative damage features; and (v) the diagnosis of the structure condition and its remaining useful life (cognitive systems can be used with this aim). The EMI method is discussed in more detail in Section 3.2.

Figure 24 – Typical examples of SHM applications

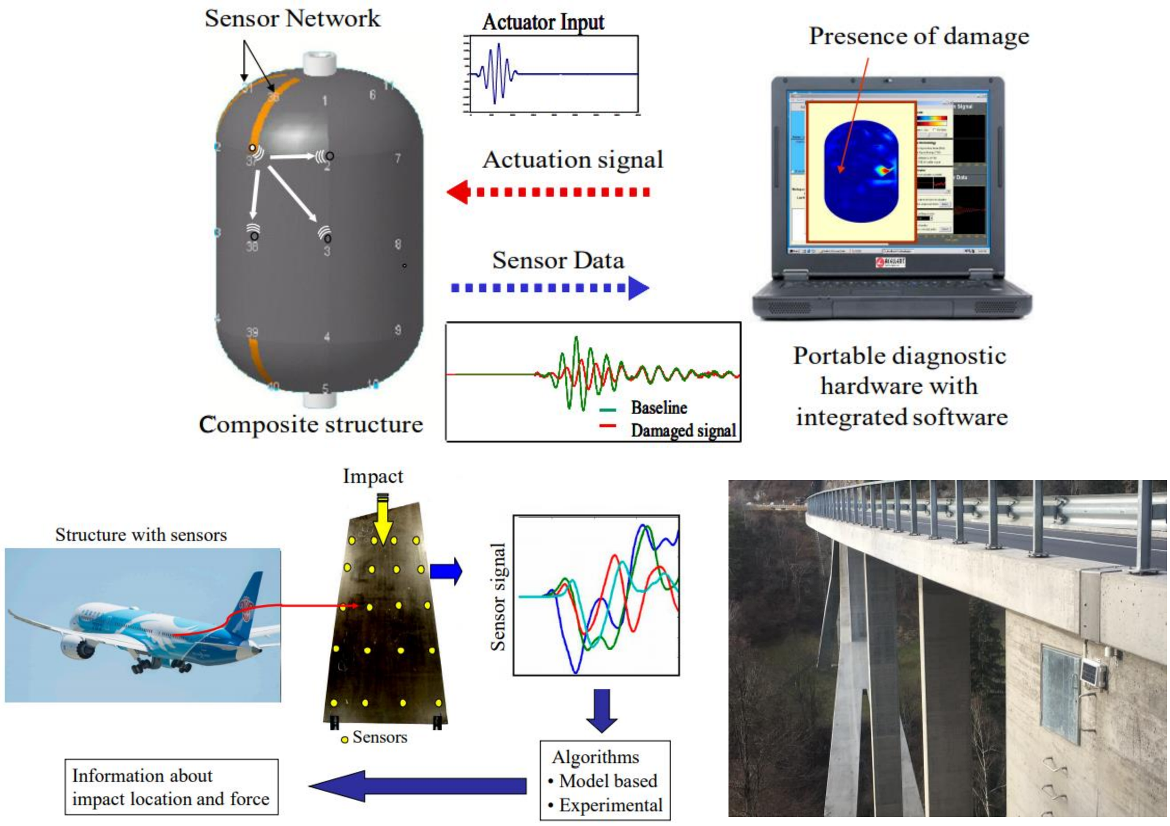

Source: (QING *et al.*, 2019; STRUCTURAE, 2017)

3.2 Electromechanical impedance method

In this section, the basic concepts of the electromechanical impedance are elaborated. The PZT transducers and the EMI principle will be introduced as well as the transducer sensitivity assessment and damage indices used in SHM will be described.

3.2.1 Piezoelectric effects

According to IEEE-ANSI (1987), the piezoelectric effect occurs in a material which, when subjected to stress, produces a voltage output through the formation of an electric dipole in the material itself. The reverse effect also occurs, i.e. by applying an electric voltage to the opposite surfaces of the piezoelectric material, a mechanical deformation is obtained. Thus, there is an interaction between the electrical and mechanical characteristics of the piezoelectric material. Based on these considerations, the direct piezoelectric effect (sensor) and reverse piezoelectric effect (actuator) in the transducer are given by Equations (1) and (2), respectively

$$D_i = d_{ikl}T_{kl} + \varepsilon_{ik}^T E_k \tag{1}$$

$$S_{ij} = s_{ijkl}^E T_{kl} + d_{kij}E_k \tag{2}$$

where, d_{ikl} and d_{kij} are the piezoelectric constants, respectively; E_k is the electric field, D_i is the electrical displacement, S_{ij} is the strain component, ε_{ik}^T is the permittivity component at constant stress, s_{ijkl}^E is the elastic compliance at a constant electric field; T_{kl} is the traction vector component, and the subscripts i, j, k, and l indicate the natural coordinate system of the piezoelectric crystal (values of 1, 2, 3) (FREITAS *et al.*, 2017).

3.2.2 PZT diaphragm transducers

Typically, the piezoelectric transducers used in SHM applications have been PZT ceramics or, in many cases, microfiber composite (MFC) patches. However, in the past few years, the use of low-cost thin-disk piezoelectric diaphragms (PZT diaphragms) has attracted researchers in SHM areas, especially when performing with EMI method. According to Freitas; Baptista (2016), PZT diaphragms are characterized by simple construction (Figure 25), consisting of a circular piezoelectric ceramic layer (active element) mounted on a circular metal plate (diaphragm). The ceramic layer is coated with a thin and a metallic film operating as an electrode. Typically, the piezoelectric material is barium titanate or PZT (not pure but doped), and the metal diaphragm can be brass, nickel alloy or stainless steel.

Freitas; Baptista (2016) presented an experimental study of the feasibility of PZT diaphragms for detecting structural damages based on the EMI method. PZT diaphragms of different sizes were compared with a conventional PZT ceramic (Figure 26a). The results indicate that a diaphragm of similar size (7BB-20-6) have reproducibilities and sensitivities to damage detection similar to a conventional PZT ceramic. As confirmed in Figure 26b, the PSDs obtained from the conventional ceramic and the PZT diaphragm exhibited similar trends.

Figure 25- PZT diaphragm

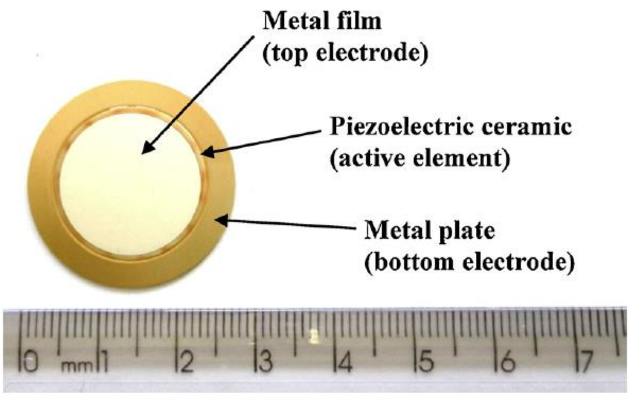

Source: (FREITAS; BAPTISTA, 2016)

Figure 26- Comparision between PZT diaphragms and conventional ceramic: (a) different sizes evaluated; (b) frequency response

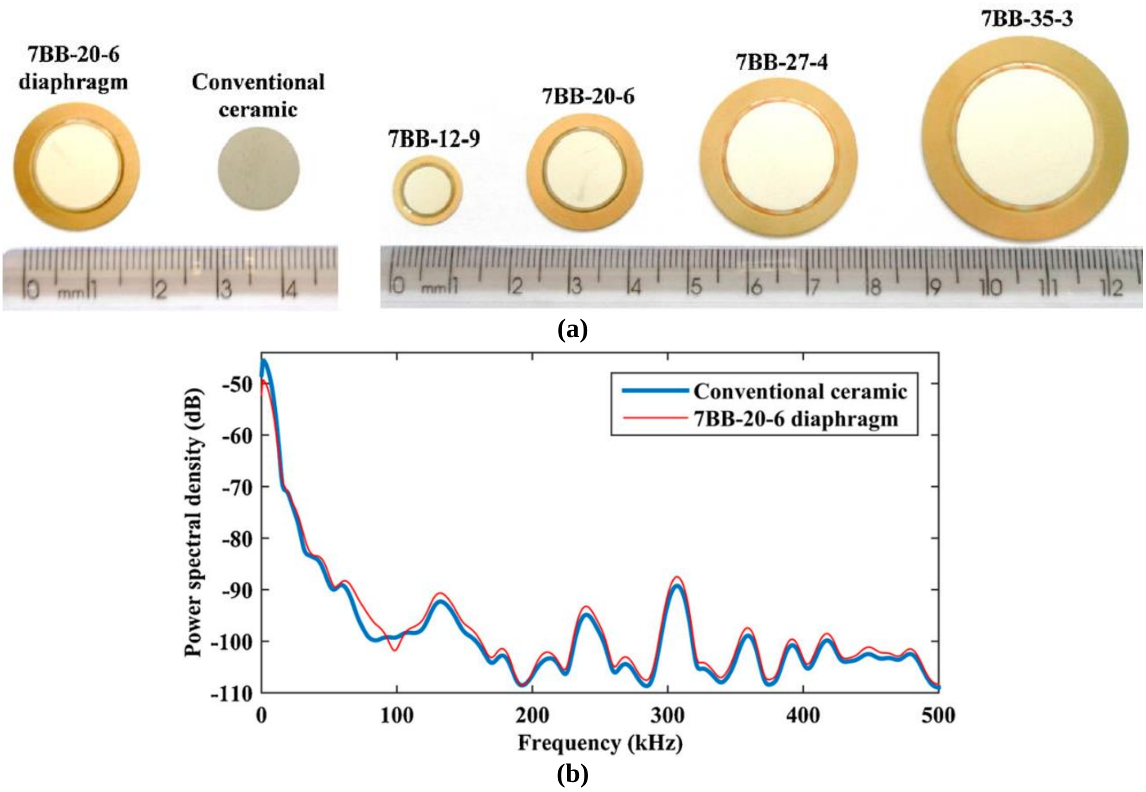

Source: (FREITAS; BAPTISTA, 2016)

3.2.3 EMI principle

The EMI method is based on the frequency response function (FRF) and uses the piezoelectric properties of PZT devices (BAPTISTA; VIEIRA FILHO, 2009; RABELO *et al.*, 2017). The transducer is usually bonded or embedded to the host component, and the EMI method employs both direct and reverses piezoelectric effects of the transducer. In this context, the self-sensing of piezoelectric material allows the transducer to obtain FRFs between input and output of the measurement system (FAN *et al.*, 2018). Consequently, the mechanical vibration response is transmitted to the PZT in the form of electrical response, i.e. when a structural modification (such as damage) occurs, this is observed in the electrical response of the transducer (RABELO *et al.*, 2017).

As shown in Figure 27, the deformation of the piezoelectric material occurs in all directions. In this context, three-dimensional (3-D) electromechanical models have been derived to relate the electrical properties of the transducer with the mechanical properties of the structure (ALMEIDA; BAPTISTA; AGUIAR, 2015; GOPAL; ANNAMDAS; SOH, 2007). However, since PZT devices are sufficiently thin and the propagation medium has a low damping coefficient, only one deformation in the longitudinal direction (axis x_1 in Figure 27) can be considered (ALMEIDA; BAPTISTA; AGUIAR, 2015; BAPTISTA; VIEIRA FILHO, 2010).

Figure 27- Directions of piezoelectric deformation

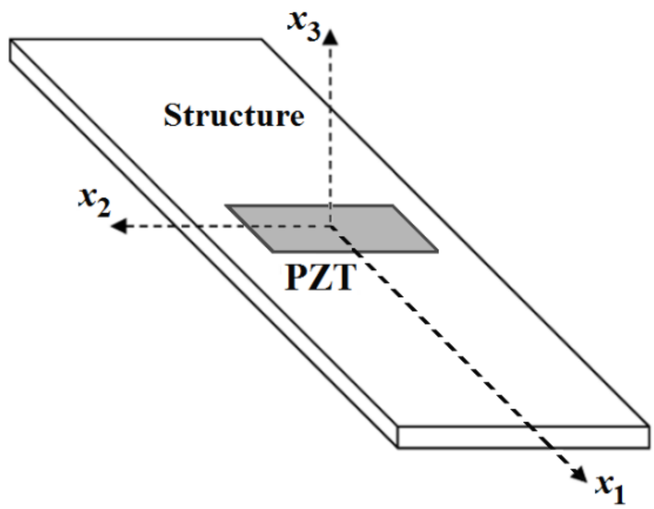

Source: Adapted from (SILVEIRA; CAMPEIRO; BAPTISTA, 2017)

Based on a one-dimensional (1-D) assumption, the piezoelectric constitutive Equations (1) and (2) can be simplified as follows (FREITAS *et al*., 2017):

$$D_3 = d_{31}T_1 + \varepsilon_{33}^{T}E_3 \tag{3}$$

$$S_1 = s_{11}^{E}T_1 + d_{31}E_3 \tag{4}$$

From Equations (3) and (4), the electrical impedance of a generic piezoelectric transducer can be calculated using a simplified theoretical model proposed by Liang et al. (LIANG, C.; SUN; ROGERS, 1994), given as follows

$$Z_E(\omega) = \frac{1}{j\omega C}\left(1 - \frac{d_{31}^2}{s_{11}^E \varepsilon_{33}^T} \frac{Z_s(\omega)}{Z_s(\omega) + Z_p(\omega)}\right)^{-1} \tag{5}$$

where $Z_E(\omega)$ is the electrical impedance of the transducer at an angular frequency ω; $Z_p(\omega$ is the mechanical impedance of the transducer; $Z_s(\omega)$ is the mechanical impedance of the monitored structure; $d_{31}, \varepsilon_{33}^T$, and s_{11}^E are the piezoelectric, dielectric, and elastic compliance constants of the piezoelectric materials; C is the static capacitance of the transducer, and j is the unit imaginary number.

Alternatively, in a recent study by Freitas *et al*. (2017), a 1-D theoretical electromechanical model specific to PZT diaphragms was proposed. In particular, the proposed model relates to the electrical impedance of the PZT diaphragms considering the additional effects of their brass plate. Thus, these authors obtained:

$$Z_D = \frac{1}{j\omega C_0} \Big\| \left\{ \left(\frac{2s_{11}^E}{\pi \emptyset_p d_{31}}\right)^2 \left[Z_{P1} + Z_{B1} + \frac{Z_{B2}(Z_{B1} + Z_S)}{Z_{B1} + Z_{B2} + Z_s}\right]\right\} \tag{6}$$

where $Z_D(\omega)$ is the electrical impedance of the PZT diaphragm at an angular frequency ω; Z_s is the mechanical impedance of the structure under inspection; Z_{P1} and Z_{P2} are the electromechanical impedance of the active element; Z_{B1} and Z_{B2} are the electromechanical impedance of the brass plate; $\emptyset_p$ is the active element diameter (see, for instance, Figure 26); C_0 is the static capacitance; and the term 1/jωC_0 is the capacitive reactance, where the symbol ‖ indicates a parallel connection.

From Equation (6), the authors obtained the complete equivalent circuit of the PZT diaphragm attached to the structure under inspection as shown in Figure 28. Further details about the proposed equivalent circuit and electromechanical model can be found in Freitas *el al*. (2017).

Typically, the electrical impedance measurements are performed with commercial data acquisition (DAQ) systems which are based on impedance analyzers (SILVEIRA; CAMPEIRO; BAPTISTA, 2017). On the other hand, numerous alternative measurement systems, including time-domain, frequency-domain, and wireless-based methods, are available in the literature (CORTEZ; VIEIRA FILHO; BAPTISTA, 2013; MARUO *et al.*, 2015; PARK, SEUNGHEE *et al.*, 2008; PEAIRS; PARK; INMAN, 2004). As an example, Baptista; Vieira Filho (2009) proposed an alternative EMI measurement system (Figure 29), whose hardware consists of an inexpensive DAQ device and a personal microcomputer (PC) laptop. In this method, the PC is equipped with an appropriate LabView software which is used to record the impedance signatures. The communication between the PC and the DAQ device is performed through a universal serial bus (USB) port.

Figure 28 – Equivalent circuit based on a 1-D vibration assumption of a PZT diaphragm

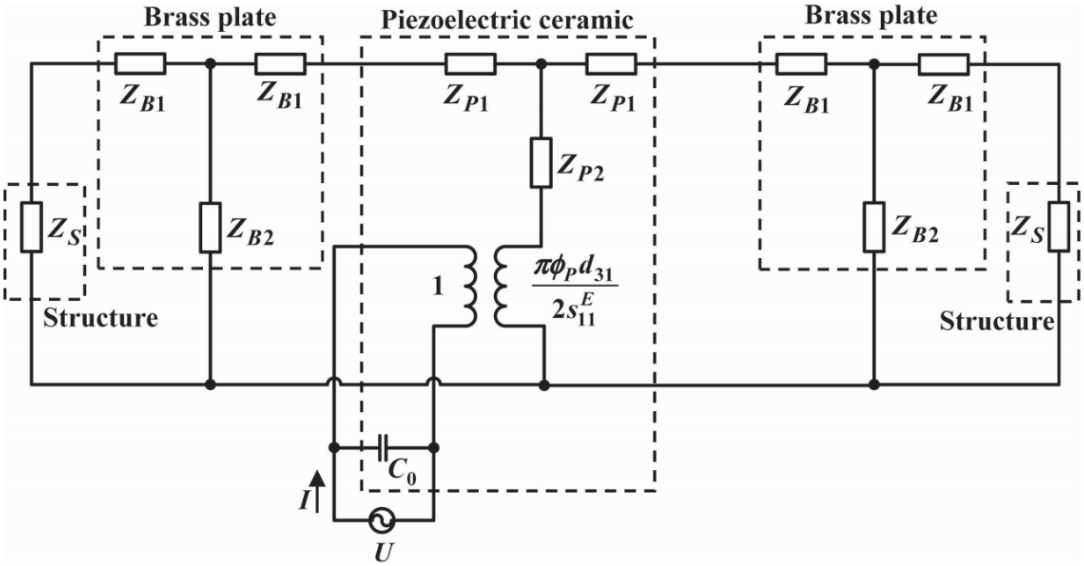

Source: (FREITAS *et al.*, 2017)

Figure 29- Alternative EM measurement system proposed by Baptista and Vieira Filho

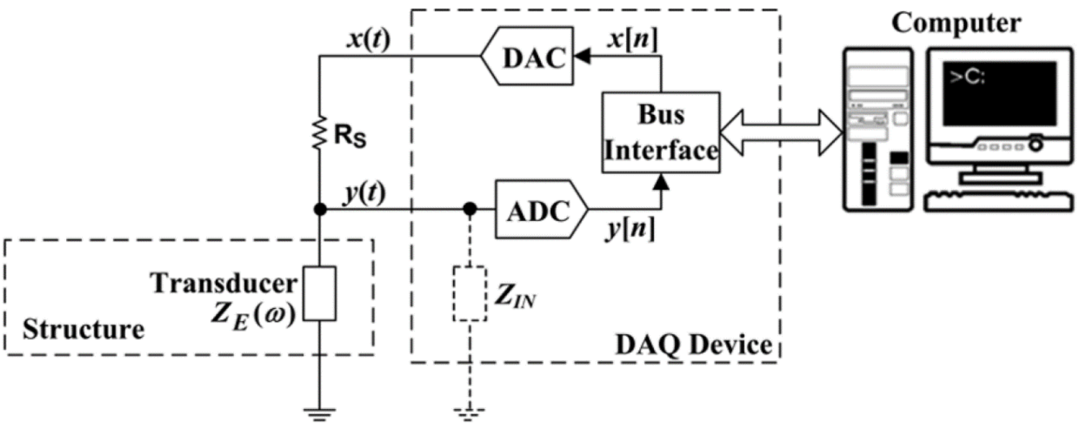

Source: (SILVEIRA; CAMPEIRO; BAPTISTA, 2017)

The transducer is connected to the DAQ device through a resistance R_s, as illustrated in Figure 29. In addition, the DAQ device provides the excitation signal $x(t)$ through the digital-to-analog converter (DAC) and acquired the response signal $y(t)$ from the transducer through the analog-to-digital converter (ADC). Finally, the signals $x[n]$ and $y[n]$ are the digital forms of the transducer excitation and response signals, respectively, to be subjected to signal processing procedures on PC. In Figure 29, Z_{IN} is the impedance of the analog input, which may be disregarded if it is sufficiently high when compared with $Z_E(\omega)$ (SILVEIRA; CAMPEIRO; BAPTISTA, 2017).

3.2.4 PZT diaphragm transducers sensitivity assessment

3.2.4.1 Pencil-Lead Break Method

The pencil-lead break (PLB) is a well-known method to characterize acoustic emission sensors (SAUSE, 2011). Recently, the use of the PLB test to characterize piezoelectric transducers, in particular, the PZT diaphragm, has received increasing attention. Almeida; Baptista; Aguiar (2015) proposed the use of the PLB to assess the sensitivity of PZT transducers for structural damage detection based on the EMI principle. The results conclusively demonstrate a very good match between the PSD obtained by the PLB method and the damage indices computed using the electrical impedance signatures. Therefore, the PLB method can be considered a simple and effective tool to experimentally assess the sensitivity of piezoelectric transducers for damage detection by using the EMI technique. The basic experimental configuration, used by Almeida; Baptista; Aguiar (2015), is shown in Figure 30a.

The PLB is carried out by breaking a pencil lead on the structure or holder on which the transducer is mounted. The pencil-lead rupture releases an impulsive elastic wave that reaches the piezoelectric transducer which generates an impulsive voltage signal. This method is a reliable way of creating a wideband signal to analyze the propagation of waves in the investigated structure as well as the frequency response of PZT transducers (ALMEIDA; BAPTISTA; AGUIAR, 2015). This method is a cheap and operational way to characterize an acoustic source following the basic procedure presented in Figure 30b. In addition, it has been adopted as a standard, according to (E976) (2010).

Figure 30- PLB method: (a) the basic configuration of the method; (b) the basic procedure for PLB experiments

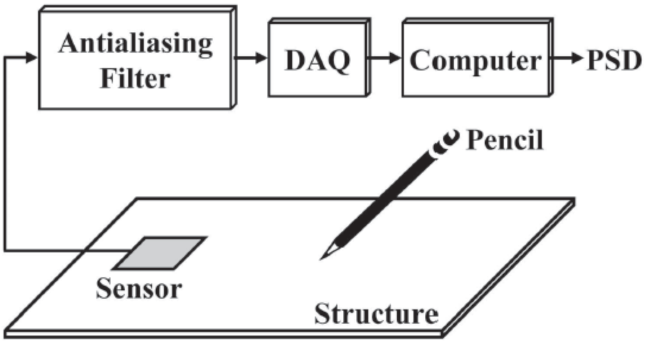

(a)

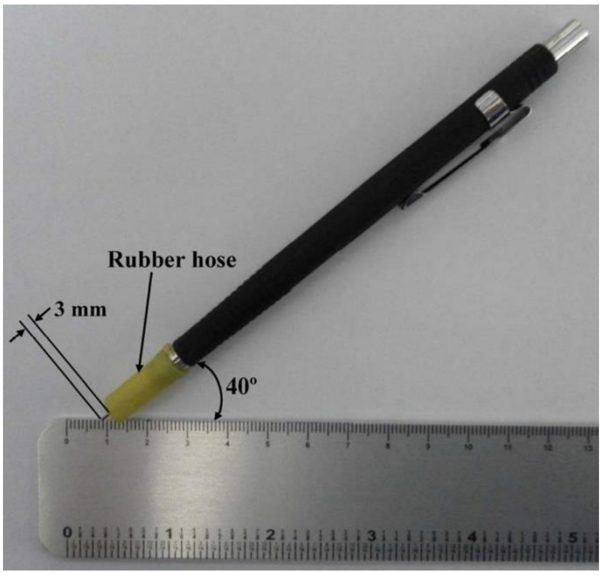

(b)

Fonte: (ALMEIDA; BAPTISTA; DE AGUIAR, 2015)

3.2.4.2 Damage indices

When the PZT transducers are attached to the structure under inspection, the electrical impedance displays peaks corresponding to the natural frequencies of the structure, and changes in these peaks are related to the onset of structural damages. The damages thus can be qualitatively detected by comparing the electrical impedance of the transducer obtained when the structure is in an initial condition (baseline), with the electrical impedance of the transducer obtained when the structure has suffered possible damages. This comparison is performed using representative damage metrics, such as the root mean square root deviation (RMSD) and the correlation coefficient deviation metric (CCDM). The RMSD index is based on the Euclidean norm and, according to Farrar (2013), is defined as

$$RMSD = \sum_{k=\omega_l}^{\omega_F} \sqrt{\frac{\left[Re(Z_{k_D}) - Re(Z_{k_H})\right]^2}{\left[Re(Z_{k_H})\right]^2}} \tag{7}$$

where the subscripts H and D represent the healthy and damaged conditions, respectively, while Re is the real part of impedance signatures of the structure under healthy (Z_{k_H}) and damaged (Z_{k_D}) conditions, respectively, measured at a frequency k ranging from ω_1 (initial frequency) to ω_F (final frequency).

On the other hand, the CCDM index is based on the correlation coefficient (CC), defined by Farrar (2013) as follows

$$CCDM = 1 - \frac{cov\left[Re(Z_{k_H}), Re(Z_{k_D})\right]}{\sigma_H \sigma_D} \tag{8}$$

where cov is the covariance of the impedance signatures (real parts), and σ_H and σ_D are the respective standard deviations of each signature.

3.3 Improved damage diagnosis through EMI

Typically, the structural damages based on the EMI database are qualitatively identified and categorized through the previously mentioned damage metrics (i.e.: RMSD and/or CCDM). However, this procedure cannot promote a classification in terms of location and severity directly from the nature of the damage. In addition, an improved damage diagnosis through EMI is sometimes critically dependent upon the selection of optimal features (MIN *et al.*, 2012). The selection of the optimal excitation frequency range, for example, is important to ensure high sensitivity to damage detection, good repeatability between the measurements, and avoid the acquisition or storage of any unnecessary data (BAPTISTA; VIEIRA FILHO, 2010). Owing to that, there are many damage diagnosis enhancement methodologies, such as those based on the numerical analysis (e.g.: finite and spectral element methods, as addressed by Fairweather; Craig (1998), and Peairs; Inman; Park (2007)), wavelet transform through time-domain feature extraction (Inman; Vieira; Guimar (2011), Xingyu Fan; Hao (2016), Zahedi; Huang (2017)), new signal processing algorithms for structure feature extraction under environment conditions (Castro; Baptista; Ciampa (2019a,b) and Castro *et al.* (2019)), and drone technology (Na, Wongi; Baek (2016)). Among them, the combination of the EMI technique machine learning with the is increasing every day. One of the trends is those investigations using ANN and fuzzy logic where it has provided detailed information such as the damage type and severity, as well as autonomous selection of damage-sensitive frequency ranges (OLIVEIRA; MONTEIRO; VIEIRA FILHO, 2018; MIN *et al.*, 2012; NA; BAEK, 2018).

Several researchers have attempted to realize an optimal damage diagnosis based on EMI using ANN and fuzzy logic. For example, in the research of Min *et al.* (2012), an innovative EMI incorporating an ANN-based pattern analysis tool was proposed to identify damage-sensitive frequency ranges autonomously and to provide detailed information, such as the damage type and severity in a simply supported aluminum beam. At the end, the proposed approach efficiently provided damage information for various damage cases with autonomously pre-determined damage-sensitive frequency ranges. Oh *et al.* (2017) proposed an ANN-based strength estimation technique using several kinds of strength related factors of concrete materials. The variations in mechanical properties of concrete were measured through the EMI method using an embedded PZT transducer (Figure 31). The trained ANN was verified with conventional strength estimation models throughout a series of experimental studies. The results showed that the proposed technique could be very effectively applied to estimate the strength of concrete.

Figure 31 – Combination of ANN with the EMI technique for predicting the strength of concrete

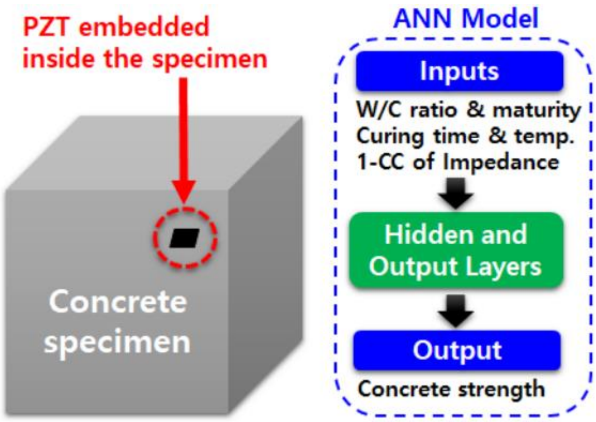

Source: (OH *et al.*, 2017)

Palomino; Steffen; Finzi (2012) combined the EMI with fuzzy cluster for identification, localization, and classification of two types of damage: cracks and rivet losses. The results demonstrated that the proposed approach was effective in accomplishing these tasks. In the research of Choi *et al.* (2018) an EMI-based fuzzy logic tool was used to estimate and predict the concrete strength in a nuclear power plant (NPP). The estimated strength was compared with the actual strength of concrete and, according to the results, the proposed approach was useful for forecasting the stability of structures. Oliveir; Inman (2017) evaluated the performance of the simplified fuzzy ARTMAP network (SFAN) and probabilistic neural network (PNN) and applied to the progression of structural damage using the EMI method. The comparison was made on the basis of the analysis of suitable parameters of the NNs. The results showed that both methods were suitable for the problem of damage growth, although the SFAN method was better suited in regard to training and testing times.

In a recent study, Oliveira; Monteiro; Vieira Filho (2018) proposed a novel strategy for damage detection in aluminum structures via the combination of the EMI and the convolutional neural network (CNN). The procedure included the following three phases (Figure 32): (i) electrical impedance measurements through an EMI DAQ system using three PZT transducers; (ii) formation of the frames which are based on the construction of a dataset for both training and test phases; and (iii) the dataset was therefore used as input for the CNN during the training process. The authors highlighted that the CNN-based method showed significant enhancement in terms of the overall success rate identifying the four damage scenarios (H, D1, D2, and D3) with higher accuracy.

Figure 32 Combination of CNN with EMI for damage detection in aluminum structures

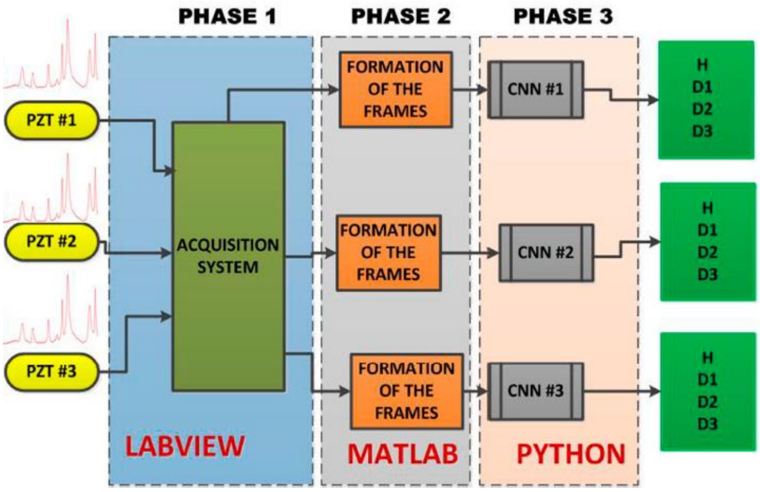

Source: (OLIVEIRA; MONTEIRO; VIEIRA FILHO, 2018)

The next chapter details the thesis experimental procedures and equipment.

Chapter 4

MATERIAL AND METHODS

In this chapter, the modeling of the problem, the test facilities, and instruments that were used to the experimental analysis and measurements will be explained. The effectiveness of the proposed approach was evaluated on the basis of two broad experimental tests. In addition to the single-point dressing operation, where the wear development of stationary single-point dressing tools was evaluated (experimental test case #1), the proposed approach was also tested for a multipoint dressing tool (experimental test case #2), thus ensuring its applicability for a broader situation.

4.1 Experimental test case #1

Experimental dressing tests were conducted on a SULMECANICA RAPH 1055 surface-grinding machine, using a conventional NORTON 38A150L6VH aluminum oxide grinding wheel (355.6 × 25.4 × 127 mm). Figure 33 presents a general view of the experiments. For comparison purposes, a first testing series with a stationary conical single-point dresser made of synthetic diamond with PCD without binder (referred as CVD diamond), and a second testing series with a stationary conical single-point dresser made of natural diamond was performed to study the tool wear development (Figure 34). A complete specification of the grinding machine, dressing conditions and test facilities can be found in Table 3. In relation to single-point dressing parameters adopted in the experiments, an $U_d = 1$ was set at the beginning of the experiment, in line with the recommendations addressed by Cearsolo *et al.* (2016); Marinescu *et al.*, (2016); and Pombo *et al.* (2017). The other main parameters were: the constant dressing depth equal to 40 µm and the constant dressing speed set at 3.45 mm/s. Both testing series were conducted without application of cutting fluid, i.e., in dry-dressing conditions, similar to that used in the research of Cearsolo *et al.* (2016), since, under these conditions, wear is accelerated, allowing a reasonable timeframe of experimentation.

Each test consisted of dressing passes throughout the grinding wheel surface until the end of the grinding wheel lifespan. The experiment with the CVD diamond dresser involved as many as 600 dressing passes. On the other hand, the experiment with the natural diamond dresser involved as many as 300 dressing passes.

Figure 33- Schematic diagram of the experimental test bench

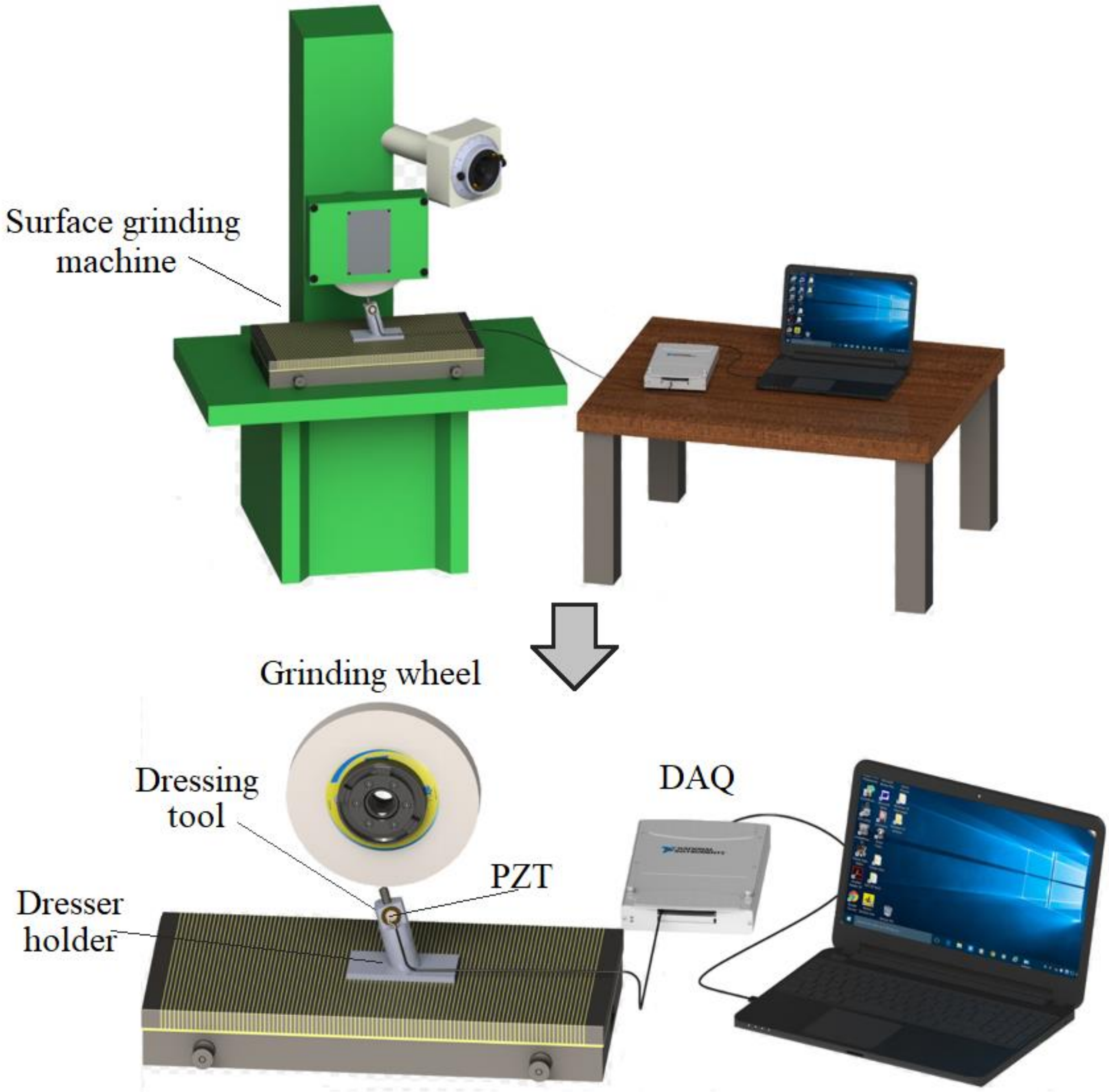

Source: Author

The wear development of the diamond dressing-tools was accurately measured using a DNT DIGIMICRO 2.0 digital microscope, with 10× to 200×, equipped with computer-aided design (CAD) software to measure distances and areas. The macro images of the diamond tips were captured for both top and side views, and the magnification of 20× was adopted. In addition, the tool wear area was measured from the side and top positions of the dressers.

Figure 34- Experimental test case #1: stationary conical single-point dressers, top and side views of both diamond tips, PZT diaphragms attached to the tool holder, and temperature monitoring procedure

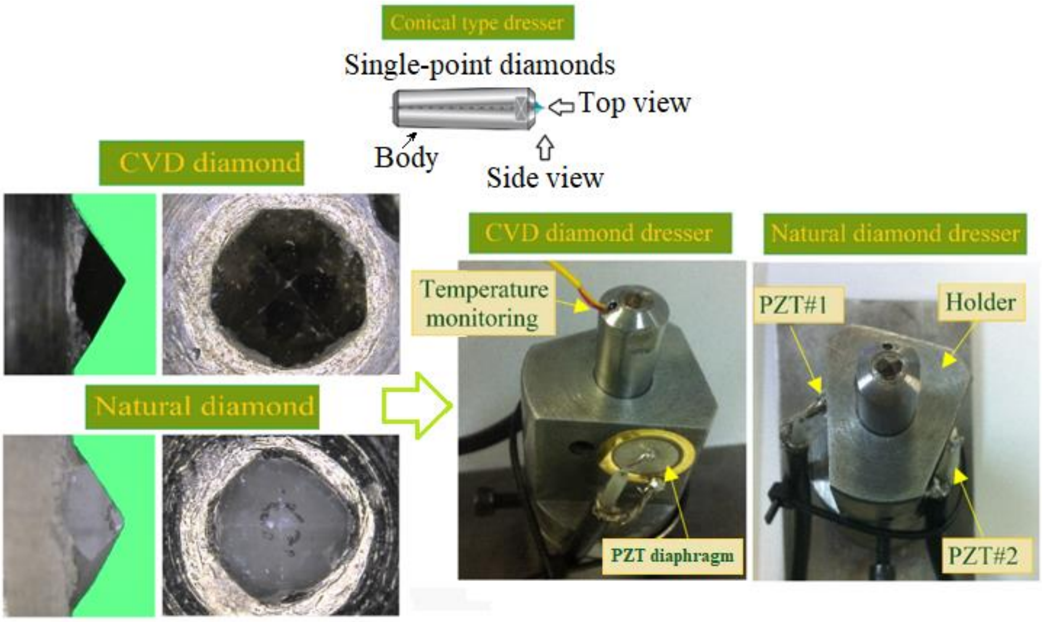

Source: Author

Table 3 - Experimental test specification

Parameter	Specification
Grinding machine	SULMECANICA RAPH 1055 surface-grinding machine
Grinding wheel	NORTON 38A150L6VH aluminum oxide (355.6 × 25.4 × 127 mm)
Dressing tool	ROYAL DIAMOND CDV and natural diamond single-point conical type dressers
U_d	1 at the beginning
Traverse dressing feed v_d	3.45 mm/s
Dressing depth a_d	40 µm
Cooling	Dry-dressing
Number of dressing passes	600 for CVD diamond and 300 for natural diamond
Temperature monitoring	MINIPA MT455 using a type K thermocouple
State wear analysis	
DAQ system	NATIONAL NI USB-6221 DAQ device
Transducers	Two patches MURATA 7BB-20-6

4.1.1 Data acquisition system

Two MURATA 7BB-20-6 PZT diaphragms with brass plate and active element diameters of 20 mm 14 mm, respectively, were used in the experiments (Figure 34). Both PZT diaphragms (PZT#1 and PZT#2) were attached to the dresser holder in opposite equidistant directions for the purpose of carry out comparisons. The electrical impedance signatures of the transducers were measured through the alternative EMI measurement system proposed by Baptista; Vieira Filho (2009), which was summarized in Chapter 3 (see, for instance, Figure 29). A NATIONAL NI USB-6221 DAQ device and a computer equipped with LabVIEW® software were used to acquire the signatures from both PZT diaphragms simultaneously, at a sampling rate of 250 kS/s (with an ADC resolution of 16 bits). During the measurements, the transducers were excited through a chirp signal with a magnitude of 1 V, a frequency range from 0 to 125 kHz, period of 262,144 ms, and a resistor of 2.2 kΩ. A complete schematic view of the data acquisition procedure is shown in Figure 35.

Figure 35- Schematic diagram of the data acquisition system

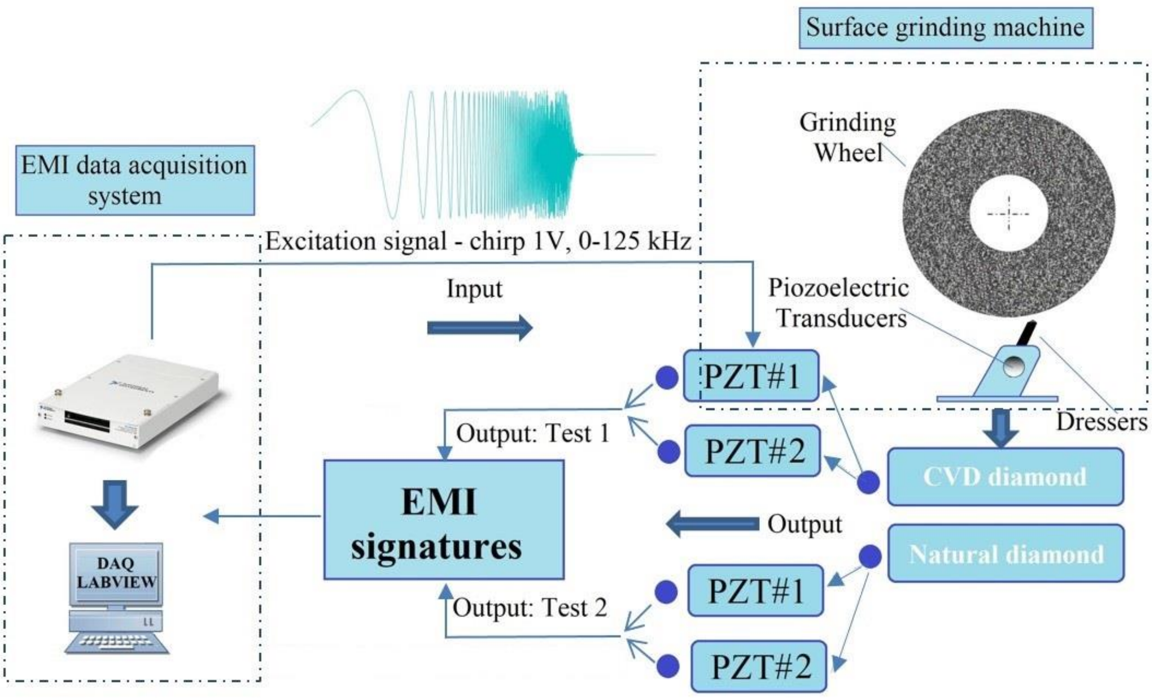

Source: Author

4.1.2 PLB method and temperature control

The PLB experiment was performed in line with the procedures reported in (ALMEIDA; BAPTISTA; DE AGUIAR, 2015) and E976 standard (E976-10, 2010). The lead break was obtained manually through a mechanical pencil equipped with a 2H lead type with a length of 3 mm and a diameter 0.5 mm. The angle between the structure and the lead was 40º and the lead was broken at a distance of 50 mm from the transducer (Figure 36). In addition, the lead was broken on each dresser diamond tip in order to compare the response of both PZT diaphragms (i.e.: PZT#1 and PZT#2) for both CVD and natural diamond dressing tools. The output voltage signals were collected at sampling frequency 2 MS/s by a YOKOGAWA DL850 oscilloscope. An average value vector of the raw response signal was obtained from 10 PLB repetitions for each PZT diaphragm. The signal analysis was performed in the frequency domain by means of PSD using the Welch method with a Hanning window of 256 points and an overlap of 50%.

As it is well known, the electrical impedance signatures have been proven to vary with change in temperatures. Consequently, this kind of influence can issue a false positive diagnosis (BAPTISTA *et al.*, 2014; NA, WONGI; BAEK, 2018). Therefore, the impedance measurements were performed at a constant temperature of 30° C. The temperature was only controlled at the moment of the impedance measurement, using a digital thermometer, model MT455 by MINIPA, equipped with a type K thermocouple. To fix the thermocouple, a hole was made in the dresser body (Figure 34 and Figure 36) near the diamond, where the thermal conductivity is high, i.e. 1000 W/(mK) (in steel it is 50.2 W/(mK)) (POMBO *et al.*, 2017). Although the dressing tests were performed without coolant to induce wear damage more rapidly, the machine cooling system was used for the host structure of the PZT diaphragms (tool holder), ensuring that the transducers were protected against any thermal damage.

Figure 36 - PLB setup and temperature monitoring procedures

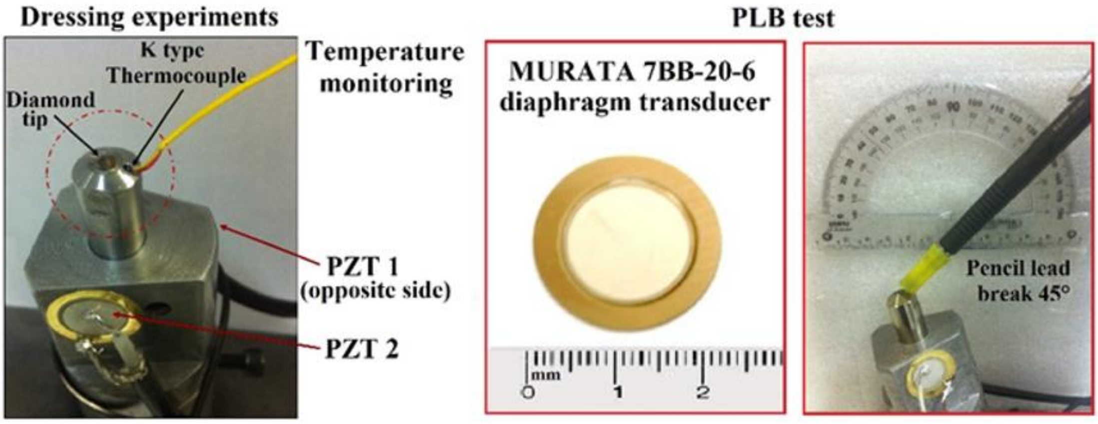

Source: Author

4.1.3 Sensor signal feature extraction

During the experiments, each damage class was experimentally defined every 200 dressing passes (i.e.: damage 1 (D1) at 200 passes, damage 2 (D2) at 400 passes, and damage 3 (D3) at 600 passes) to the CVD diamond dresser, and every 100 dressing passes (i.e.: damage 1 (D1) at 100 passes, damage 2 (D2) at 200 passes, and damage 3 (D3) at 300 passes) to the natural diamond dresser. In addition, the impedance signature related to the dressing tools in an undamaged state (fresh tool) was adopted as a reference (baseline) for both testing series. For the purpose of comparisons, an average of 10 repetitive impedance measurements were taken for each tool condition class. To analyze the signals, the real part of the impedance $Re\ (Z_E(\omega))$, which is related as the most susceptible to structural damages and least susceptible to temperature variations (BHALLA; NAIDU; SOH, 2003; NA, S.; LEE, 2013), was adopted.

As previously mentioned, the present research work was dived into two tasks: (i) TCM for dressing tool wear and failure in grinding process through EMI along with PZT diaphragms sensorial data processing; (ii) enhancement of damage identification in (i) through machine learning. For the purpose of experimental test case #1, the sequence of activities was developed in line with the framework illustrated in Figure 37. The idea was to focus on the tool wear development during the dressing operation. This way, the tool wear information was extracted by using RMSD and CCDM indices for various damage cases (tool conditions) at different frequency bands. At the end, an intelligent diagnosis system was constructed to select the most damage-sensitive features based on the optimal frequency band recognized in the process of learning validation following the approach presented in Min *et al.* (2012), and Yang; Divsholi (2010).

Figure 37 – The proposed framework for experimental test case #1

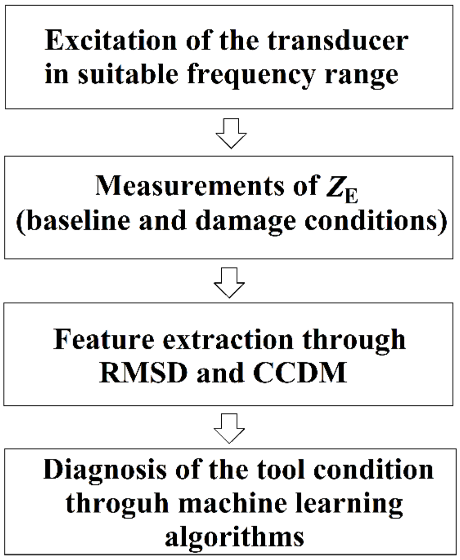

Source: Author

At first, the damage indices were calculated for the impedance signatures related to those damage classes previously defined. It has been well-known, however, that each transducer has a frequency range that is more suitable for calculating RMSD and CCDM indices when they are attached at different positions, as well as when different types of structure are monitored

(MARCHI *et al.*, 2015; SILVEIRA; CAMPEIRO; BAPTISTA, 2017). Moreover, according to Table 4, six appropriate frequency sub-ranges were defined, considering over a wide frequency range of 0-120 kHz, with each frequency band spanning 20 kHz. This wide frequency range was considered due to the sampling rate of the DAQ device used in this research work (i.e.: 250 kS/s). However, the final frequency was set at 120 kHz instead of 125 kHz for the purpose of carried out a proprer division of the frequency sub-range (i.e. every 20 kHz). In addition, the choice of the frequency sub-range value was optimally selected for the present application based on experimental impedance signatures and on the values obtained from the damage metrics. It was further supported by the related literature (MARCHI *et al.*, 2015; SILVEIRA; CAMPEIRO; BAPTISTA, 2017). Figure 38 illustrates the frequency sub-range selection.

Table 4- Sub-ranges of frequency chosen

Nomenclature	Frequency bands for RMSD and CCDM calculation
@fb#1	0-20 kHz
@fb#2	20-40 kHz
@fb#3	40-60 kHz
@fb#4	60-80 kHz
@fb#5	80-100 kHz
@fb#6	100-120 kHz

Figure 38- Frequency sub-range selection

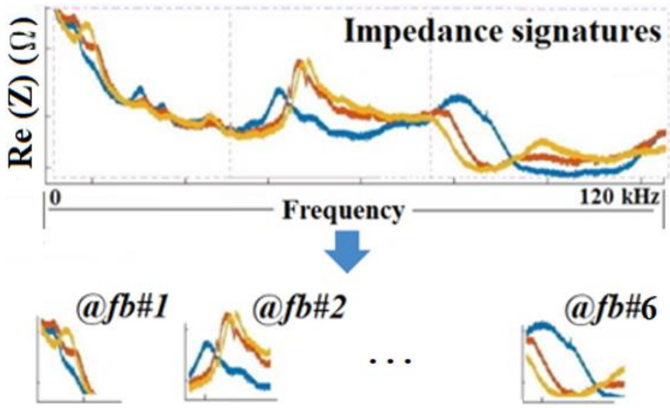

Source: Author

The damage indices were therefore computed for each frequency sub-range (Table 4) with a step of 10 Hz to construct a grouping of feature patterns (feature vector). Accordingly, each group of the feature vector corresponding to each tool condition consists of 2,000 feature patterns, and a complete chart for the three damage classes D1, D2, and D3 consists of 6,000 feature patterns. Figure 39 illustrates the feature extraction procedure.

Figure 39 – Feature extraction procedure

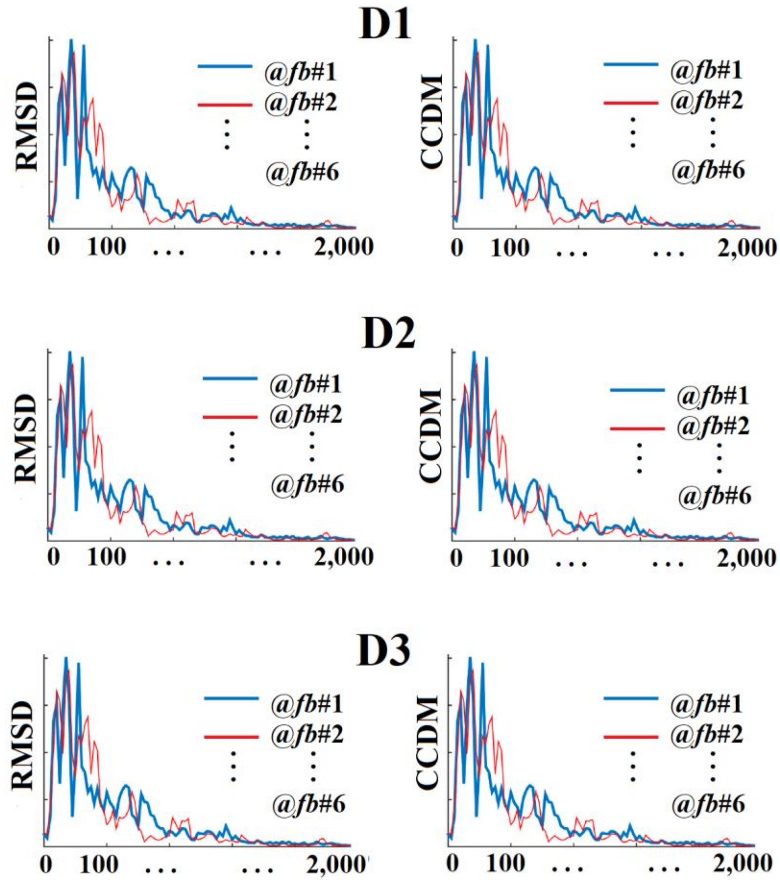

Source: Author

4.1.4 Machine learning-based intelligent diagnosis system

An ANN-based machine learning approach was proposed to construct the intelligent diagnosis system previously mentioned. To accomplish this goal, a supervised multi-layer feed-forward neural network (NN) with a BP algorithm was employed. The ANN-based machine learning framework can be further summarized as follows: for a given transducer (PZT#1 or PZT#2), for a given damage metrics (RMSD or CCDM) and for a given frequency sub-range (0-20 kHz or 20-40kHz or 40-60 kHz or 60-80 kHz or 80-100 kHz or 100-120 kHz), the NN input training database was made of feature vectors with representative tool condition information. A schematic representation of the feature vector as well as the NN architecture is illustrated in Figure 40.

A study was conducted to identify the best NN configuration through different combinations of several learning parameters. To this end, eight NN models were constructed (Table 5), i.e.: *model#1*, *model#2*, *model#3*, and *model#4* to the testing series with CVD diamond dresser, and *model#5*, *model#6*, *model#7*, and *model#8* to the testing series with natural diamond dresser.

Each model was trained and tested by combining the feature vector of two consecutive frequency sub-ranges, in agreement with the following references (JUNIOR, P.O. *et al.*, 2017; MARTINS, CESAR H. R. *et al.*, 2014), to yield a combination of two frequency sub-ranges capable to provide the reliable monitoring of the dressing tool condition instead of a single.

Figure 40- Illustration of the RMSD and CCDM indices calculation

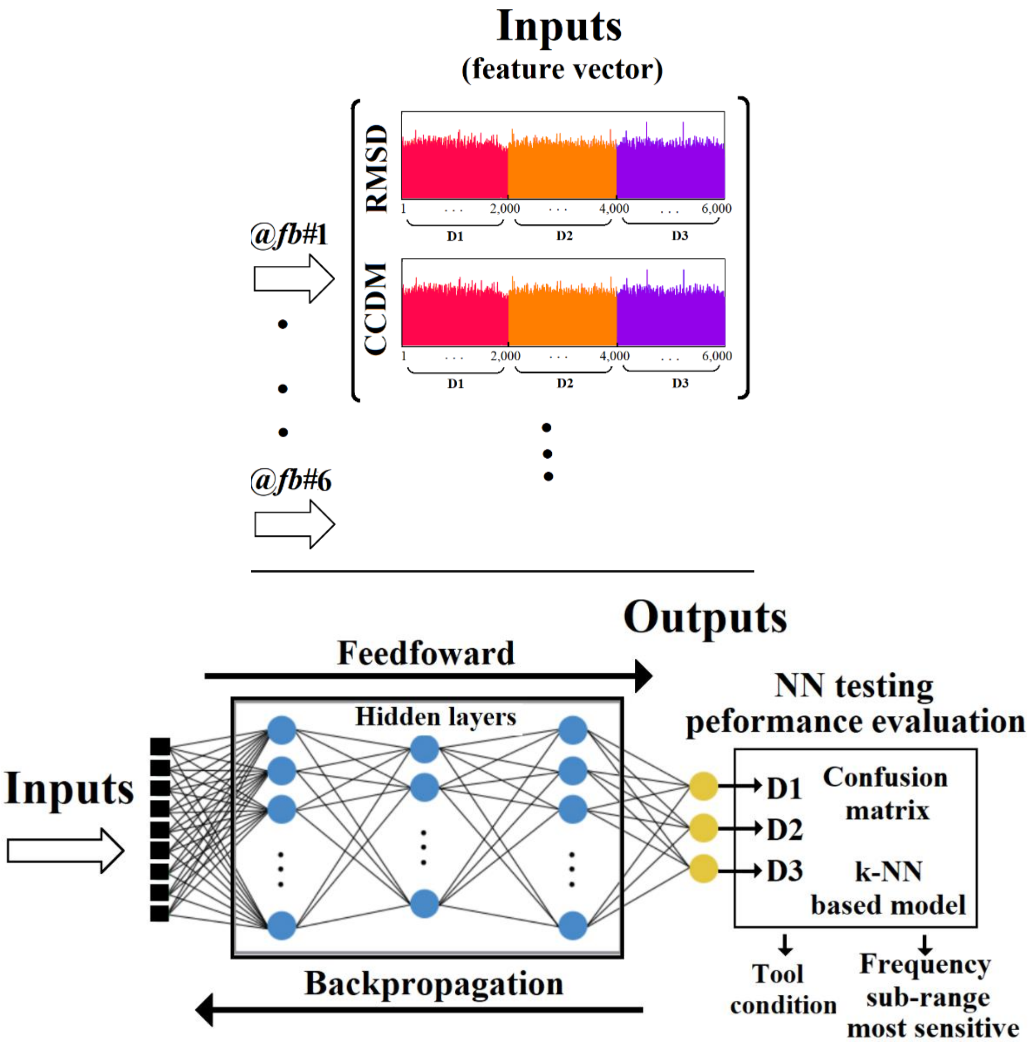

Source: Author

A binary matrix that considered those three damage conditions D1, D2 and D3 was built as a target for the NN output. A logic value 1 was used to activate the features corresponding to each damage class D1, or D2, or D3. Multi-layer perceptron networks architectures (Figure 41) with 1 to 3 hidden layers were created, varying the number of neurons from 5 to 40 per layer. The supervised BP algorithm under the Levenberg-Marquardt optimization function was implemented through MATLAB® software. To evaluate the repeatability of the proposed configuration, each NN model was trained five times for each set of feature vectors and 10%

of the features were kept aside for validation purposes. The entire flowchart that summarizes the proposed machine learning algorithm, is illustrated in Figure 41.

Table 5- NN input sets

Experimental test case	Parameter	identification
Testing series with CVD diamond dressers	PZT#1 CVD RMSD	*model#1*
	PZT#2 CVD RMSD	*model#2*
	PZT#1 CVD CCDM	*model#3*
	PZT#2 CVD CCDM	*model#4*
Testing series with natural diamond	PZT#1 natural RMSD	*model#5*
	PZT#2 natural RMSD	*model#6*
	PZT#1 natural CCDM	*model#7*
	PZT#2 natural CCDM	*model#8*

Figure 41- Flowchart of the proposed machine learning algorithm

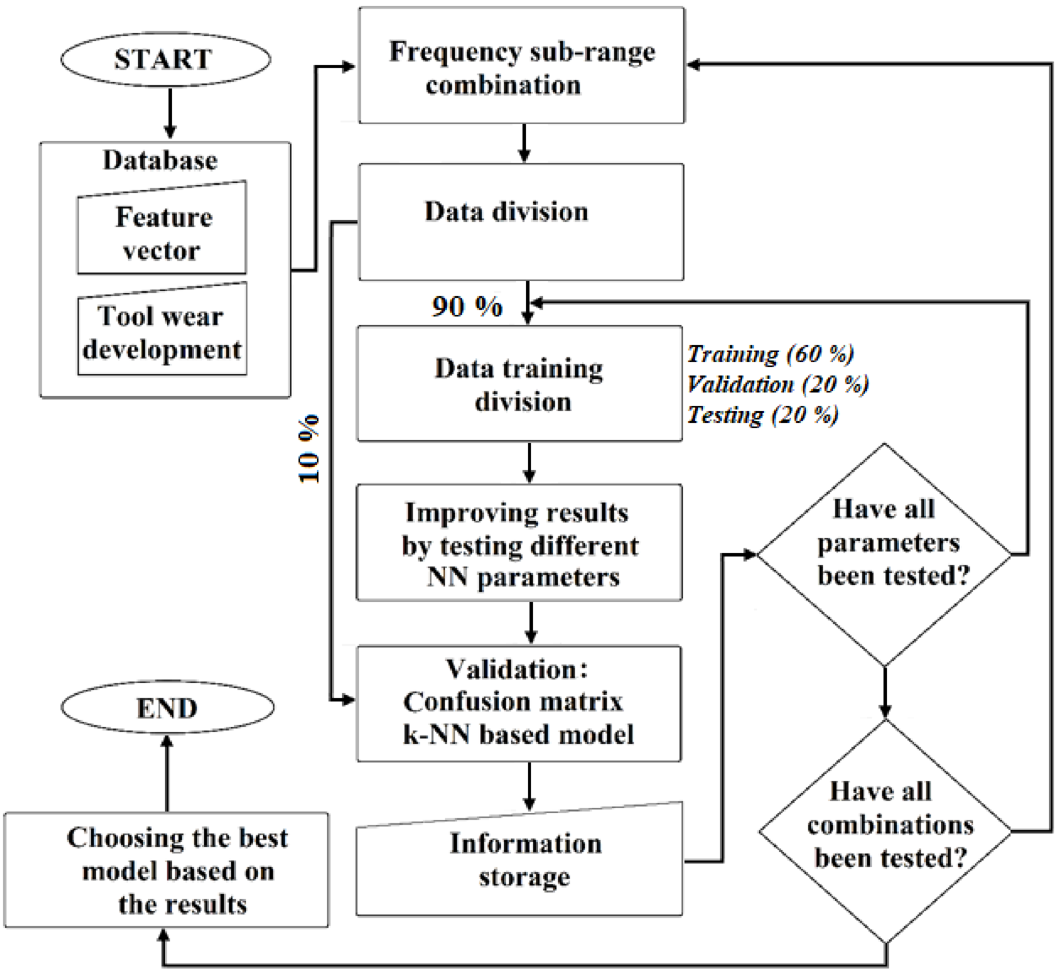

Source: Author

4.2 Experimental test case #2

An additional experimental test was conducted on a multipoint stationary dressing tool of CVD diamond (20 × 15 × 5 mm of metallic dresser body, and seven 0.6 × 10 mm diamond sticks), which is commonly known as fliesen dresser or surface plate. Unlike tool wear monitoring previously studied, the idea was to simulate other dressing tool structural failures (breakage, CTF, impacts) and thus expanding the feasibility of applying the EMI method for TCM. The damages were inserted at three positions (Figure 42) on the top of the surface plate by drilling two sequentially holes at each position, whose diameters and depths of cut were 1.5 mm and 0.5 mm, respectively (i.e. each hole was totally drilled until 1 mm of depth cut into two steps of 0.5 mm). An industrial ZOCCA S30 column-drilling machine was used to perform the holes. As shown in Figure 42, the three distinct positions of the holes were 3 mm (P1), 8.5 mm (P2), and 13.5 mm (P3), respectively. As an NDE trial, this procedure changes the mechanical impedance of the host structure similarly to failures but provides the advantage of not permanently damaging the dressing tool, since the holes were made in the dresser body instead of the diamond position (Figure 42).

Figure 42 – Tool damage insertion procedure

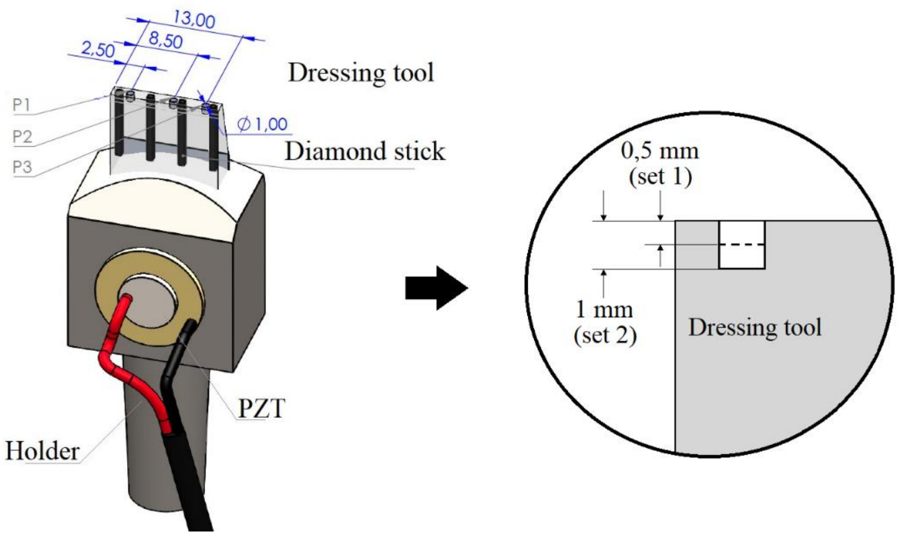

Source: Author

4.2.1 Data acquisition sytem

The procedures adopted for data acquisition were the same as those previously adopted to the experimental test case #1 (i.e. the same EMI measurement system and DAQ device were adopted). A MURATA 7BB 12-9 PZT diaphragm (PZT#1) with bronze disc diameter of 12 mm and an active element diameter of 9 mm and another (MURATA 7BB 15-11 – PZT#2) with bronze disc diameter of 15 mm and an active element diameter of 11 mm were glued to the dresser body (Figure 42) in opposite directions. The impedance signatures were acquired at each set as given in both Table 6 and Table 7. At the end, six different scenarios that correspond to the impedance signatures of the dressing tool under damage conditions were taken for comparison purposes with the baseline signature (healthy). In order to ensure good accuracy, an average of five measurements were taken at every tool condition acquired.

Table 6 – Main features of the experimental test case #2

Parameter	Specification
Dressing tool	The multipoint diamond stationary dressing tool
Transducers	PZT MURATA 7BB 15-11 and 7BB 12-9
Temperature	27.5° C constant during the impedance measurements
Damage induction	Holes drilled at 3 positions from top of the dressing tool
Set	Each hole was drilled until 1 mm of depth cut in two steps of 0.5 mm, i.e., set#1 and set#2
DAQ device	NATIONAL NI USB-6221

Table 7 – Description of the experiment

Conditions	Damage type	Set
1	Damage introduced at 3 mm from top of the dressing tool (P1)	1
2	Damage introduced at 3 mm from top of the dressing tool (P1)	2
3	Damage introduced at 8.50 mm from top of the dressing tool (P2)	1
4	Damage introduced at 8.50 mm from top of the dressing tool (P2)	2
5	Damage introduced at 13 mm from top of the dressing tool (P3)	1
6	Damage introduced at 13 mm from top of the dressing tool (P3)	2

The temperature control procedures were adopted in agreement with those described in Section 4.1 (experimental test case #1). However, the experimental teste case #2 was conducted under environmentally controlled conditions and all impedance measurements were performed at a temperature of 27.5 ° C. In addition, for the purpose of the experimental test case #2, macro images of the induced damages were also captured during the experiments. To this end, a TESA-VISIO-200 microscope with 6,5× optical magnification (0,7× to 4,5×), equipped with 200 × 100 mm measuring table and a TESA-REFLEX interface software. The macro images of the diamond tips were captured for both top and side views, and the magnification of 0,7× was adopted.

4.2.2 Sensor feature extraction

To analyze the signals of both PZT diaphragms (PZT#1 and PZT#2), the real part of the impedance was also used for calculation ($Re(Z_E)$). Likewise, the RMSD and CCDM metric were applied for feature extraction purposes. According to Table 8, 12 frequency sub-ranges were experimentally chosen in line with the procedures previously reported for the experimental test case #1 considering over a wide frequency range of 0-120 kHz, with each frequency sub-range spanning 10 kHz.

Table 8 – Frequency sub-ranges chosen

Nomenclature	Frequency sub-range
@fb#1	0-10 kHz
@fb#2	10-20 kHz
@fb#3	20-30 kHz
@fb#4	30-40 kHz
@fb#5	40-50 kHz
@fb#6	50-60 kHz
@fb#7	60-70 kHz
@fb#8	70-80 kHz
@fb#9	80-90 kHz
@fb#10	90-100 kHz
@fb#11	100-110 kHz
@fb#12	110-120 kHz

4.2.3 Fuzzy-based intelligent diagnosis system

Unlike experimental test case #1, the intelligent diagnosis system was constructed on the basis of a fuzzy logic model. To this end, the dressing tool damage information extracted from the RMSD and CCDM calculation at those frequency sub-ranges previously mentioned (Table 8) was considered. The fuzzy models were implemented by using the Fuzzy logic toolbox of the MATLAB® software. The inference system was established based on the Mamdani method given by Mamdani; Assilian (1975), and the centroid method was chosen for defuzzification purposes. The Gaussian type membership functions were used to the fuzzy logic system (*gaussmf*), which are related in literature as a better behavior and smooth transition in situations of a sudden spike, as addressed by Alexandre *et al.* (2018). The mean characteristics of the proposed fuzzy system are given in Table 9.

In accordance with the literature (Alexandre *et al.* (2018), Miranda *et al.* (2015); Silva; Castro; Miranda (2012)), the terms linguistic Low, Medium and High were also used to represent the membership functions. These terms were defined considering the values minimum and maximum of the RMSD and CCDM (PZT#1 database only) in each one of those six-damage conditions that were given in Table 7. These linguistic variables are capable to convert the input pattern (numeric values) into concepts to be applied to the fuzzification based on sets of the membership functions. The PZT#2 database, which is not presented during metal model construction, is used to validate the proposed fuzzy system for a broader situation. Figure 43 illustrates the membership function and the adopted concepts. The framework of the proposed intelligent diagnosis system is illustrated in Figure 44.

Table 9 - Mean characteristics of the proposed fuzzy system

Parameter	**Specification**
Fuzzy inference type	*Mamdani* (MAMDANI; ASSILIAN, 1975)
Membership functions (MF)	Gaussian type (*gaussmf*)
Number of clusters	3 (P1, P2, and P3)
Number of rules	9 (LOW, MEDIUM, and HIGH × 3 clusters)
Defuzzification method	Centroid
Validation	PZT#2 database

Figure 43– Membership functions representation

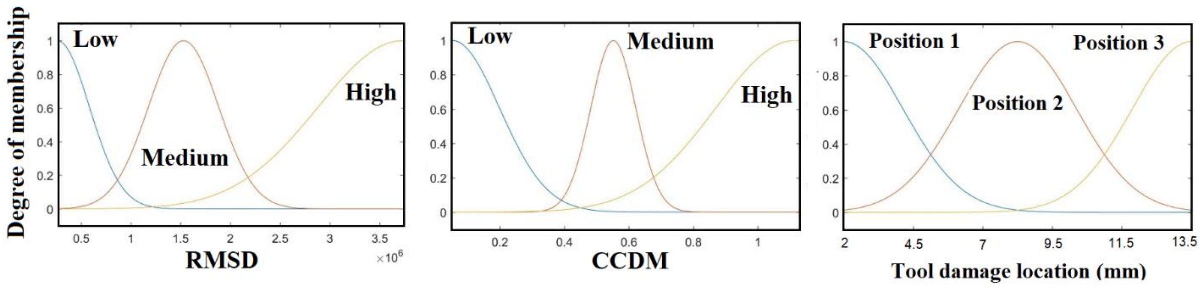

Source: Author

Figure 44 – Proposed intelligent diagnosis system based on fuzzy logic

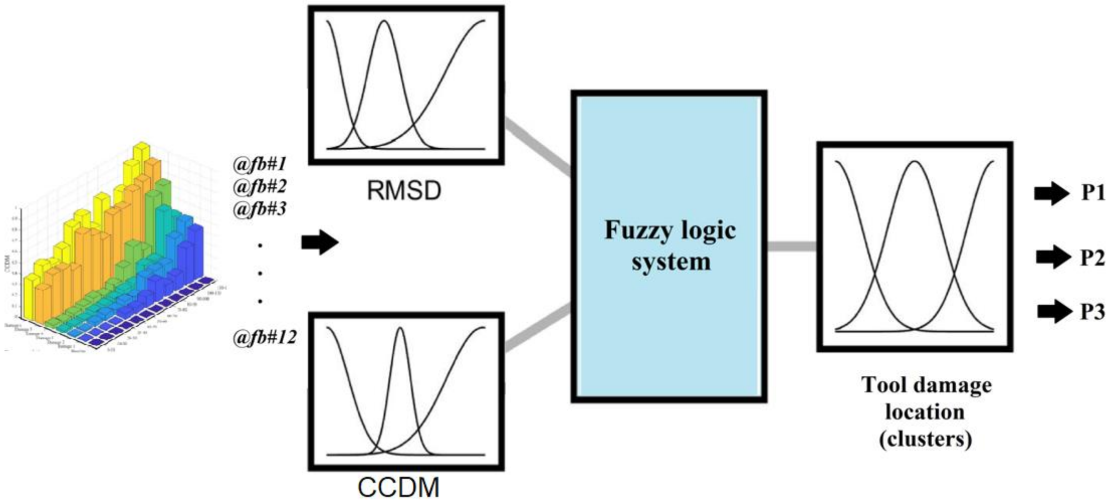

Source: Author

Regarding the system output, those determined clusters P1, P2 and P3, respectively, were adopted. This means that the output of the system, namely the position of the damage (P1, P2, or P3), is classified according to the three sets of linguistic variables (Low, Medium, and High). To this end, the system should be capable to classify two damage types to each position (i.e. set#1 and set#2, as it was given in Table 7). In addition, the values corresponding to the real position of the induced damages in the dressing tool (i.e. 2.5 mm, 8.5 mm, and 13 mm) were assigned to the output membership functions, as given in Figure 43. Therefore, nine rules to manipulate the linguistic data were generated as given in Table 10.

Table 10 – Set of rules

Input		**Set of rules (tool damage location)**		
		Low	Medium	High
RMSD and CCDM	Low	Position 1 (P1)	Position 1 (P1)	Position 2 (P2)
(from @*fb#1* to @*fb#12*)	Medium	Position 1 (P1)	Position 2 (P2)	Position 3 (P3)
	High	Position 2 (P2)	Position 3 (P3)	Position 3 (P3)

The generated rules are further summarized as follows:

- (1) If (RMSD is Low) and (CCDM is Low) then (Location is P1);
- (2) If (RMSD is Medium) and (CCDM is Medium) then (Location is P2);
- (3) If (RMSD is High) and (CCDM is High) then (Location is P3);
- (4) If (RMSD is Low) and (CCDM is Medium) then (Location is P1);
- (5) If (RMSD is Low) and (CCDM is High) then (Location is P2);
- (6) If (RMSD is Medium) and (CCDM is Low) then (Location is P1);
- (7) If (RMSD is Medium) and (CCDM is High) then (Location is P3);
- (8) If (RMSD is High) and (CCDM is Low) then (Location is P2);
- (9) If (RMSD is High) and (CCDM is Medium) then (Location is P3);

The next chapter presents the most relevant results obtained with the proposed approach.

Chapter 5

RESULTS AND DISCUSSION

This chapter discusses the most relevant results obtained with the proposed approach. At first, the results obtained with the experimental test case #1 are presented. Subsequently, the results obtained with the experimental test case #2 are evaluated.

5.1 Results of the experimental test case #1

This section presents the results obtained with experimental test case #1 as follows: (i) results and discussion on the analysis of tool wear state (5.1.1); (ii) results and discussion on PZT diaphragms characterization (5.1.2); and (iii) results and discussion on the NN-based machine learning performance (5.1.3).

5.1.1 Results and discussion on the analysis of tool wear state

Considering that the purpose of the experimental test case #1 was to find a correlation between the wear state of the dressing tool and the impedance signatures, Figure 45 shows the microscopic photographs of the CVD diamond dressing tool after 200, 400 and 600 dressing passes, respectively, as well as its wear development as a function of the number of dressing passes. The industrial diamond manufacturing process is characterized by stochastic components and depends on various factors, such as the impurities in natural diamonds, the methods to produce CVD diamonds, the metallization and characterization processes. These effects are well covered in the literature (see, for instance, Fraimovitch *et al.* (2017)). For this reason, even though two diamonds with the same reference, well-defined geometry, and under the same dressing conditions were used in this study, the number of passes for the CVD diamond dresser differs from the number of passes for the natural diamond dresser (summarized next). Accordingly, for the CVD diamond dresser, it was verified that this material presented such a high wear resistance that it was not possible to reach the end of its life since the grinding wheel life was over before the end of dresser tool life due to excessive reduction of grinding wheel diameter.

Figure 45 - Analysis of the CVD diamond wear state: (a) top view; (b) wear area; and (c) side view

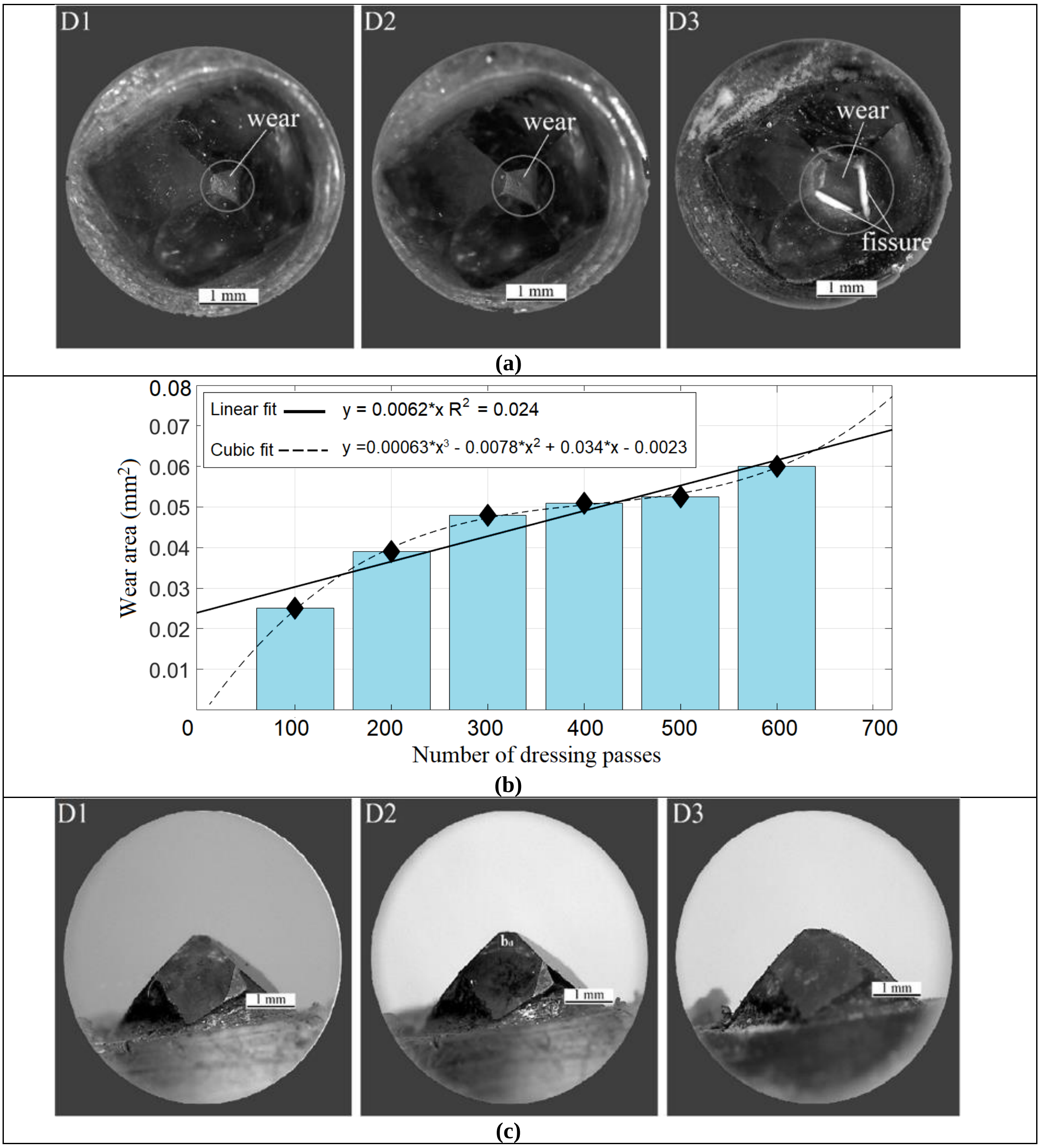

Source: Author

Figure 45a shows that the condition of the CVD diamond dresser did not change significantly with the increasing number of passes, i.e., it is possible to observe only small wear and some fissures at 600 dressing passes in the top views. Moreover, in the side views (Figure 45c), for a value of overlap ration U_d = 1 at the beginning of the dressing and for constant values of dressing depth, ad, and dressing feed rate, v_d, the width of action, b_d, does not suffer considerable changes that could increase the contact area between grinding wheel and diamond, directly influencing the final quality of the dressing process. Figure 45b showed the evolution of the CVD diamond tip wear. The side worn area of the CVD diamond tip was measured every 100 dressing passes using CAD software and plotted vs. the number of passes showing an increasing trend of the wear development. However, this trend was not exactly linear as the dressing passes took place. Thus, in accordance with previous observations by microscopy photographs (Figure 45a,c), the effects of the high wear resistance presented by this material was also evident in Figure 45b, since, the worn area increased at the beginning (100, 200, and 300 passes, respectively), and then, after 300 dressing passes it was not presented significant increases up to 500 passes, i.e. it kept similar values at approximately 0.05 mm^2. After 500 passes, it increased again up to 600 passes. The CVD diamond dresser presented less than 10% of the worn area for 600 passes due to its very high wear resistance (loss of 0.06 mm^2). This result is in agreement with previous research work, such as: (JUNIOR, P.O. *et al.*, 2017; MARTINS, CESAR H. R. *et al.*, 2014), in which authors addressed wear condition assessment of single-point dresser. In particular, high standard deviations were observed by these authors, probably due to different friability properties of the utilized diamonds.

As said before, clear difference emerges when comparing the results obtained with different dressing-tool diamonds, as expected. This way, Figure 46 shows microscopic photographs of the natural diamond-dressing tool after 100, 200 and 300 dressing passes, respectively, as well as the evolution of the tool wear as a function of the number of dressing passes. It can now be observed a significant difference in the diamond conditions as the dressing passes progresses, showing much lower resistance to wear than that corresponding to the CVD diamond-dressing tool, previously showed. According to Figure 46a and Figure 46c, it can be observed that the condition of the diamond changed significantly as a function of dressing passes evolution. It is possible to observe, from top and side views, the evolution of the wear at 100 dressing passes as well as severe damage at 200 and 300 dressing passes (such as: excessive wear, fracture, and breakage). In this case, the increase of the contact area between the grinding wheel and diamond was very high and there was a significant increase of the parameter bd, for a constant value of dressing depth ad equal to 40 µm and a constant dressing feed v_d, set at 3.45 mm/s.

Figure 46b shows the worn area of the natural diamond, which has been measured every 100 dressing passes. The wear area of the natural diamond tip increased as the dressing passes took place, as expected. In contrast with the evolution of the CVD diamond dresser wear, presented in Figure 46b, a linear trend is observed in Figure 46b.

Figure 46 - Analysis of the natural diamond wear state: (a) top view; (b) wear area; and (c) side view

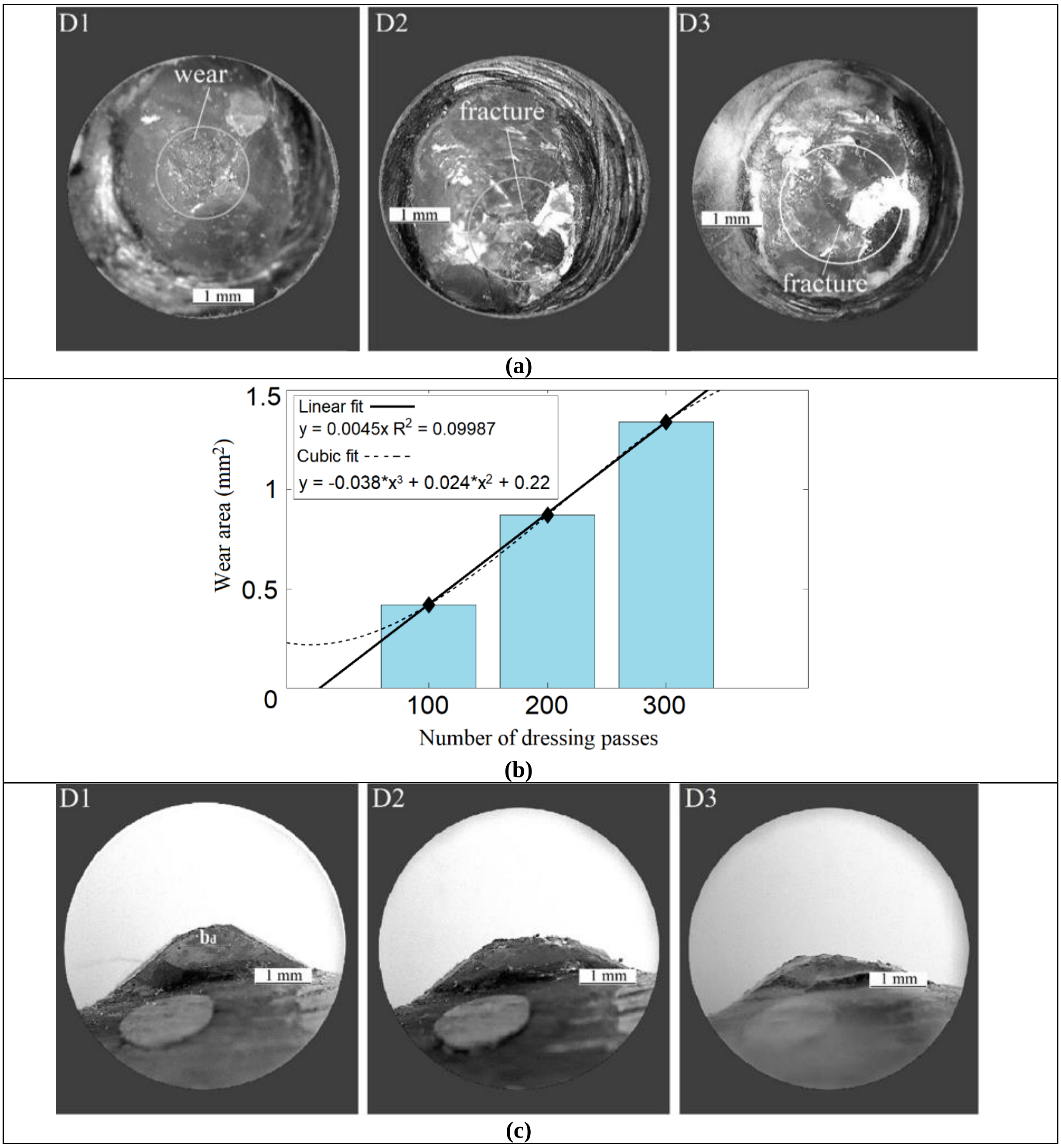

Source: Author

Nevertheless, it was possible to determine the actual state of the dressing tool and predict its influence on the grinding operation. In fact, up to 100 dressing passes, U_d increased (the contact area increased) and, consequently, the sharpness that the dressing operation produces on the grinding wheel decreased. However, after 200 dressing passes, the contact surface shows an increase rate, and it grows constantly up to 300 dressing passes. Thus, the behavior of the dressing tool becomes erratic due to the occurrence of fractures and micro-cracks, i.e. catastrophic failures of the diamond dressing tool structure at 300 dressing passes. In accordance with previous observations, the material properties of the natural diamond dressers were also evident, since, in contrast with the CVD diamond tool wear results, the natural diamond dresser was largely affected by the increase of dressing passes.

It is worth noting that in Pombo *et al.* (2017), this fact was considered evidence that the tool wear progressively increased the actual contact area between the grinding wheel and diamond tool. As result, it leads to higher power consumption during the dressing process. In addition, the effect of wear in the dressing tool is also evident in the present results: in Figure 46b, the natural diamond presented a very high level of worn area after 200 dressing passes and a CTF at 300 dressing passes. As indicated by the $R^2 = 0.9987$ for $y = 0.0045x$, a proportional trend between the number of the dressing passes and the dressing tool wear level was found. Such results showed that the structure of the natural diamond dresser can have a strong influence on the dressing results as well as on the dressing tool life. This result agrees with previous results obtained in Oliveira Junior *et al.* (2017); and Martins *et al.* (2014) where the diamond wear increase with increasing number of dressing passes was clearly evidenced.

Overall, the CVD diamond (Figure 45) presented more wear resistance than natural diamond (Figure 46) for the present application. One of the reasons if the fact that, unlike natural diamonds, CVD diamonds (i.g. synthetic diamonds made with PCD without binder) present very high fracture strength because of its homogenous polycrystalline structure. In addition, their wear resistance is the same in all directions, as reported by Jackson, Davim (2011).

5.1.2 Results and discussion on PZT diaphragms characterization

Figure 47 reports a plot of voltage signals in the time domain, for both diaphragms PZT#1 and PZT#2, detected during the PLB for both CVD and natural diamond dressing tools. The signals from PZT#1 were similar in terms of voltage levels for both CVD and natural diamond dressing tools. In contrast, the signals from PZT#2 presented a lower magnitude under the same conditions, which can be attributed to some minor distance differences between the two transducers and the PLB location due to asymmetric testing conditions. In addition, PZT characteristics, such as the capacitance, can vary up to 20%, according to Freitas; Baptista (2016); Freitas *et al*. (2017); and Silveira; Campeiro; Baptista (2017). The PSD of these signals was computed, as reported in Figure 48.

Figure 47- PLB results: Voltage signals

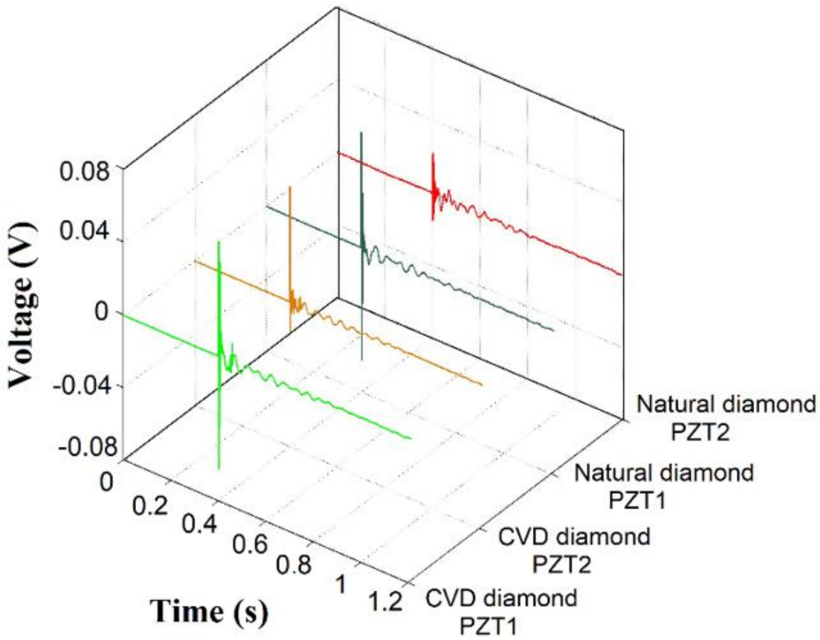

Source: Author

Figure 48 - PLB results: (a) frequency response analysis via PSD; and (b) enlarged view into the range of 0-100 kHz

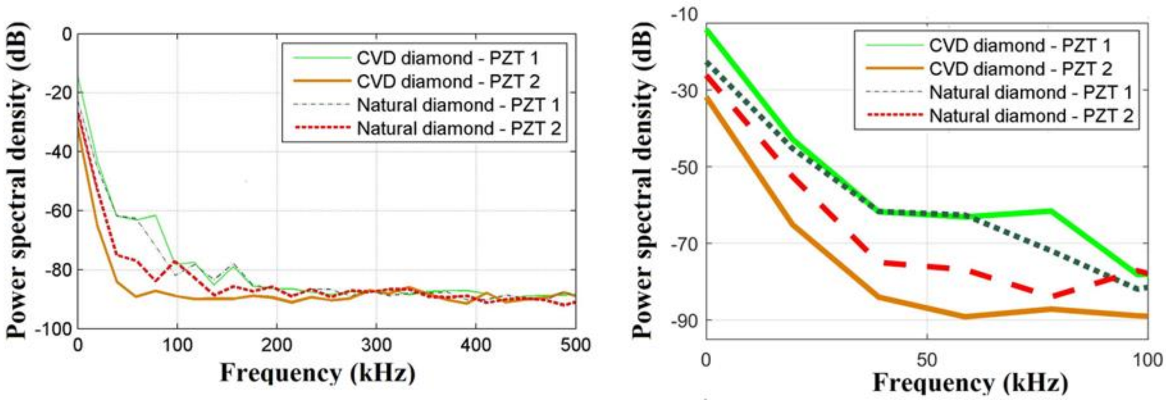

Source: Author

As expected, the same magnitude behavior as in the time domain is observed also in the frequency domain for both PZT#1 and PZT#2 diaphragms. However, according to the enlarged view into the range of 0-100 kHz shown in Figure 48b, magnitude differences can be better verified in the frequency domain, where a significant difference of up to 30 dB in CVD diamond dressing tool was observed for the PZT#1 (set at approximately at -60 dB) and PZT#2 (set at approximately at -90 dB). Also, the dresser diamond material (CVD and natural diamonds) influenced the PZT diaphragm frequency response as shown by the fact that the magnitude differences between both transducers are much smaller for the natural diamond dresser when compared with the CVD diamond dresser results. Moreover, it can be clearly noted that, in general, the transducers display more sensitivity in terms of damage detection for frequencies below 200 kHz.

5.1.3 Results and discussion on the NN-based machine learning performance

5.1.3.1 Impedance signatures behavior

It is worth mentioning that the different behaviors of the CVD and natural diamond dressers in terms of mechanical properties, as described in Fraimovitch *et al.* (2017) and Zhang, Chunhe; Shin (2003), can also contribute to the different behaviors of the impedance signatures for both PZT#1 and PZT#2 diaphragms, as shown in Figure 49. Furthermore, because impedance signatures differ, each transducer has a specific frequency range that is more relevant to analyze. To support this claim, it is possible to find examples in the literature (MARCHI *et al.*, 2015; SILVEIRA; CAMPEIRO; BAPTISTA, 2017). The frequency range was initially analyzed from 0 to 125 kHz. However, specific frequency bands that were more sensitive to damage are observed in Figure 49: the reference to the specific frequency bands allows analyzing the impact of each transducer mounting location (PZT#1 and PZT#2) as well as of each tool type (CVD and natural diamond dressing tools) on the sensitivity of the monitoring approach for dressing tool damage condition identification. Figure 49 also shows that impedance signatures are significantly different for diverse experimental conditions.

According to results presented in Figure 49, the proposed sensor monitoring approach was able to detect structural damage in dressing tools, for all the considered test conditions, since considerable impedance signature variations can be observed between healthy (H) and damaged tool conditions (wear levels). The effectiveness of the proposed sensor monitoring approach for tool wear detection can be additionally evaluated through an analysis based on the RMSD and CCDM damage indices, calculated for the frequency ranges displaying the highest sensitivity to tool wear. However, the selection of the most appropriate frequency ranges for the RMSD and CCDM indices calculation needs to be carried out through analytical approaches or machine learning paradigms (BAPTISTA; VIEIRA FILHO 2010; HUYNH; DANG; KIM, 2018; YANG; DIVSHOLI 2010). As previously mentioned (Chapter 4), present research work considered an ANN-based machine learning approach, whose results are presented in the next subsection.

Figure 49 - Impedance signatures for both PZT1 and PZT2 diaphragms

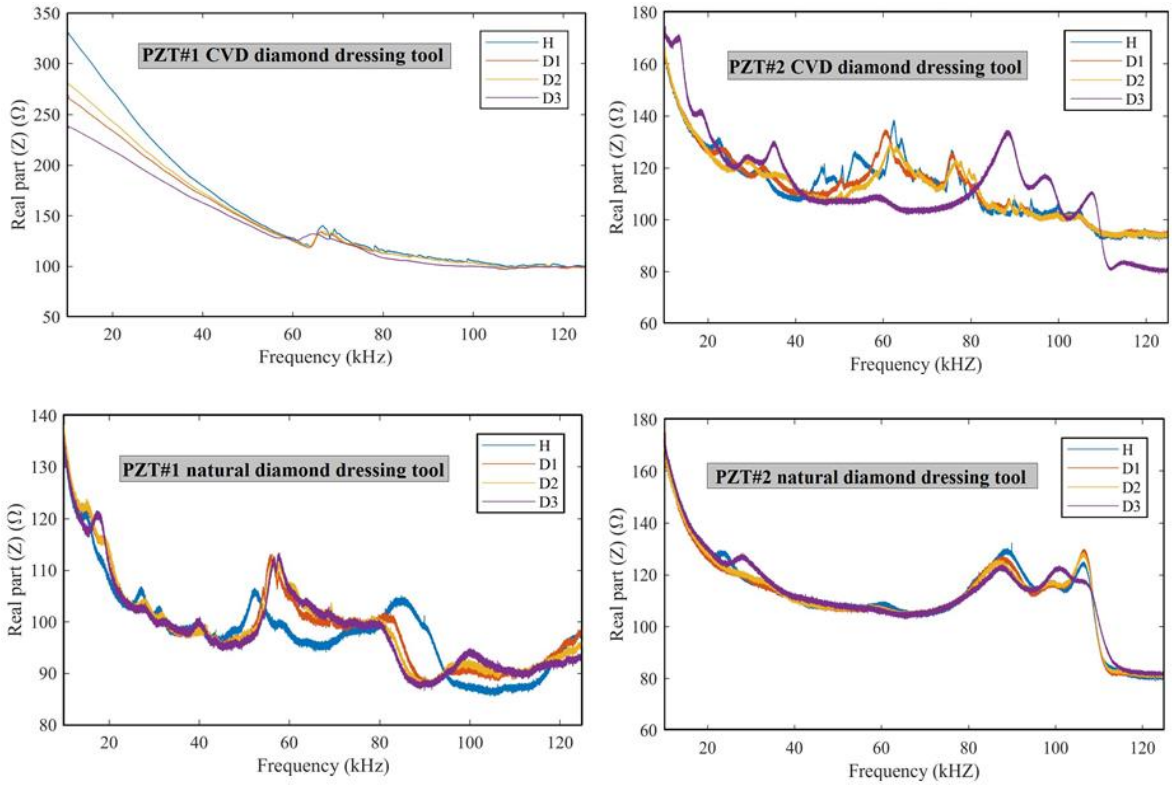

Source: Author

5.1.3.2 NN performance assessment through confusion matrix and *k*-NN-based decision boundary graphic: CVD diamond dressing tool

This subsection presents the validation process following the training performed with the NN using the LVM BP algorithm for each NN model constructed as reported in Chapter 4. The main characteristics of each model are presented in Table 11. In order to identify the best frequency range to be utilized, an average error was computed for each combined frequency sub-ranges considered. Table 11 shows that the combined feature vector related to the combined frequency sub-ranges [*@fb#3* + *@fb#4*], corresponding to [40-60 kHz + 60-80 kHz], presented the lowest overall testing error for CVD diamond dresser wear classification. This combined feature vector presented a high percentage of testing errors for some models, in particular, *model#2* and *model#4*. However, when compared with the other two combined frequency sub-ranges, this combined feature vector provides a much better accuracy. It worth mentioning that the other two combined feature vectors presented errors higher than 10 % for some models, in particular model *#2* and *#3* for combined feature vector [*@fb#1* + *@fb#2*], and *model#3* for combined feature vector [*@fb#5* + *@fb#6*] (Table 11). On the other hand, the errors of the combined feature vector related to the combined frequency sub-ranges [*@fb#3* + *@fb#4*] were lower by 10% for all models, which is an interesting result for real-time monitoring implementation. In summary, this combined feature vector presented an average error of 3.2%, against 9.1 % and 6.5% for the other two combined feature vectors, and its standard deviation was 2.6%, against 8.1% and 5% for the other two combined feature vectors.

From Table 11, it can be seen that the best NN models for the combined feature vector related to the combined frequency sub-ranges [40-60 kHz + 60-80 kHz] were *model#1* (using PZT#1 transducer and RMSD metric) and *model#3* (using PZT#2 transducer and RMSD metric) presenting errors of 1.1% and 0.9%, respectively.

Table 11- Mean features of NN models for CVD diamond dresser

Input models		**Combined frequency bands**		
		@fb#1 (0-20 kHz) *@fb#2*(20-40kHz)	*@fb#3*(40-60 kHz) *@fb#4*(60-80 kHz)	*@fb#5* (80-100 kHz) *@fb#6*(100-120 kHz)
model#1	PZT#1 RMSD	1.7 %	1.1 %	9.8 %
model#2	PZT#1CCDM	14.5 %	5.9 %	2.6 %
model#3	PZT#2 RMSD	17.6 %	0.9 %	11.9 %
model#4	PZT#2 CCDM	2.6 %	5.2 %	1.9 %
Average error		**9.1 %**	**3.2 %**	**6.5 %**
Standard deviation		**8.1**	**2.6**	**5**

Table 12 shows the main characteristics resulting from the two best NN models identified during the validation phase. The first column shows the considered parameters in the feature extraction process: combined feature vector, neuron structure, training function and k-NN rule for dressing tool wear classification. The second column reports the specifications for each parameter. According to the results, both *model#1* and *model#3* presented a simple structure with three hidden layers of 10-10-5 neurons and two hidden layers of 5-15 neurons, respectively, which is very attractive in terms of implementation effectiveness. Further comparisons and analyses are illustrated in Figure 50 and Figure 51, where confusion matrices and decision boundary graphics present the best NN performances for CVD diamond dresser wear classification. Confusion matrices are often used to summarize the performance of a classification model (MARTINS, CESAR H. R. *et al.*, 2014). Accordingly, the results of *model#1* and *model#3* are presented in Figure 51a and Figure 51b, respectively.

Table 12- Mean features of the best NN models for CVD diamond dresser

Parameters	Specification	
Best input model of the test	PZT#1 CVD RMSD *model*#1	PZT#2 CVD RMSD – *model*#3
Structure (layers and neurons)	2 - 10 - 10 - 05 – 3	2 -05 - 15 - 00 - 3
Feature vector	[@*fb#3* + @*fb#4*]	
Optimally combined frequency sub-ranges	[40-60 kHz + 60-80 kHz]	
Training function	LVM BP	
Max number of epochs	2000	

Figure 50- Confusion matrices of the best NN models for CVD diamond dresser: (a) *model#1*; (b)*model#3*

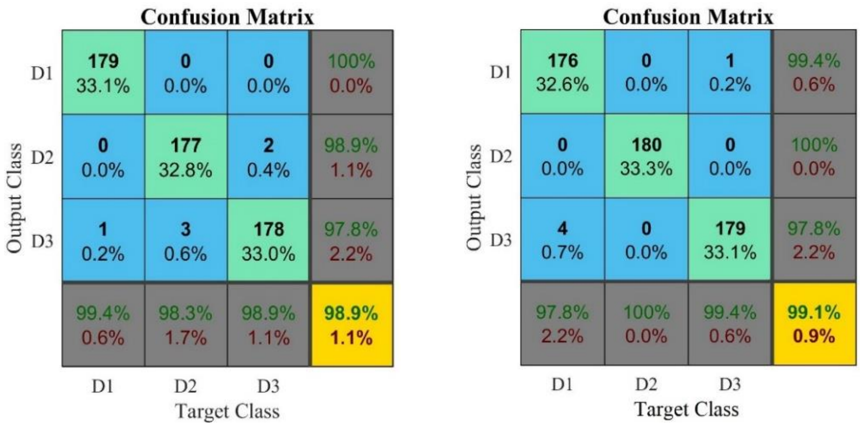

(a) (b)

Source: Author

As regards *model#1* (Figure 50a), for the D1 damage class, the NN presented a predictive capability of 100 % and a sensitivity of 99.4 %. For D2, the predictive capability was 98.9% and the sensitivity was 98.3%, corresponding to the occurrence of false-positive diagnostics. For D3, the confusion matrix showed a predictive capability of 97.8 % and a sensitivity of 98.9 %. The overall accuracy rate of the NN for *model#1* was 98.9 %, which is attractive for actual implementation.

Figure 50b presented the results of *model#3*: the overall accuracy rate of the NN for this model was 99.1 %, i.e. the network was able to accurately distinguish the data at this level of tool wear and the features were classified correctly. For the D1 damage class, the NN presented a good performance: 99.4 % and 97.8 % for predictive capacity and sensitivity parameters, respectively. For D2, both predictive capability and sensitivity parameters were 100%. For D3, the predictive capacity was 97.8%, corresponding to false negatives, and the sensitivity was 99.4%. For this reason, this model is very attractive in terms of practical implementation for dressing tool condition monitoring. This result agrees with the findings related by Martins *et al.* (2014) where most of the best NN models, with small overall classification error, also presented false negatives for the worn dresser condition (e.g. the NN predicted that the dresser was in half-life condition whereas it was fully worn instead).

Figure 51 reports the decision boundary graphics based on the *k*-NN classifier for the best models achieved by NN for CVD diamond dresser, according to Table 11.

Figure 51- *k*-NN results via decision boundary graphics for CVD diamond dresser (a) *model#1 and (b) model#3*

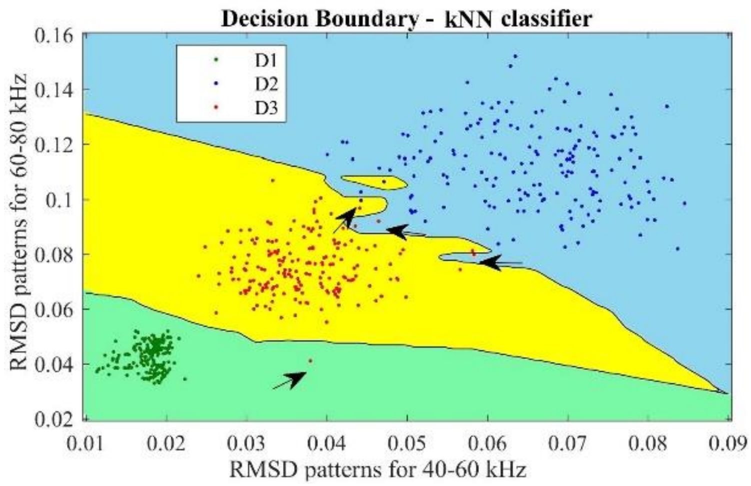

Source: Author

(a)

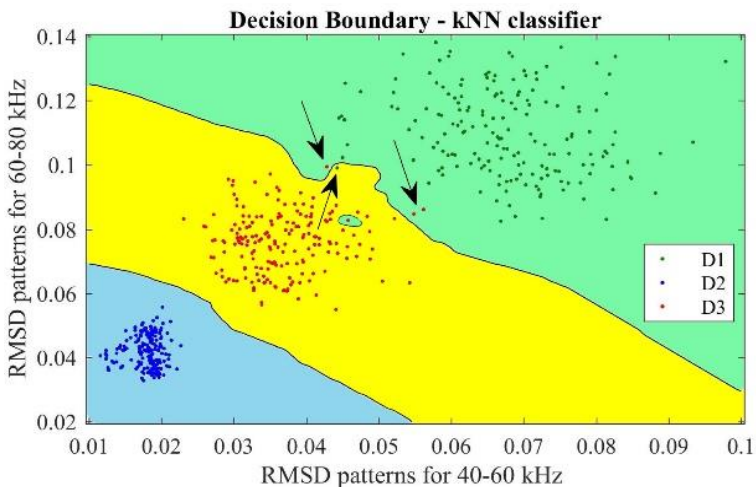

(b)

Source: Author

Boundary regions graphic is a visual way to analyze the results of the k-NN procedure; this approach is based on an overfitting process, according to Franc; Hlavác (2004). In this kind of graph, the location of each point refers to the real damage condition, while its color shows the classification performed by the *k*-NN based on the successful training of the NN. In Figure 51, the arrows indicate the features that have not been classified correctly.

Since *model#1* and *model#3* presented good results, the classification performance is very high with only a few numbers of features misclassified in the k-NN procedure. In Figure 51a (*model#1*), it can be observed that some features belonging to the D3 damage class were classified as D1 and D2. On the other hand, only one feature belonging to the D2 damage class was classified as D3. In Figure 51b (*model#3*), it is possible to see that one feature belonging to the D1 damage class was classified as D3 as well as some features belonging to D3 were classified as D2. This result again agrees with the literature, since most of the damage features erroneously classified occurred in regions close to the borders, as reported in Oliveira Junior *et al.* (2017) in which the authors did not consider them as serious errors because these boundaries can be difficult to determine.

5.1.3.3 NN performance assessment through confusion matrix and *k*-NN-based decision boundary graphic: natural diamond dressing tool

This subsection presents the results obtained from the NN models for the testing series with the natural diamond dresser. The main characteristics of each NN model are reported in Table 13, following the same characteristics previously adopted for testing series with CVD diamond dresser (Table 11). From Table 13, it can be seen that the combined feature vector related to frequency sub-ranges [*@fb#3* + *@fb#4*], corresponding to [40-60 kHz + 60-80 kHz], again presented the lowest overall error equal to 2.8 % against 12.8 % and 5.8 % for the other two combined frequency sub-ranges. Again, this combined feature vector presented a high percentage of testing errors for some models, such as *model#6* and *model#8*. However, when compared with the other two combined frequency sub-ranges, its performance was much better. It is worth mentioning that, according to Table 13, again the other two combined feature vectors displayed testing errors > 10% for some models, which is not attractive in terms of accuracy for actual implementation. Besides this, for the natural diamond dresser, the testing errors of the best-combined feature vector were less than 10%, and the NN models presented a much better accuracy than all other combinations. This result is very interesting for real-time system monitoring implementation.

It is clear from Table 13 that the best models for the combined feature vector related to the combined frequency sub-ranges [40-60 kHz and 60-80 kHz] were *model#5* (using PZT#1 transducer and RMSD metric) and *model#7* (using PZT#2 transducer and RMSD metric) with testing errors 1.1% and 0.9%, respectively. This means that the RMSD metric presented better results than the CCDM metric for both testing series (CVD and natural diamond dressers). Table 14 reports the main characteristics for both best models identified in the validation step, following the same characteristics previously adopted for testing series with CVD diamond dresser. According to the results, both *model#5* and *model#7* presented a simple structure with three and two hidden layers with 5-5-5 and 5-15 neurons, respectively, which again is very attractive in view of implementation. Accordingly, these results are consistent with the previously reported results for testing series with CVD diamond dresser and confirm the validity of the proposed approach for a broader situation.

Table 13- Mean features of the NN models for natural diamond dresser

Input models		**Combined frequency bands**		
		@fb#1 (0-20 kHz) *@fb#2*(20-40kHz)	*@fb#3*(40-60 kHz) *@fb#4*(60-80 kHz)	*@fb#5* (80-100 kHz) *@fb#6*(100-120 kHz)
model#5	PZT#1 RMSD	45.2 %	1.1 %	9.3 %
model#6	PZT#1CCDM	1.7 %	4.8 %	2.4 %
model#7	PZT#2 RMSD	1.7 %	0.6 %	8.9 %
model#8	PZT#2 CCDM	2.8 %	5.0 %	2.6 %
Average error		**12.8 %**	**2.8 %**	**5.8 %**
Standard deviation		**21.5**	**2.3**	**3.8**

Table 14- Mean features of the best NN model for natural diamond dresser

Parameters	**Specification**	
Best input model of the test	PZT#1 CVD RMSD *model*#5	PZT#2 CVD RMSD *model*#7
Structure (layers and neurons)	2 - 05 - 05 - 05 – 3	2 -05 - 15 - 00 - 3
Input pattern	[*@fb#3* + *@fb#4*]	
Optimal combined frequency ranges	[40-60 kHz + 60-80 kHz]	
Training function	LVM BP	
Max number of epochs	2000	

In Figures 52 and 53, respectively, confusion matrices and decision boundary graphics present the best NN performance for natural diamond dresser. Figure 52a shows the confusion matrix for *model#5*. For damage class D1, the predictive capability was 99.4 %, corresponding to the occurrence of only one false positive, and the sensitivity was 97.2 %. For damage class D2, the NN presented a very high performance with 100% for both predictive capability and sensitivity. For damage class D3, the sensitivity was 99.4 % and the predictive capability was 97.3 %. The overall accuracy rate of the NN for this combined feature vector was 98.9 %, which is a decidedly attractive result for dressing tool condition monitoring. Figure 52b shows the confusion matrix for *model#7*. The results of this NN model showed the best performance of all cases presented in experimental test case *#1* as its overall accuracy rate was 99.4 %, i.e. very close to 100 %, with only 0.6 % of testing error (Table 13). For this reason, this NN model is very attractive for actual implementation at low-cost in industrial grinding processes. For damage condition D1, the NN presented 98.4 % of predictive capability and 100 % of sensitivity. For damage condition D2, the predictive capability was 100 % and the sensitivity was 98.3 %. For damage class D3, both sensitivity and predictive capability were 100%.

Figure 52- Confusion matrices of the best NN model for natural diamond dresser: (a) *model#5*; and (b) *model#7*

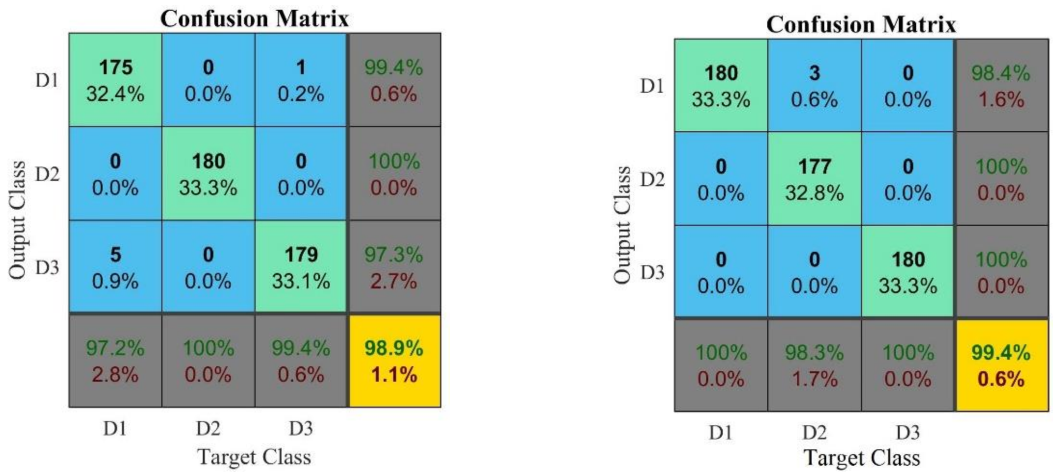

(a) (b)

Source: Author

For testing series with natural diamond dresser, the results show that the proposed approach provides for a more robust diagnosis as the system was able to diagnose the catastrophic tool failure that the natural diamond dresser suffers at 300 dressing passes. This result is in agreement with the results obtained for CVD diamond dresser, where the overall accuracy rates were similar and close to 100%.

Figure 53 shows the decision boundary graphics based on the *k*-NN classifier for the best model achieved by the NN to the testing series with the natural diamond dresser, according to Table 13.

Figure 53- *k*-NN results via decision boundary graphics to the best NN models for natural diamond dresser: (a) *model#5*; and (b) *model#7*

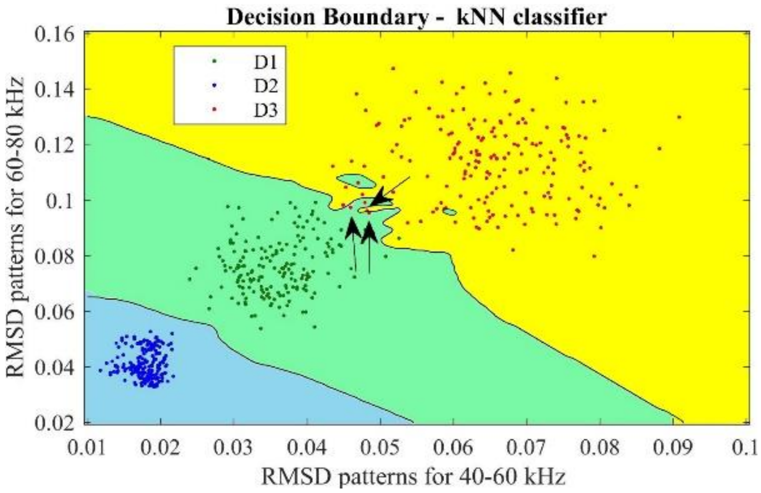

(a)

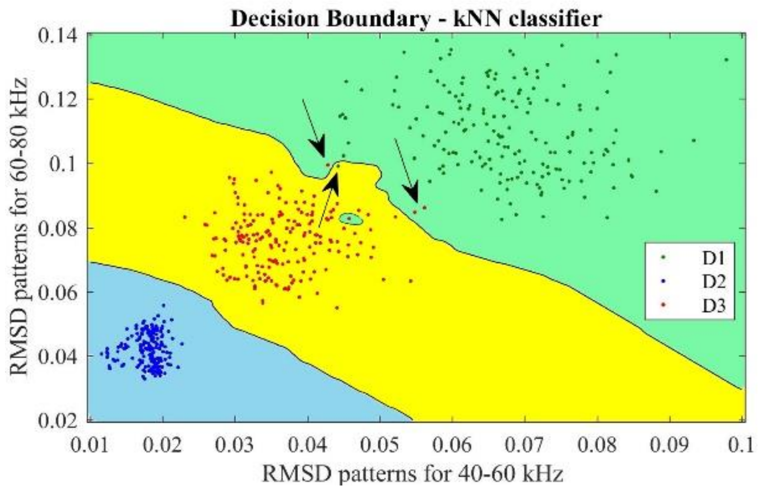

(c)

Source: Author

Again, this result is consistent with the previous results obtained in the present research work to the CVD diamond dresser, as well as with those obtained in literature (Oliveira Junior *et al.* (2017), Martins *et al.* (2014)) cited before, since, the *model#5* and *model#7* presented good and accuracy results. This way, only a few numbers of patterns were not classified correctly in the *k*-NN process. In Figure 53a (*model#5*), and in Figure 53b (*model#7*), it can be observed that some features pertaining to D3 class were classified as D2. On the other hand, only one feature pertaining D2 class was classified as D3. Note that, again the damage features erroneously classified occurred in regions close to the borders, which is not a big problem, as related in Oliveira Junior *et al.* (2017).

5.2 Results of the experimental test case #2

This section presents the results obtained with experimental test case #2. To this end, only the most representative results obtained through the defuzzification process is presented. Therefore, after testing those 12 frequency sub-ranges, only two of them were chosen, i.e. 40-50 kHz and 110-120 kHz, from which the proposed fuzzy logic system presented its best performance (i.e. the other ten frequency sub-ranges presented considerable overall testing errors and were not suitable for the proposed approach).

At first, the macro images of the dressing tool (top views) are shown in Figure 54. As shown in Figure 54, it is possible to see the different locations of the diamond sticks, as well as the induced damages (P1, P2, and P3). With respect to the fuzzification process, Table 15 presents the membership functions information based on the rules previously extracted.

Figure 54 – Damage induction results

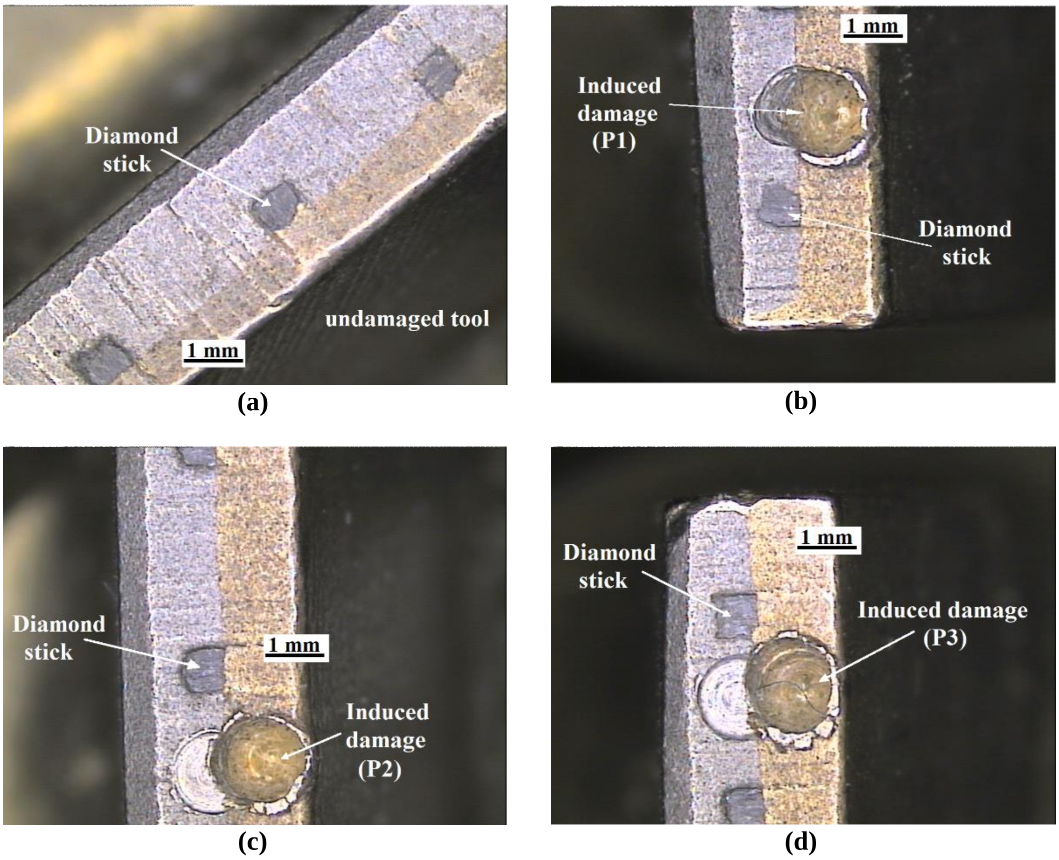

Source: Author

Table 15- Fuzzification results

Best	**RMSD**			**CCDM**			**Output (mm)**		
@fb#	MF1	MF2	MF3	MF1	MF2	MF3	MF1*	MF2*	MF3*
40-50 kHz	[$1.2*10^5$ $2.4*10^5$]	[$3.41*10^5$ $1.7342*10^6$]	[$5*10^5$ $3.0105*10^6$]	[0.0441 0.392]	[0.0518 0.6021]	[0.111 1.1290]	[1.9 2.5]	[1.9 8.5]	[1.9 13.5]
110-120 kHz	[$2.5*10^5$ $8.44*10^5$]	[$1.06*10^5$ $1.7610*10^6$]	[$7.31*10^5$ $3.8393*10^6$]	[0.1192 0.1]	[0.0887 0.4343]	[0.206 1.1296]	[1.9 2.5]	[1.9 8.5]	[1.9 13.5]
	[$2.8*10^5$ $8.45*10^5$]	[$1.44*10^5$ $2.1099*10^6$]	[$3.2590*10^5$ $3.71*10^6$]	[0.0558 0.3]	[0.0372 0.60]	[0.1010]	[1.9 2.5]	[1.9 8.5]	[1.9 13.5]

MF1 – membership function 'Low':'gaussmf'
MF2 – membership function 'Medium':'gaussmf'
MF3 – membership function 'High':'gaussmf'
MF1* – membership function 'Position 1':'gaussmf'
MF2* – membership function 'Position 2':'gaussmf'
MF3* – membership function 'Position 3':'gaussmf'

The intervals of the membership functions are in accordance with the knowledge of the problem (dressing tool damage information), i.e. the interval between $1.2*10^5$ and $3.71*10^6$ that is related to the terms linguistic Low, High, and Medium, respectively (MF1, MF2, and MF3 in Table 15), represents the input pattern corresponding to the RMSD metric. In a similar way, the interval between 0.0441 and 1.137 represents the feature pattern corresponding to the CCDM metric. On the other hand, the interval between 1.9 and 13.5 of the output membership functions (i.e.: the clusters P1, P2, and P2 previously defined) corresponding to the position of the induced damages at the dressing tool (for this reason, these values are given in millimeters).

Based on the set of rules previously obtained, two fuzzy models that represent the frequency sub-ranges of 40-50 kHz, 110-120 kHz, respectively, were initially generated. Firstly, to observe the input and output effects of the fuzzy models, 3D surfaces were obtained. Secondly, a matrix consisting of distinct values (PZT#2 database) that were not used before was taken into account to validate the proposed fuzzy system. Then, the process of defuzzification could be initiated in order to verify the effectiveness and robustness of the proposed approach.

Figure 55 shows the 3D surfaces generated for the fuzzy model related to the frequency sub-range of 40-50 kHz. It is possible to see at different colors the clusters P1, P2, and P3 well defined in areas in relation to the set of rules. Based on Figure 55, it is possible to confirm that the combined inputs resulted in different influences on damage location in the dressing tool. Furthermore, according to the rules surface, when the RMSD and CCDM have a low value, the damage cases reach the position 1 (P1). On the other hand, when the RMSD and CCDM have intermediate values, the damage cases reach position 2 (P2). Similarly, when the RMSD has an intermediate value and CCDM has a high value, the damage cases also reach the position 2 (P2). Finally, when the RMSD and CCDM have high values, the damage cases reach the position 3 (P3). This model, however, presents some discontinuities and abrupt transitions at the boundaries of the areas, which occurs due to the range of values of the damage metrics RMSD and CCDM corresponding to the frequency sub-range of 40-50 kHz. In addition, this result is in agreement with (ALEXANDRE *et al.*, 2018), i.e. during the evaluation of the grinding wheel condition through fuzzy models, the average and standard deviation values of the ROP metric had a high influence on the smoothness of transitions on 3D surfaces.

Figure 56 shows the response of the proposed approach to the fuzzy model that corresponds to the frequency sub-range of 40-50 kHz. The matrix has three distinct regions that represent those three clusters P1, P2 and P3, which were named as Position 1, Position 2 and Position 3, respectively. The defuzzified values (μ) were normalized between 0 and 1.

Figure 55 -3D surface generated to the fuzzy model corresponding to 40-50 kHz

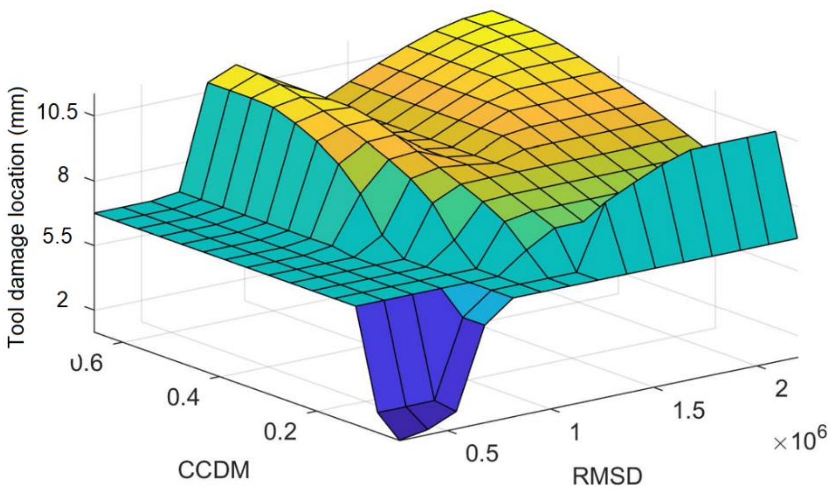

Source: Author

Figure 56 - Validation results considering the fuzzy model corresponding to 40-50 kHz

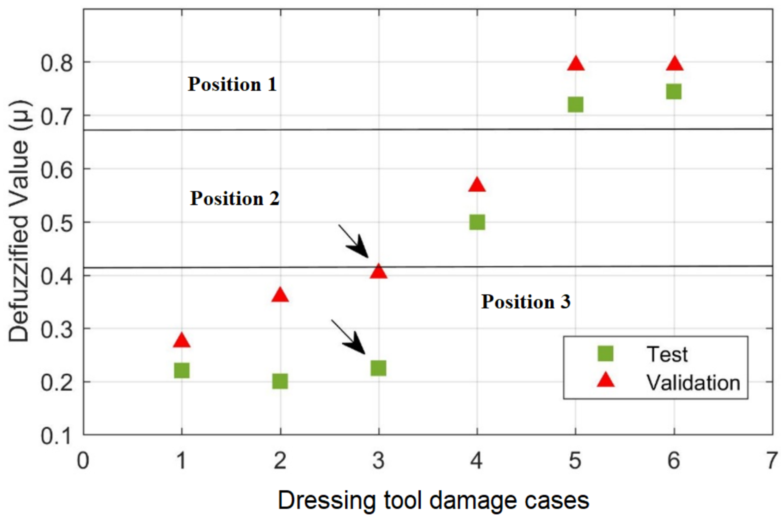

Source: Author

The result showed in Figure 56 indicates high assertiveness with only one case for test and one for validation (corresponding to D3 damage case) that were misclassified, i.e. the fuzzy system classified the location of the damage as Position 1 (P1) while it is, in fact, a damage that was induced at Position 2 (P2). On the other hand, the error case corresponding to the validation database, however, is located very close to the border. In accordance with literature (Alexandre *et al.* (2018), Miranda *et al.* (2015)), it is not a serious error in practical applications, since, when the system scores damage near the line corresponding to the real region it is reasonable to assume that the error is asymptotically normal due to distribution based on process uncertainty. In addition, it is important to point out that this defuzzification was acceptable in terms of accuracy rate taking into account possible cases with no clear symptoms, i.e. those damage cases that present high similarity between their values and limits. This assumption is made in accordance with related literature (ALEXANDRE *et al.*, 2018; KATUNIN; AMAROWICZ; CHRZANOWSKI, 2015; MIRANDA *et al.*, 2015)

Figure 57 shows the 3D surfaces generated for the fuzzy model related to the frequency sub-range of 110-120 kHz. In contrast with the 3D surfaces of the previous model, the surfaces of Figure 57 presented a better symmetry. In addition, the distinct areas corresponding to the clusters P1, P2 and P3 are better defined. However, both abrupt and smooth transitions are observed between areas. Furthermore, it is possible to confirm in Figure 57 certain stability, in terms of performance at the same level, to the intermediate values for both RMSD and CCDM metrics as expected, since, this area corresponds to the P2 cluster, which is responsible to divide the low and high values. Again, it is possible to confirm the different influences of the input combination on the results based on the same reasons supported before.

Figure 58 shows the response of the proposed approach to the fuzzy model that corresponds to the frequency sub-range of 110-120 kHz. In this case, it is possible to see only one case of error related to the D1 damage case corresponding to the PZT#1 database (test). This way, the fuzzy system scored the case as damage at Position 2 (P2) while it is, in fact, the damage that was induced at Position 1 (P1). Therefore, in terms of practical applications this model was one of the best with the highest assertiveness between results of this research work. Based on the same reasons supported before (e.g. high similarity between values and limits, and accuracy rate taking into account possible cases with no clear symptoms), in terms of practical implementation, the error of this model is not considered serious and the defuzzification was acceptable.

Figure 57 -3D surface generated to the fuzzy model corresponding to 110-120 kHz

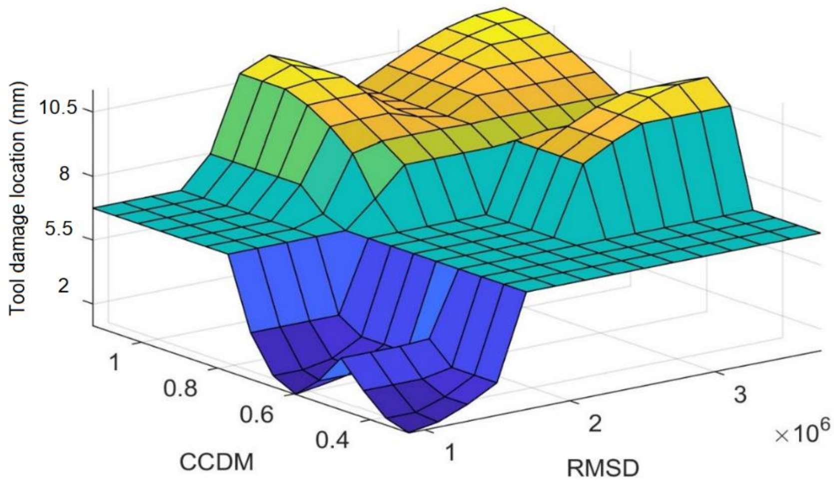

Source: Author

Figure 58 - Validation results considering the fuzzy model corresponding to 110-120 kHz

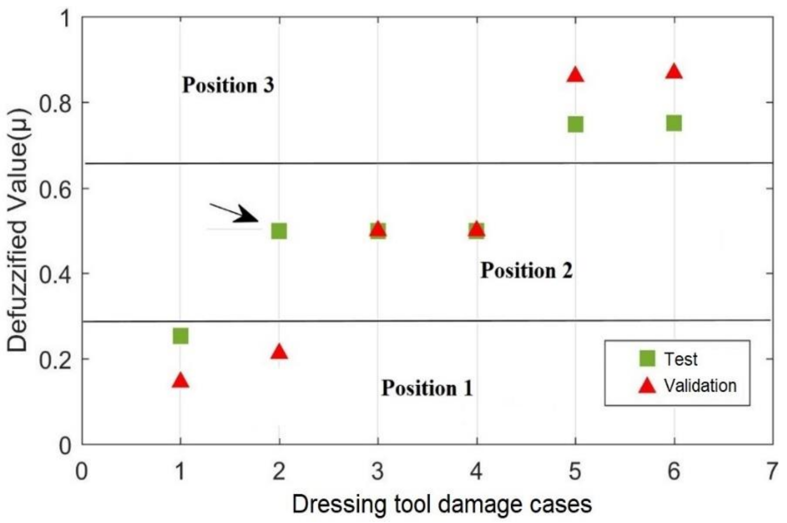

Source: Author

In order to verify the effectiveness of the proposed approach for a more robust situation than that studied before, an additional model was generated to be considered as input. To this end, those two models that presented the best results with the proposed fuzzy system were taking into account, i.e. the frequency sub-ranges of 40-50 kHz and 110-120 kHz, respectively. Therefore, Figure 59 shows the 3D surfaces generated for the fuzzy model related to this combination. It is possible to see a greater number of levels between the areas of the clusters P1, P2 and P3 (low, medium and high values) due to the broader range of values for both RMSD and CDDM metrics. Smooth transitions at different levels of damage, in addition to a good surface symmetry, are also observed in Figure 59.

Figure 59 -3D surface to the fuzzy model corresponding to 40-50 kHz and 110-120 kHz

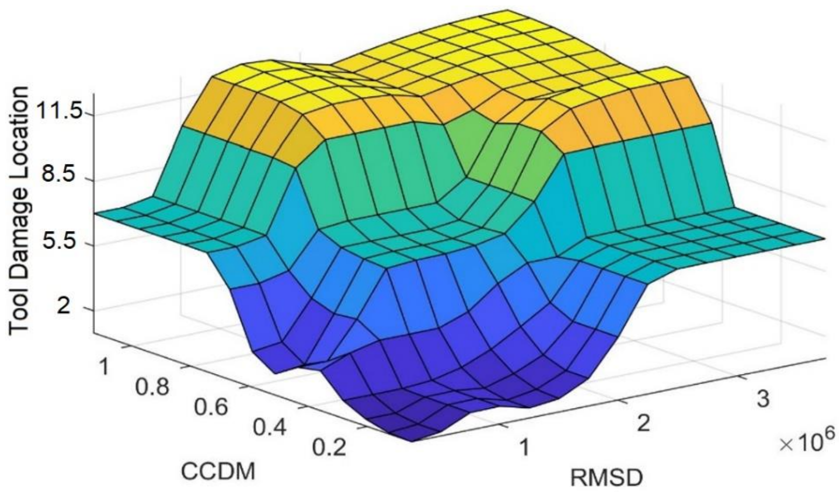

Source: Author

Note that the combined inputs again resulted in different influences on the final damage location, in particular in this case in view of the two frequency bands used together. In (MIRANDA *et al.*, 2015), in order to monitor the wear of single-point dressing tools using fuzzy models, authors also tested a model considering different frequency sub-ranges as input (210-260 kHz and 0-13 kHz between ROP and RMS of AE and vibration signals). With two inputs, the fuzzy model proposed by authors presented good results and proved to be effective and easier to implement for predicting the dressing tool wear. Figure 60 shows the response of the proposed approach to the fuzzy model related to the combination of the frequency sub-ranges of 40-50 kHz and 110-120 kHz, respectively.

The result given in Figure 60 indicates a good assertiveness with a few numbers of misclassified cases taking into account the number of inputs and the accuracy rate of the fuzzy system for possible cases with no clear symptoms. This way, one case corresponding to PZT#2 database was classified as damage at Position 1 (P1) while it is, in fact, a damage that was induced at Position 2 (P2). Another case, corresponding to both PZT#1 and PZT#2 databases, was classified as damage at Position 2 (P2) while it is, in fact, the damage that was induced at Position 3 (P3). Finally, one last error occurred to a case corresponding to PZT#2 database that was classified as damage at Position 2 (P2) while it is, in fact, damage that was induced at Position 3 (P3). Furthermore, an example of the tool damage location is presented in Figure 61.

Figure 60 - Validation results considering the fuzzy model corresponding to 40-50 kHz + 110-120 kHz

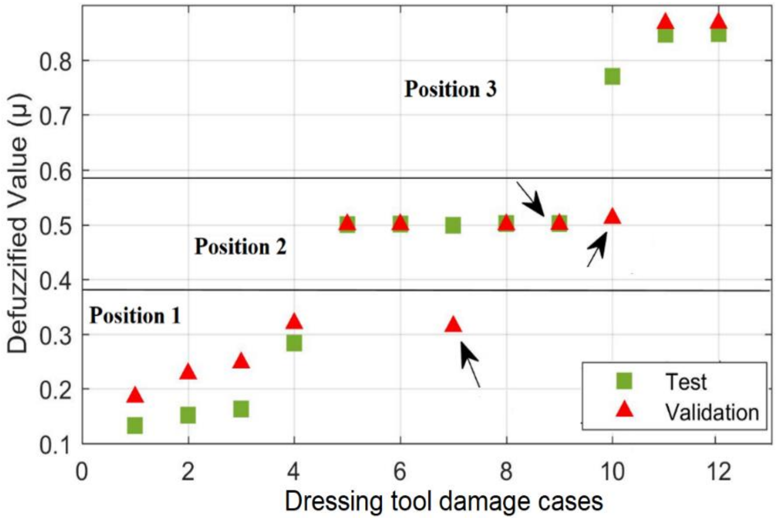

Source: Author

Figure 61 - Validation results considering the fuzzy model corresponding to 40-50 kHz and 110-120 kHz

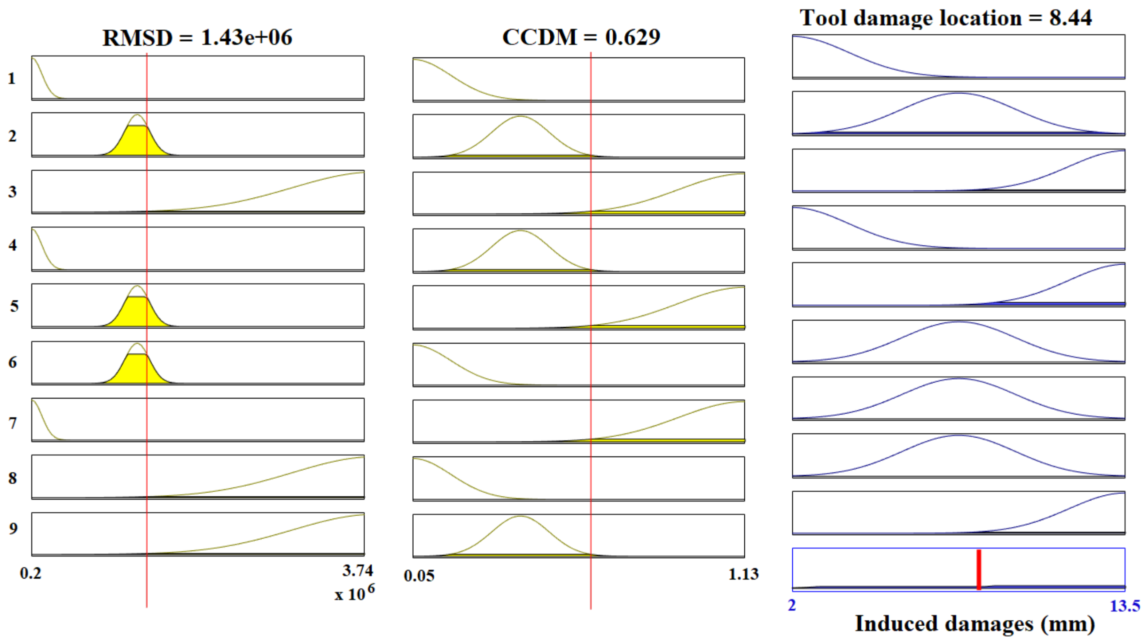

Source: Author

Therefore, based on the set of rules previously extracted, Figure 61 shows the inputs (first two columns related to RMSD and CCDM) and the output (last column where the numeric values corresponding to the real damage location given in millimeters). As a case study, the given values of RMSD and CCDM corresponding to the induced damage at Position 2 (P3) were used. This way, Figure 60 shows the inputs (RMSD equal to 1.43*10^6 and CCDM equal to 0.629) and the output of the system (position equal to 8.44 mm). The real damage location, however, was at 8.50 mm. A similar result was obtained in the research of Vieira *et al.* (2007), where fuzzy techniques were applied to detect corrosion at flat structures using impedance-based SHM. To this end, five cases of corrosion were induced at different locations of an aluminum flat structure. Representative damage indexes were obtained for each case and a fuzzy-based meta-model was built for prediction purposes. Similar to the present work, authors also verified the position of the corrosion by plot a graphic like that shown in Figure 61. In a similar way, the predict position of the corrosion was different from the real position for some cases (predict position was equal to 4.43 cm against the real position equal to 6.25 cm). According to these authors, many factors can be responsible for the correct tuning of the identification system such as the definition of the irregular fuzzy sets for the inputs and output, and the number of discrete points used to represent the membership functions.

Nevertheless, although errors showed in Figure 60 and Figure 61, the results are consistent and agreement with related literature cited above, since, this model proved to be more robust against previous models in view of the input number. Accordingly, in terms of practical application a fuzzy model that considering two different frequency bands is more attractive for the manufacturing industry, engineers and technicians responsible for the grinding and dressing operation than those that are limited to only one frequency band. However, this model is considered more complex in terms of implementation than those previous models because of the number of rules.

Chapter 6

CONCLUSION AND FUTURE DEVELOPMENTS

This chapter concludes the thesis, summarizing its contributions to the existent knowledge, as well as future developments and challenges

6.1 Conclusion

This research work presented an approach for TCM in the dressing process through EMI and machine learning. The effectiveness of the proposed approach was evaluated on the basis of two broad experimental tests. To carry out the experimental test case #1, a first testing series with a stationary single-point dresser made of CVD diamond and a second testing series with a stationary single-point dresser made of natural diamond was performed to study the tool wear development. Three damage classes (i.e.: D1, D2, and D3) were obtained for both testing series (CVD and natural diamond dressers) for comparison purposes with baseline (fresh tool). Microscopic analyses of the dresser wear state were essential to support the results, since, the tool wear increased as the dressing passes took place. Likewise, the dressing tool information was analyzed by considering the real part of the impedance signatures that were obtained with two PZT diaphragms attached to the dressing tool holder. Moreover, an ANN-based machine learning approach was proposed to construct an intelligent diagnosis system whose representative features were learned directly from the dressing tool condition information obtained from RMSD and CCDM metrics at six-frequency sub-ranges carefully chosen. At the end, the proposed intelligent diagnosis system was able to promote the tool wear level classification on the basis of the optimal frequency band recognized in the learning validation process. Furthermore, the frequency sub-ranges most sensitive achieved, which were 40-60 kHz and 60-80 kHz, respectively, showed less than 2% of general average errors to determine the feature patterns of the dressing tools through D1, D2, and D3 classes. Accordingly, the best models showed overall testing errors of 0.6%, 0.9%, and 1.1 %, considering the RMSD metric, which was most sensitive than CCDM for both CVD and natural diamond dressers.

To confirm the results, the research activities proposed in this thesis were also tested for a multipoint dressing tool. To this end, an additional experimental test (experimental test case #2) was conducted on a multipoint stationary dresser made of CVD diamonds. Six different damage scenarios were induced by drilling holes at three distinct positions (P1, P2, and P3) and impedance signatures were acquired from two PZT diaphragms attached to the dressing tool body. A fuzzy logic model was implemented and validated on the basis of the dressing tool damage information extracted from the representative damage indices RMSD and CCDM at various frequency sub-ranges. The results indicated that the frequency sub-ranges of 40-50 kHz and 110-120 kHz achieved much better accuracy than others to determine the damage location by those defined clusters: P1, P2, and P3, respectively. The best fuzzy model was further obtained through the combination of these two frequency sub-ranges (40-50 kHz + 110-120 kHz). This model presents high assertiveness with a minimum number of errors that are acceptable in terms of accuracy rate taking into account possible cases with no clear symptoms. In addition, in terms of practical application, a fuzzy model that considers two different frequency bands is more attractive than those that are based on a single one.

Overall, the research activities proposed in this thesis involved in diagnosing different wear and failure ranges on dressing tools through experimental tests of dressing operation into different dressing conditions. The proposed system was also tested for sensory position independence and for different types of stationary dressing tools to ensure its capability for real-time application. The experimental results provided high diagnostic accuracy for dressing tool condition monitoring and opens the door for its wide application in industrial grinding operations. Accordingly, the effective implementation of the proposed approach for grinding processes in industry can be taken into account in CNC machines at low cost and without significant changes in the usual cycle times due to the simplicity of the EMI technique and its inexpensive PZT transducers. From this, a cut in manufacturing costs can be expected because the tool replacement will be based on the actual tool condition, i.e., the proposed approach avoids that the dressing tool being substituted before their end of life or that the dressing operation being performed with damaged tools Finally, the application of machine learning algorithms, such as ANNs and fuzzy logic has a great potential to improve the impedance-based grinding process monitoring due to the very high sensitivity to the differences in process conditions and the success in adapting to uncertainties. In addition, after the appropriated training process (wich take two hours of timeframe for the present application), these algorithms completed their tasks in a reasonable timeframe (few minutes).

6.2 Future developments, outlook, and challenges

While the use of the EMI method for SHM applications is increasing every day, manufacturing process monitoring through the EMI is in the very beginning stage of research. On the other hand, as the Industry 4.0 approaches, an efficient sensor monitoring system lies within multi-functional sensing applications, giving the possibility of the EMI method not only to SHM but also to be used in smart factories for advanced monitoring of machining operations. Essentially, future manufacturing maintenance technology can demand such a technique as the EMI is suitable for detecting damage at a very early stage. However, one of the main challenges regarding the implementation of the EMI method is the effects caused by environmental conditions, which may severely affect the process of damage diagnosis. Owing to that, the SHM based on the EMI method has been conducted mainly under a well-controlled environment. On the other hand, the present research work showcases a sample of real applications: targeting a grinding case with particular focus to the stationary dressing process. The most critical problems identified were: (i) the need for a temperature control procedure in the factory floor; (ii) the robustness of the results obtained which were valid only for the particular conditions adopted in the present research work. Future research work, however, will entail deeper studies of the dressing tool configuration to include rotary dressing tools and different dressing conditions. In the same way, the effectiveness and reliability of the proposed approach can also be tested for other machining operations (e.g.: drilling, milling, turning, etc.). Likewise, more in-depth machine learning approaches (e.g.: deep NN, neuro-fuzzy systems, etc.) can be implemented to expand the intelligent diagnosis system proposed in this thesis work.

REFERENCES

ABDI, Agência Brasileira de Desenvolvimento Industrial. *Agenda brasileira para a Indústria 4.0: **O Brasil preparado para os desafios do futuro***. Available in: <http://www.industria40.gov.br/>. Accessed on: Out, 10, 2019.

ABEDINI, R. *et al.* The Prediction of Undersaturated Crude Oil Viscosity: An Artificial Neural Network and Fuzzy Model Approach. ***Petroleum Science and Technology***, v. 30, n. 19, p. 2008–2021, jul. 2012.

AGUIAR, Paulo R. *et al.* Monitoring the dressing operation in the grinding process. ***International Journal of Machining and Machinability of Materials***, v. 5, n. 1, 2009.

ALEXANDRE, Felipe Aparecido *et al.* Tool condition monitoring of aluminum oxide grinding wheel using AE and fuzzy model. ***The Internacional Journal of Advanced Manufacturing Technology***, v. 96, p. 67–79, 2018.

ALMEIDA, Vinicius Augusto Dare; BAPTISTA, Fabricio Guimaraes; AGUIAR, Paulo Roberto. Piezoelectric transducers assessed by the pencil lead break for impedance-based structural health monitoring. ***IEEE Sensors Journal***, v. 15, n. 2, p. 693–702, 2015.

ARUN, A *et al.* Tool Condition Monitoring Of Cylindrical Grinding Process Using Acoustic Emission Sensor. ***Materials Today: Proceedings***, International Conference on Materials Manufacturing and Modelling, ICMMM - 2017, 9 - 11, March 2017, v. 5, n. 5, Part 2, p. 11888–11899, 2018.

AULESTIA VIERA, Martin A. *et al.* A Time-Frequency Acoustic Emission-Based Technique to Assess Workpiece Surface Quality in Ceramic Grinding with PZT Transducer. ***Sensors***, v. 19, n. 18, p. 3913, 11 set. 2019.

AZMI, A I. Monitoring of tool wear using measured machining forces and neuro-fuzzy modeling approaches during machining of GFRP composites. ***Advances in Engineering Software***, v. 82, p. 53–64, 2015.

BADGER, Jeffrey; MURPHY, Stuart; DONNELL, Garret E O. Acoustic emission in dressing of grinding wheels : AE intensity, dressing energy, and quantification of dressing sharpness and increase in diamond wear- flat size. ***International Journal of Machine Tools and Manufacture***, v. 125, n. July 2017, p. 11–19, 2018.

BAPTISTA, F.G. *et al.* An experimental study on the effect of temperature on piezoelectric sensors for impedance-based structural health monitoring. ***Sensors***, v. 14, n. 1208–27, 2014.

BAPTISTA, F.G.; VIEIRA FILHO. A new impedance measurement system for PZT based structural health monitoring. ***IEEE Trans. Instrum. Meas***, v. 58, n. 3602–8, p. 3602–3608, 2009.

BAPTISTA, F.G.; VIEIRA FILHO, J. Optimal Frequency Range Selection for PZT Transducers in Impedance-Based SHM Systems. ***IEEE Sensors Journal***, v. 10, n. 8, p. 1297–1303, 2010.

BAPTISTA, F.G.; VIEIRA FILHO, J.; INMAN, D.J. Influence of Excitation Signal on Impedance-based Structural Health Monitoring. ***Journal of Intelligent Material Systems and Structures***, v. 21, n. 14, p. 1409–1416, 2010.

BATISTA SILVA, Rosemar *et al.* Electromechanical impedance (EMI) technique as an alternative to monitor workpiece surface damages after the grinding operation. ***International Journal of Advanced Manufacturing Technology***, v. 98, n. 9–12, p. 2429–2438, 2018.

BHALLA, Suresh; NAIDU, Akshay S. K.; SOH, Chee Kiong. Influence of structure-actuator interactions and temperature on piezoelectric mechatronic signatures. ***Smart Materials, Structures, and Systems***, v. 262, n. 9, p. 50–62, 2003.

BHUIYAN, M.S.H.; CHOUDHURY, I.A. Review of Sensor Applications in Tool Condition Monitoring in Machining. ***Comprehensive Materials Processing***. Elsevier, 2014. p. 539–569.

BOBYR, Maxim V; YAKUSHEV, Aleksey S; DORODNYKH, Aleksandr A. Fuzzy devices for cooling the cutting tool of the CNC machine implemented on FPGA. ***Measurement,*** v. 152, p. 107378, 2020.

BOST. ***Bost Machine Tools Company***. Available in: <http://www.bost.es/pt-br/>. Accessed on: 28 Nov. 2019.

BUDOYA, Danilo *et al.* Analysis of Piezoelectric Diaphragms in Impedance-Based Damage Detection in Large Structures. ***Proceedings,*** v. 2, n. 6, p. 131, 2017.

BUDOYA, Danilo E.; CAMPEIRO, Leandro M.; BAPTISTA, Fabricio G. Sensitivity Enhancement of Piezoelectric Transducers for Impedance-Based Damage Detection via a Negative Capacitance Interface. ***IEEE Sensors Journal***, p. 1–1, 2019.

BUDOYA, Danilo E.; BAPTISTA, Fabricio Guimaraes. A Comparative Study of Impedance Measurement Techniques for Structural Health. ***IEEE Trans. Instrum. Meas***, v. 67, n. 4, p. 912–924, 2018.

BYRNE, G *et al.* Tool Condition Monitoring (TCM) — The Status of Research and Industrial Application. ***CIRP Annals***, v. 44, n. 2, p. 541–567, 1995.

CAGGIANO, Alessandra. Cloud-based manufacturing process monitoring for smart diagnosis services. ***International Journal of Computer Integrated Manufacturing***, v. 31, n. 7, p. 612–623, 3 jul. 2018.

CAGGIANO, Alessandra *et al.* Dimensionality Reduction of Sensorial Features by Principal Component Analysis for ANN Machine Learning in Tool Condition Monitoring of CFRP Drilling. ***Procedia CIRP***, 6th CIRP Global Web Conference – Envisaging the future manufacturing, design, technologies and systems in the innovation era (CIRPe 2018), v. 78, p. 307–312, 2018.

CARNIEL, Carlo. *Emulsifiable grinding oil for engine head resurfacing*. Available in: <https://theultimatetooling.com/en/emulsifiable-grinding-oil-head-resurfacing/>.

CASTRO, Bruno *et al.* Partial Discharge Monitoring in Power Transformers Using Low-Cost Piezoelectric Sensors. ***Sensors***, v. 16, n. 8, p. 1266, 2016.

CASTRO, Bruno A. *et al.* A chromatic technique for structural damage detection under noise effects based on impedance measurements. ***Measurement Science and Technology***, v. 30, n. 7, p. 75601, 2019.

CASTRO, Bruno A.; BAPTISTA, Fabricio Guimarães; CIAMPA, Francesco. Comparative analysis of signal processing techniques for impedance-based SHM applications in noisy environments. ***Mechanical Systems and Signal Processing***, v. 126, p. 326–340, Jul. 2019a.

CASTRO, Bruno A.; BAPTISTA, Fabricio Guimarães; CIAMPA, Francesco. New signal processing approach for structural health monitoring in noisy environments based on impedance measurements. ***Measurement***, v. 137, p. 155–167, Abr. 2019b.

CEARSOLO, A. X. *et al.* Dry-dressing for ecological grinding. ***Journal of Cleaner Production***, v. 135, p. 633–643, 2016.

CHEN, Yunzhu; XUE, Xingwei. Advances in the Structural Health Monitoring of Bridges Using Piezoelectric Transducers. ***Sensors***, v. 18, p. 4312, 2018.

CHENG, Can *et al.* Deep convolutional neural network-based in-process tool condition monitoring in abrasive belt grinding. ***Computers in Industry***, v. 106, p. 1–13, 2019.

CHOI, Sang Ki *et al.* Real-time strength monitoring for concrete structures using EMI technique incorporating with fuzzy logic. ***Applied Sciences (Switzerland)***, v. 8, n. 1, p. 1–13, 2018.

CNI, Confederação Nacional da Indústria. *Investimentos em Indústria 4.0*. Brasilia: 2018.

COELHO, R T; OLIVEIRA, J F G; CAMPOS, G P. Experimental and theoretical study of the temperature distribution on diamond dressing tools for precision grinding. ***Abrasives,*** cited By 4, n. APR./MAY, p. 7–15, 2000.

CORTEZ, Nicolás E; FILHO, Jozué V; BAPTISTA, Fabricio G. A new microcontrolled structural health monitoring system based on the electromechanical impedance principle. ***Structural Health Monitoring: An International Journal***, v. 12, n. 1, p. 14–22, 17 jan. 2013.

CUKA, Besmir; KIM, Dong-Won. Fuzzy logic based tool condition monitoring for end-milling. ***Robotics and Computer-Integrated Manufacturing***, v. 47, p. 22–36, 2017.

D'ADDONA, Doriana M. *et al.* Neural Networks Tool Condition Monitoring in Single-point Dressing Operations. ***Procedia CIRP***, v. 41, p. 431–436, 2016.

D'ADDONA, Doriana M. *et al.* Prediction of Dressing in Grinding Operation via Neural Networks. ***Procedia CIRP***, v. 62, p. 305–310, 2017.

D’ADDONA, Doriana *et al.* Tool Condition Monitoring of Single-point Dressing Operation by Digital Signal Processing of AE and AI. ***Procedia CIRP***, v. 67, p. 307–312, 2018.

DENG, Hui; XU, Zhou. Dressing methods of superabrasive grinding wheels: A review. ***Journal of Manufacturing Processes***, v. 45, p. 46–69, 2019.

DENKENA, Berend; JACOBSEN, J; KRAMER, Niklas. Dressing Monitoring by Acoustic Emission. ***Key Engineering Materials***, 2005: Trans Tech Publications, 2005. p. 195–200.

DORNFELD, D; CAI, Gao. An Investigation of Grinding and Wheel Loading Using Acoustic Emission. ***Journal of Engineering for Industry***, v. 106, n. 1, p. 28, 1984.

DORNFELD, David A; DEVRIES, M F. Neural Network Sensor Fusion for Tool Condition Monitoring. ***CIRP Annals***, v. 39, n. 1, p. 101–105, 1990.

DOTTO, Fabio R. L. *et al.* In-Dressing Acoustic Map by Low-cost Piezoelectric Transducer. ***IEEE Transactions on Industrial Electronics***, p. 1–1, 2019.

DUVAL. ***Aerospace & Aviation***. Available in: <https://www.duvalgrinding.com/precision-grinding-services-for-aerospace-components-and-faa-overhaul/>. Accessed on: Nov 28, 2019.

DYNAMIC PRECISION. ***Surface Grinding Services***. Available in: <https://www.dynamicprecision.net/surface-grinding-services.html>. Accessed on: Nov 28, 2019.

E976-10, Standard. Standard Guide for Determining the Reproducibility of Acoustic Emission Sensor Response. ***ASTM***, 2010.

EGANA, I. *et al.* Towards intelligent dressing. ***IEEE Instrumentation & Measurement Magazine***, p. 38–43, 2006.

FAIRWEATHER, James A.; CRAIG, Kevin C. Incorporating finite element techniques to simplify the impedance modeling of active structures. ***Proceedings*** v. 3323, 1998 p. 602–613.

FAN, Shuli *et al.* Damage Evaluation of Concrete Column under Impact Load Using a Piezoelectric-Based EMI Technique. ***Sensors***, v. 17, n. 2, p. 417, 2018.

FARRAR, K. Worden. ***Structural health monitoring: A machine learning perspective***. United Kingdom: John Wiley & Sons Chichester, 2013.

FERREIRA, F.I. *et al.* Electromechanical impedance (EMI) measurements to infer features from the grinding process. ***The International Journal of Advanced Manufacturing Technology***, 2019.

FERREIRA, F.I. *et al.* Inferential measurement of the dresser width for the grinding process automation. ***The International Journal of Advanced Manufacturing Technology***, v. 100, n. 9–12, p. 3055–3066, 2019.

FRAIMOVITCH, D *et al.* CVD diamond metallization and characterization. ***Nuclear Inst. and Methods in Physics Research, A***, v. 845, p. 76–79, 2017.

FRANC, V.; HLAVÁC, V. Statistical pattern recognition toolbox for Matlab—User's guide. ***Dept. Cybernetics, Czech Tech. Univ., Prague, Czech Republic, Tech. Rep***., n. 1213-2365, 2004.

FRAUNHOFER-GESELLSCHAFT. ***Trends in industrie 4.0***. Brochure 2016. Available in: < http://s.fhg.de/contact-press >. Accessed on: Jan 20, 2019.

FREITAS E.S; BAPTISTA, Fabricio G. Experimental analysis of the feasibility of low-cost piezoelectric diaphragms in impedance-based SHM applications. *Sensors & Actuators: A. Physical*, v. 238, p. 220–228, 2016.

FREITAS, E.S. *et al.* Equivalent Circuit of Piezoelectric Diaphragms for Impedance-Based Structural Health Monitoring Applications. ***IEEE Sensors Journal***, v. 17, n. 17, p. 5537–5546, 2017.

GIURGIUTIU, Victor; ZAGRAI, Andrei N. Characterization of Piezoelectric Wafer Active Sensors. ***Journal of Intelligent Material Systems and Structures***, v. 11, n. 12, p. 959–976, dez. 2000.

GOPAL, Venu; ANNAMDAS, Madhav; SOH, Chee Kiong. Three-Dimensional Electromechanical Impedance Model. I : Formulation of Directional Sum Impedance. ***Journal of Aerospace Engineering,*** v. 20, n. January, p. 53–62, 2007.

GOSTIMIROVIĆ, M. *et al.* Investigation of the Cutting Forces in Creep-Feed Surface Grinding Process. ***Journal of Production Engineering***, v. 18, n. 2, p. 21–24, 2015.

HABRAT, W.; BATSCH, A.; PORZYCKI, J. Monitoring of the single-point diamond dresser wear. ***Archives of Civil and Mechanical Engineering***, v. 1, 2005.

HAYKIN, Simon. ***Neural Networks and Learning Machines***. 3nd: Prentice-Hall, 2008.

HU, Xianyan; ZHU, Hongping; WANG, Dansheng. A Study of Concrete Slab Damage Detection Based on the Electromechanical Impedance Method. ***Sensor****s*, v. 14, n. 10, p. 19897–19909, out. 2014.

HUYNH, Thanh-Canh; DANG, Ngoc-Loi; KIM, Jeong-Tae. Preload Monitoring in Bolted Connection Using Piezoelectric-Based Smart Interface. ***Sensors,*** v. 18, n. 9, p. 2766, ago. 2018.

IEEE STANDARD ON PIEZOELECTRICITY. ***An American National Standard. IEEE-ANSI***. New York. 1987

INASAKI, I.; OKAMURA, K. Monitoring of Dressing and Grinding Processes with Acoustic Emission Signals. ***CIRP Annals - Manufacturing Technology***, v. 30, n. 1, p. 277–280, 1985.

INMAN, Daniel J. *et al.* ***Damage Prognosis: For Aerospace, Civil and Mechanical Systems***. Wiley, 2005.

INMAN, Daniel J; VIEIRA, Jozue; GUIMAR, Fabricio. Time-domain analysis of piezoelectric impedance-based structural health monitoring using multilevel wavelet decomposition.

Mechanical Systems and Signal Processing, v. 25, p. 1550–1558, 2011.

JACKSON, Mark J.; DAVIM, J. Paulo. ***Machining with Abrasives***. New York: Springer Science+Business Media LLC, 2011.

JEMIELNIAK, K; OTMAN, O. Catastrophic Tool Failure Detection Based on Acoustic Emission Signal Analysis. ***CIRP Annals***, v. 47, n. 1, p. 31–34, 1998.

JEMIELNIAK, Krzysztof. Tool Condition Monitoring in Metal Cutting. ***Soft Modeling in Industrial Manufacturing***. Springer, Cham, 2019. p. 45–74.

JFS. *CNC Grinding Service*. Available in: <https://www.jfs-steel.com/en/OEM-service/CNC-Grinding-Service/OEM-CNC-grinding.html>. Accessed on Nov 28, 2019.

KATUNIN, Andrzej; AMAROWICZ, Marcin; CHRZANOWSKI, Paweł. Faults diagnosis using self-organizing maps: A case study on the DAMADICS benchmark problem. ***Federated Conference on Computer Science and Information Systems (FedCSIS)*** p. 1673–1681, 2015.

KIM, Jinki; WANG, K W. An enhanced impedance-based damage identification method using adaptive piezoelectric circuitry. ***Smart Materials and Structures*** *PAPER*, v. 23, p. 095041, 2014a.

KIM, Jinki; WANG, K W. An enhanced impedance-based damage identification method using adaptive piezoelectric circuitry. ***Smart Materials and Structures***, v. 23, n. 9, p. 95041, 2014b.

KONG, Dongdong *et al*. Relevance vector machine for tool wear prediction. ***Mechanical Systems and Signal Processing***, v. 127, p. 573–594, 2019.

KOTHURU, Achyuth. ***Application of Audible Signals in Tool Condition Monitoring using Machine Learning Techniques***. 2017. 107 f. Rochester Institute of Technology, 2017.

KUBO, Akihiko; TAMAKI, J. Evaluation of diamond dressers and estimation of grinding performance by dressing force measurement**.** ***International Journal of Abrasive Technology***, v. 3, n. 1, 2010.

KWAK, Jaeseob; HA, Mankyung. Detection of dressing time using the grinding force signal based on the discrete wavelet decomposition. ***The International Journal of Advanced Manufacturing Technology***, v. 23, n. 1, p. 87–92, 2004.

LACH DIAMOND. *Diamond dressing tools and maintenance service*. Available in: <https://www.lach-diamant.de/english/products/diamond-dressing-tools/diamond-dressing-tools-and-maintenance-service#!%7B%22article%22:%22undefined%22%7D>. Accessed on Nov 29, 2019.

LAURO, C H *et al*. Monitoring and processing signal applied in machining processes – A review. ***Measurement***, v. 58, p. 73–86, 2014.

LEE, D E *et al*. Precision manufacturing process monitoring with acoustic emission. ***International Journal of Machine Tools and Manufacture***, v. 46, n. 2, p. 176–188, 2006.

LEE, Wo Jae; MENDIS, Gamini P; SUTHERLAND, John W. Development of an Intelligent Tool Condition Monitoring System to Identify Manufacturing Tradeoffs and Optimal Machining Conditions. ***Procedia Manufacturing***, Sustainable Manufacturing for Global Circular Economy: Proceedings of the 16th Global Conference on Sustainable Manufacturing, v. 33, p. 256–263, 2019.

LI, Ling. China's manufacturing locus in 2025: With a comparison of "Made-in-China 2025" and "Industry 4.0". ***Technological Forecasting and Social Change***, v. 135, p. 66–74, 2018.

LI, Zhixiong; LIU, Rui; WU, Dazhong. Data-driven smart manufacturing: Tool wear monitoring with audio signals and machine learning. ***Journal of Manufacturing Processes***, v. 48, p. 66–76, 2019.
LIANG, C.; SUN, F. P.; ROGERS, C. A. Coupled electromechanical analysis of adaptive material systems-determination of the actuator power consumption and system energy transfer. ***Journal of Intelligent Material Systems and Structures***, v. 5, n. 1, p. 12–20, 1994.

LIANG, Qianzhu *et al.* Low-Cost Sensor Fusion Technique for Surface Roughness Discrimination with Optical and Piezoelectric Sensors. ***IEEE Sensors Journal***, v. 17, n. 23, p. 7954–7960, 2017.

LIM, Yee Yan; SOH, Chee Kiong. Electro-Mechanical Impedance (EMI)-Based Incipient Crack Monitoring and Critical Crack Identification of Beam Structures. ***Research in Nondestructive Evaluation***, v. 25, n. 2, p. 82–98, Abr. 2014.

LIN, Shuyu; XU, Jie. Effect of the Matching Circuit on the Electromechanical Characteristics of Sandwiched Piezoelectric Transducers. ***Sensors***, v. 17, n. 2, p. 329, fev. 2017.

LINS, Romulo Gonçalves; DE ARAUJO, Paulo Ricardo Marques; CORAZZIM, Marcio. In-process machine vision monitoring of tool wear for Cyber-Physical Production Systems. ***Robotics and Computer-Integrated Manufacturing***, v. 61, p. 101859, 2020.

LIU, Wei *et al.* A method of NC machine tools intelligent monitoring system in smart factories. ***Robotics and Computer-Integrated Manufacturing***, v. 61, p. 101842, 2020.

LOPES SILVA, R.H.; DA SILVA, Márcio Bacci; HASSUI, Amauri. A probabilistic neural network applied in monitoring tool wear in the end milling operation via acoustic emission and cutting power signals. ***Machining Science and Technology***, v. 20, n. 3, p. 386–405, 2 Jul. 2016.

LOPES, W.N. *et al.* Digital signal processing of acoustic emission signals using power spectral density and counts statistic applied to single-point dressing operation. ***IET Science, Measurement & Technology***, v. 11, n. 8, p. 631–636, mar. 2017.

LUO, Ming *et al.* A wireless instrumented milling cutter system with embedded PVDF sensors. ***Mechanical Systems and Signal Processing***, v. 110, p. 556–568, 2018.

LUO, Ming; CHONG, Zenghui; LIU, Dongsheng. Cutting Forces Measurement for Milling Process by Using Working Tables with Integrated PVDF Thin-Film Sensors. ***Sensors***, v. 18, n. 11, p. 4031, 19 Nov. 2018.

MAGGIONI, Matteo F; MARZORATI, Elena. ***In-Process Quality Monitoring via sensor data***

fusion: chatter control in grinding. 2013. 112 f. Politecnico di Milano, 2013.

MAKSOUD, T. M. A.; ATIA, M. R. Review of Intelligent Grinding and Dressing Operations. ***Machining Science and Technology An International Journal***, v. 8, n. 2, p. 263–276, 2007.

MALKIN, Stephen; GUO, Changsheng. *Grinding Technology:* ***Theory and Application of Machining with Abrasives***. 2nd. ed. New York: Industrial Press Inc, 2008.

MAMDANI, E. H.; ASSILIAN, S. An Experiment in Linguistic Synthesis with a Fuzzy Logic Controller. ***Int. J. Man-Machine Studies***, v. 7, p. 1–13, 1975.

MARCHI, Marcelo *et al.* Grinding process monitoring based on electromechanical impedance measurements. ***Measurement Science and Technology***, v. 26, n. 4, p. 045601, 2015.

MARINESCU, Ioan D. *et al.* ***Handbook of Machining with Grinding Wheels***. 2nd. ed. New York: CRC Press, 2016b.

MARTINS, C.H. *et al.* Tool Condition Monitoring of Single-Point Dresser Using Acoustic Emission and Neural Networks Models. ***IEEE Transactions on Instrumentation and Measurement***, v. 63, n. 3, p. 667–679, 2014.

MARTINS, C.H. *et al.* Application of MLP and Kohonen networks for recognition of wear patterns of single-point dressers. ***IASTED Multiconferences - Proceedings of the IASTED International Conference on Artificial Intelligence and Applications***, p. 70 74, 2013.

MARUO, Isabela Iuriko Campos *et al.* Electromechanical Impedance - Based Structural Health Monitoring Instrumentation System Applied to Aircraft Structures and Employing a Multiplexed Sensor Array. ***Journal of Aerospace Technology and Management***, v. 7, n. 3, p. 294–306, set. 2015.

MIN, Jiyoung *et al.* Impedance-based structural health monitoring incorporating neural network technique for identification of damage type and severity., v. 39, p. 210–220, 2012.

MIRANDA, H.I. *et al.* Monitoring single-point dressers using fuzzy models. ***Procedia CIRP***, v. 33, p. 281-286, 2015.
MOCHIDA, Y. *et al.* Estimation of grinding wheel performance by dressing force measurement. ***Adv. Mater. R****es*, v. 76, n. 78, p. 155–160, 2009.

MOIA, D. F. G. *et al.* Tool condition monitoring of aluminum oxide grinding wheel in dressing operation using acoustic emission and neural networks. ***Journal of the Brazilian Society of Mechanical Sciences and Engineering***, v. 37, n. 2, p. 627–640, 2015.

MURATA, Manufacturing Co. ***Piezoelectric Sound Components***. Available in: <https://www.murata.com/~/media/webrenewal/support/library/catalog/products/sound/p15e.ashx>. Accessed on Jan. 20, 2020.

NA, S.; LEE, H.K. Neural network approach for damaged area location prediction of a composite plate using electromechanical impedance technique. ***Composites Science and Technology***, v. 88, p. 62–68, nov. 2013.

NA, Wongi; BAEK, Jongdae. A Review of the Piezoelectric Electromechanical Impedance Based Structural Health Monitoring Technique for Engineering Structures. ***Sensors***, v. 18, n. 5, p. 1307, Abr. 2018.

NA, Wongi; BAEK, Jongdae. Impedance-Based Non-Destructive Testing Method Combined with Unmanned Aerial Vehicle for Structural Health Monitoring of Civil Infrastructures. ***Applied Sciences***, v. 7, n. 1, p. 15, 22 dez. 2016.

NAGHDY, Fazell; COOK, Chris; ENGINEERING, Telecommunications. Monitoring of Wheel Dressing Operations for Precision Grinding. ***Industrial Technology, IEEE ICIT***, v. 02, p. 1296–1299, 2002.

NOVAK, A; WIKLUND, H. On-Line Prediction of the Tool Life. ***CIRP Annals***, v. 45, n. 1, p. 93–96, 1996.

OH, Tae-Keun *et al.* Nondestructive Concrete Strength Estimation based on Electro-Mechanical Impedance with Artificial Neural Network. ***Journal of Advanced Concrete Technology***, v. 15, n. 3, p. 94–102, 2017.

OLIVEIRA JUNIOR, P.C. *et al.* Dressing Tool Condition Monitoring through Impedance-Based Sensors: Part 2—Neural Networks and K-Nearest Neighbor Classifier Approach. ***Sensors***, v. 18, n. 12, p. 4453, Dez. 2018.

OLIVEIRA JUNIOR, P.C. *et al*. Dressing Tool Condition Monitoring through Impedance-Based Sensors: Part 1—PZT Diaphragm Transducer Response and EMI Sensing Technique. ***Sensors***, v. 18, n. 12, p. 4455, dez. 2018.

OLIVEIRA JUNIOR, P.C. *et al.* Impedance-Based PZT Transducer and Fuzzy Logic to Detect Damage in Multi-point Dressers. ***Lecture Notes in Mechanical Engineering***. Springer Nature Switzerland AG, 2019. p. 213–222.

OLIVEIRA JUNIOR, P.C. *et al.* Spectral estimation of vibration signal for monitoring the wear of single-point dresser. ***Matéria Journal Scielo***, v. 21, n. 04, p. 827–840, 2016.

OLIVEIRA JUNIOR, P.C *et al.* Wear Monitoring of Single-Point Dresser in Dry Dressing Operation Based on Neural Models. ***Proceedings of the IASTED International Conference Modelling, Identification and Control (MIC 2017)***, v. 36, n. Mic, p. 178–185, 2017.

OLIVEIRA JUNIOR, P.C *et al.* Time-domain analysis based on the electromechanical impedance method for monitoring of the dressing operation. ***Procedia CIRP***, v. 67, p. 319 – 324, 2018.

OLIVEIRA, Mario A.; INMAN, Daniel J. Performance analysis of simplified Fuzzy ARTMAP and Probabilistic Neural Networks for identifying structural damage growth. ***Applied Soft Computing***, v. 52, p. 53–63, mar. 2017.

OLIVEIRA, Mario A.; MONTEIRO, Andre V.; FILHO, Jozue Vieira. A new structural health monitoring strategy based on PZT sensors and convolutional neural network. ***Sensors***, v. 18, n. 9, 2018.

OLIVEIRA, M. Anderson De *et al.* A novel time-domain technique for damage detection applied to SHM using Savitzky-Golay filter. ***Aerospace Engineering: A Roadmap to Intelligent Structures - Proceedings of the 9th International Workshop on Structural Health Monitoring, IWSHM***, v. 1, p. 996–1003, 2013.

OLIVEIRA, J. F. Gomes; DORNFELD, David A. Application of AE Contact Sensing in Reliable Grinding Monitoring. ***Annals of the CIRP***, v. 50, n. 1, p. 217–220, 2001.

OLIVEIRA, J.F. Gomes; DORNFELD, David A.; WINTER, B. Dimensional Characterization of Grinding Wheel Surface Through Acoustic Emission. ***Annals of the CIRP***, v. 44, n. 1, p. 291–294, 1994.

OLIVEIRA, J F G; BOTTENE, A C; FRANC, T V. A novel dressing technique for texturing of ground surfaces. ***CIRP Annals - Manufacturing Technology***, v. 59, p. 361–364, 2010.

OLIVEIRA, J F G; BOTTENE, A C; FRANÇA, T V. A novel dressing technique for texturing of ground surfaces. ***CIRP Annals***, v. 59, n. 1, p. 361–364, 2010.

PALOMINO, Lizeth Vargas; STEFFEN, Valder; FINZI, Roberto Mendes. Fuzzy Cluster Analysis Methods Applied to Impedance Based Structural Health Monitoring for Damage Classification. ***Topics in Modal Analysis II***. New York: Springer New York, 2012. p. 205–212.

PARK, Gyuhae *et al.* Overview of Piezoelectric Impedance-Based Health Monitoring and Path Forward. ***The Shock and Vibration Digest***, v. 35, n. 6, p. 451–463, 2003.

PARK, Seunghee *et al.* Electro-Mechanical Impedance-Based Wireless Structural Health Monitoring Using PCA-Data Compression and k -means Clustering Algorithms. ***Journal of Intelligent Material Systems and Structures***, v. 19, n. 4, p. 509–520, 10 Abr. 2008.

PEAIRS, Daniel M.; INMAN, Daniel J.; PARK, Gyuhae. Circuit Analysis of Impedance-based Health Monitoring of Beams Using Spectral Elements. ***Structural Health Monitoring***, v. 6, n. 1, p. 81–94, 2007.

PEAIRS, Daniel M.; PARK, Gyuhae; INMAN, Daniel J. Improving Accessibility of the Impedance-Based Structural Health Monitoring Method. ***Journal of Intelligent Material Systems and Structures***, v. 15, n. 2, p. 129–139, 27 Feb. 2004.

PHYSICAL-ACOUSTIC. *R15I-AST* ***Sensor-Integral Preamplifier Sensor***. Available in: < https://www.physicalacoustics.com/by-product/sensors/R15I-AST-150-kHz-Integral-Preamp-AE-Sensor> Accessed on Jan. 20, 2020.

POMBO, I. *et al.* Experimental and numerical analysis of thermal phenomena in the wear of single-point diamond dressing tools. ***Journal of Manufacturing Processes***, v. 27, p. 145–157, 2017.

POMBO, I; PORTILLO, E. Dry-dressing for ecological grinding. ***Journal of Cleaner Production***, v. 135, p. 633–643, 2016.

QING, Xinlin *et al.* Piezoelectric Transducer-Based Structural Health Monitoring for Aircraft Applications. ***Sensors,*** v. 19, n. 3, p. 545, 28 Jan. 2019.

RABELO, D.S. *et al.* Impedance-based structural health monitoring and statistical method for threshold-level determination applied to 2024-T3 aluminum panels under varying temperature. ***Structural Health Monitoring***, v. 16, n. 4, p. 365–381, 2017.

RABIEY, Mohammad. ***Dry Grinding with CBN Wheels, The Effect of Structuring***. 2010. 174 f. Universität Stuttgart, 2010.

REHORN, Adam G.; JIANG, Jin; ORBAN, Peter E. State-of-the-art methods and results in tool condition monitoring: A review. ***International Journal of Advanced Manufacturing Technology***, v. 26, n. 7–8, p. 693–710, 2005.

REN, Qun *et al.* Type-2 fuzzy tool condition monitoring system based on acoustic emission in micromilling. ***Information Sciences***, v. 255, p. 121–134, 2014.

RIBEIRO, Danilo M. S. *et al.* Spectra Measurements Using Piezoelectric Diaphragms to Detect Burn in Grinding Process. ***IEEE Transactions on Instrumentation and Measurement***, v. 66, n. 11, p. 3052–3063, nov. 2017.

ROWE, W. Brian. ***Principles of Modern Grinding Technology***. 2nd. ed. Oxford: Elsevier, 2014.

RUI SILVA, G. Condition monitoring of the cutting process using a self-organizing spiking neural network map. ***Journal of Intelligent Manufacturing***, v. 21, n. 6, p. 823–829, 19 Dez. 2010.

SAUSE, M. Investigation of Pencil Lead Breaks as Acoustic Emission Sources. ***Journal of Acoustic Emission***, v. 29, p. 184–196, 2011.

SELVA, Pierre *et al.* Smart monitoring of aeronautical composites plates based on electromechanical impedance measurements and artificial neural networks. ***Engineering Structures***, v. 56, p. 794–804, 2013.

SHI, Chengming *et al.* Anomaly Detection via Unsupervised Learning for Tool Breakage Monitoring. ***International Journal of Machine Learning and Computing***, v. 6, n. 5, p. 256–259, out. 2016.

SILVA, Macedo; CASTRO, Adriana R.; MIRANDA, Vladimiro. Transformer failure diagnosis by means of fuzzy rules extracted from Kohonen Self-Organizing Map. ***International Journal of Electrical Power & Energy System****s*, v. 43, n. 1, p. 1034–1042, Dez. 2012.

SILVEIRA, Ricardo Zanni; CAMPEIRO, Leandro Melo; BAPTISTA, Fabricio G. Performance of three transducer mounting methods in impedance-based structural health monitoring applications. ***Journal of Intelligent Material Systems and Structures***, v. 1, n. 14, 2017.

STRUCTURAE. *Structural health monitoring at Cugnielertobel Bridge II and Lavoitobel Bridge*. Disponível em: <https://structurae.net/en/products-services/structural-health-monitoring-at-cugnielertobel-bridge-ii-and-lavoitobel-bridge>.

SWAIN, Samarjit *et al.* Adaptive tool condition monitoring system: A brief review. ***Materials Today: Proceedings***, 2019.

TETI, R. *et al.* Advanced monitoring of machining operations. ***CIRP Annals - Manufacturing Technology***, v. 59, n. 2, p. 717–739, Jan. 2010.

TETI, R. Advanced IT Methods of Signal Processing and Decision Making for Zero Defect Manufacturing in Machining. ***Procedia CIRP***, v. 28, p. 3–15, 2015.

TETI, Roberto. A Review of Tool Condition Monitoring Literature Database. ***CIRP Annals***, v. 44, n. 2, p. 659–666, 1995.

TETI, Roberto *et al.* Smart Multi-Sensor Monitoring in Drilling of CFRP/CFRP Composite Material Stacks for Aerospace Assembly Applications. ***Applied Sciences***, v. 10, n. 3, p. 758, 21 jan. 2020.

TETI, Roberto. Tool Wear State Identification by Fuzzy Logic Processing of Fused Sensor Data. ***CIRP ICME***, v. 1, p. 687–691, 1998.

TIAN, Wei. *Signature Analysis of OD Grinding Processes with Applications in Monitoring and Diagnosis*. 2009. 89 f. **Worcester Polytechnic Institute**, 2009.

TÖNSHOFF, H K; FRIEMUTH, T; BECKER, J C. Process Monitoring in Grinding. ***CIRP Annals***, v. 51, n. 2, p. 551–571, 2002.

VENU ANNAMDAS; CHEE KIONG SOH. Application of Electromechanical Impedance Technique for Engineering Structures: Review and Future Issues. ***Journal of Intelligent Material Systems and Structures***, v. 21, n. 1, p. 41–59, jan. 2010.

VIEIRA, Reis *et al.* Fuzzy Logic Applied to Damage Characterization through SHM Techniques. ***Allen Institute for Artificial Intelligence by Semantic Scholar***, p. 1–8, 2007.

VIERA, Martin A. Aulestia *et al.* Low-cost piezoelectric transducer for ceramic grinding monitoring. ***IEEE Sensors Journal***, v. 19, n. 17, p. 7605–7612, 2019.

WANG, Chonghua. *A Study of Membership Functions on MamdaniType Fuzzy Inference System for Industrial Decision-Making*. *Mechanical Engineering Commons*. Lehigh University, 2015

WEGENER, K. *et al.* Conditioning and monitoring of grinding wheels. ***CIRP Annals - Manufacturing Technology***, v. 60, n. 2, p. 757–777, jan. 2011.

WEHMEIER, M; INASAKI, I. Investigation and utilization of the acoustic emission signal for monitoring the dressing process. ***Proceedings of the Institution of Mechanical Engineers, Part B: Journal of Engineering Manufacture***, v. 216, n. 4, p. 543–553, 2002.

WIRZ-DIAMANT. *Diamond Dressing Tools Catalog*. 2014. Available in: <https://www.meycotools.ch/PDF/Gesamtkatalog_EN.pdf>. Accessed on: Jan. 20, 2020.

XINGYU FAN, Jun Li; HAO, And Hong. Piezoelectric impedance-based damage detection in truss bridges based on time-frequency ARMA model. ***Smart Structures and Systems***, v. 18, n. 3, 2016.

YANG, Yaowen; DIVSHOLI, Bahador Sabet. Sub-Frequency Interval Approach in Electromechanical Impedance Technique for Concrete Structure Health Monitoring. ***Sensors***, v. 10, p. 11644–11661, 2010.

YANG, Yaowen; LIM, Yee Yan; SOH, Chee Kiong. Practical issues related to the application of the electromechanical impedance technique in the structural health monitoring of civil structures: I. Experiment**. *Smart Materials and Structures***, v. 17, n. 3, p. 035008, jun. 2008.

ZAHEDI, F; HUANG, H. Time-frequency analysis of electro-mechanical impedance (EMI) signature for physics-based damage detections using piezoelectric wafer active sensor (PWAS). ***Smart Materials and Structures***, v. 26, n. 5, p. 55010, 2017.

ZĘBALA, Wojciech; STRUZIKIEWICZ, Grzegorz. Aspects of Monitoring of Machining in the Context of Industry 4.0. ***Lecture Notes in Mechanical Engineering***. Springer Nature Switzerland AG, 2020. p. 233–242.

ZHANG, Chunhe; SHIN, Yung C. Wear of diamond dresser in laser assisted truing and dressing of vitrified CBN wheels. ***International Journal of Machine Tools and Manufacture***, v. 43, p. 41–49, 2003.

ZHANG, Cunji *et al.* Tool Condition Monitoring and Remaining Useful Life Prognostic Based on a Wireless Sensor in Dry Milling Operations. ***Sensors***, v. 16, n. 6, p. 795, May 2016.

ZHONG, Ray Y *et al.* Intelligent Manufacturing in the Context of Industry 4.0: A Review. ***Engineering***, v. 3, n. 5, p. 616–630, 2017.

ZHOU, Pin; WANG, Dansheng; ZHU, Hongping. A Novel Damage Indicator Based on the Electromechanical Impedance Principle for Structural Damage Identification. ***Sensors***, v. 18, n. 7, p. 2199, Jul. 2018.

ZHOU, Yuqing; XUE, Wei. A Multisensor Fusion Method for Tool Condition Monitoring in Milling. ***Sensors***, v. 18, n. 11, p. 3866, 10 Nov. 2018.

ZHOU, Z.D *et al.* Integrated Condition Monitoring and Fault Diagnosis for Modern Manufacturing Systems. ***CIRP Annals***, v. 49, n. 1, p. 387–390, 2000.